



Title	AN NMR STUDY OF MOLECULAR MOTION IN A SERIES OF LIQUID CRYSTALLINE COMPOUNDS
Author(s)	Miyajima, Seiichi
Citation	大阪大学, 1981, 博士論文
Version Type	VoR
URL	https://hdl.handle.net/11094/24339
rights	
Note	

The University of Osaka Institutional Knowledge Archive : OUKA

<https://ir.library.osaka-u.ac.jp/>

The University of Osaka

AN NMR STUDY OF MOLECULAR MOTION
IN A SERIES OF LIQUID CRYSTALLINE COMPOUNDS

BY

Seiichi Miyajima

M. S., Osaka University, 1978

Thesis

Submitted to
The Graduate School of Faculty of Science,
Osaka University,
in Partial Fulfilment of the Requirements
for the Degree of Doctor of Science

1981

Doctoral Comittee:
Professor Hideaki Chihara, Chairman,
Professor Keiji Kuwata,
Professor Hiroshi Suga.

Acknowledgments

This work was carried out in the laboratory of Professor Chihara during the author's graduate course in Osaka University, Toyonaka.

I wish to express sincere thanks to Professor Hideaki Chihara for his kind guidance and encouragement and also for critical reading of this manuscript.

I would like to thank Associate Professor Nobuo Nakamura for many valuable suggestions. It was fortunate for me to be able to enjoy discussion with him almost every day throughout this work. The main results of the present thesis will soon be published jointly by Drs. N. Nakamura, H. Chihara, and the present author.

The samples used in this work was prepared by Dr. Kazuhiro Tsuji of Kwansei Gakuin University. I am deeply indebted to him for his friendship to provide me the excellent samples.

I would like to thank Professor Hiroshi Suga and Associate Professor Michio Sorai for providing me a chance to use the polarizing microscope, and for their kind encouragement.

The NMR spectrometers used in this work are the products of collaboration of the many workers in our laboratory, for which Dr. N. Nakamura and Messrs. Toshihiro Tsuneyoshi, Kiyoshi Ichimura, and Keita Sasaki are mainly responsible.

I will not forget the joyful days we've had with many friends in Professor Chihara's laboratory.

Contents

Abstract		1
Chapter I	Introduction	3
§ I-1	Introductory Remarks	3
§ I-2	Survey of the Studies on the Physical Properties of the Three Compounds	8
I-2-1	HBAB	8
I-2-2	HBAC	10
I-2-3	HBT	10
	References to Chapter I	12
Chapter II	Theory of Nuclear Spin-Lattice Relaxation due to Orientational Fluctuation in Smectic Liquid Crystals	14
§ II-1	Description of Order	14
§ II-2	Elastic Continuum Theory of the Smectic System ——— A Simplified Review of the Theory ———	16
§ II-3	Dynamics of Undulation	21
§ II-4	Nuclear Spin-Lattice Relaxation Rate due to Undulation Mode	22
§ II-5	Nuclear Spin-Lattice Relaxation due to Three-Dimensional Director Fluctuation in Smectic A System	31
	References to Chapter II	34
Chapter III	Experimental	35
§ III-1	Samples	35

§ III-2	Differential Thermal Analysis (DTA)	35
§ III-3	Texture Observations	37
§ III-4	NMR Lineshape Observations	37
§ III-5	NMR Spin-Lattice Relaxation Measurements	38
	References to Chapter III	42
Chapter IV	Phase Relations and Textures	43
§ IV-1	HBAB	43
§ IV-2	HBAC	45
§ IV-3	HBT	48
	References to Chapter IV	59
Chapter V	Molecular Motion in the Nematic Liquid	
	Crystalline Compound, HBAB	60
§ V-1	Major Objectives of the NMR Study	60
§ V-2	The Crystalline Phases	60
V-2-1	Second Moments	60
V-2-2	Spin-Lattice Relaxation Rates	64
§ V-3	Orientational Order in the Nematic Phase	68
§ V-4	Molecular Dynamics in the Nematic Phase	77
§ V-5	Molecular Dynamics in the Isotropic Phase	82
§ V-6	Summary	83
	References to Chapter V	86
Chapter VI	Molecular Motion in the Smectic Liquid	
	Crystalline Compound, HBAC	88
§ VI-1	Purposes of This Study	88
§ VI-2	The Crystalline State	89
§ VI-3	The Phase III	91
§ VI-4	The Smectic B Mesophase	95

§ VI-5	The Smectic A Mesophase and the Isotropic Liquid Phase	105
§ VI-6	Summary	105
	References to Chapter VI	107
Chapter VII	Molecular Motion in HBT	108
§ VII-1	Purposes of This Study	108
§ VII-2	The Crystalline States	108
§ VII-3	The Nematic and the Isotropic Liquid Phases	111
§ VII-4	The Metastable Smectic B Mesophase	115
§ VII-5	Summary	117
	References to Chapter VII	123
Chapter VIII	A Phenomenological Theory of Viscosity and Self-Diffusion in Nematic Liquid Crystals	124
§ VIII-1	Theory	124
§ VIII-2	Comparison with Experiment	129
§ VIII-3	Discussion	132
	References to Chapter VIII	134
Chapter IX	Summary	135
Appendix	Kinetics of Phase Transition between Two Crystalline Modifications of HBAB as Studied by Nuclear Magnetic Relaxation	139
	Abstract	139
	Introduction	140
	Experimental	143

Results and Discussion	144
Johnson-Mehl Mechanism	144
A Refined Treatment of Impingement among Growing Domains	146
Cahn's Mechanism of Grain Boundary Nucleated Growth	148
On the Mechanism of Phase Transition in HBAB	149
References to Appendix	151

Abstract

NMR studies are carried out in a series of liquid crystalline compounds, HBAB, HBAC, and HBT, which are the p'-substituents (cyano-, chloro-, and methyl-) of p-n-hexyloxybenzylidene-aniline (HBA). Various motional aspects which are exhibited in a variety of thermodynamical phases in this series of compounds are examined with special emphasis on successive excitation of motional modes and their time-scales.

Theory of spin-lattice relaxation due to orientational fluctuation in smectic liquid crystals is developed on the basis of elastic continuum theory. The order of magnitude of proton spin-lattice relaxation and its frequency-, temperature-, and angular-dependences are deduced theoretically.

The low temperature crystalline phases of HBAB and HBT are revealed to be the ordered states. The nature of disorder in the high temperature phases of these compounds are examined by proton NMR second moments and T_1^{-1} .

The transition from crystal to smectic mesophase is characterized by melting of the alkoxy chain and excitation of self-diffusion, which result in qualitative change in NMR lineshape. NMR spectrum in the smectic B and A mesophases consists of a narrow central peak (which is well approximated by a Lorentzian) and a pair of doublets. The frequency-, temperature-, and angular-dependences of T_1^{-1} in the smectic mesophases are most satisfactorily accounted for by assuming collective excitation of orientational fluctuation.

The orientational order parameters of nematic HBAB and HBT reveal the failure of mean field theories on nematic liquid crystals based on anisotropic intermolecular dispersion forces. Comparative studies on the second rank orientational order parameter $\langle p_2 \rangle$ for the two compounds suggest the effect of terminal substituent on lowering $\langle p_2 \rangle$ and on stability enhancement of the nematic state. The spin-lattice relaxation rates in the nematic HBAB is analyzed quantitatively by the theory of T_1^{-1} due to translational self-diffusion.

The apparent activation enthalpies for diffusion in the isotropic liquid phases of the three compounds are greater than that of nematic HBAB, and the mechanism of self-diffusion in the isotropic phase is discussed.

A phenomenological theory of viscosity and self-diffusion in nematic liquid crystals is developed on the basis of Eyring's theory of significant liquid structure, and is compared with the experimental data on PAA, MBBA, and HBAB.

An appendix is given for the study of kinetics of the intercrystalline phase transition (CII/CI) of HBAB. An application of NMR technique to the study of transition kinetics is presented. The mechanism of the transition is discussed on the basis of the experimentally obtained master curve of the transition.

Chapter I Introduction.

§ I-1. Introductory Remarks

The nature of liquid crystal has been investigated extensively, and many of the macroscopic properties of them have been successfully understood phenomenologically by the elastic continuum theory of liquid crystals.¹⁾ But, compared to this, the microscopic nature on the molecular level and the dynamical nature of the liquid crystal have not been well understood up to the present. The liquid crystal which consists of a molecule with elongated shape is one of the extreme cases in which melting of the crystal takes place in a stepwise manner, the other extreme case being the plastic crystal which consists of a globular molecule.²⁾ The study of the molecular dynamics of these special kinds of mesophase will give us well-resolved informations on the successive excitation of motional modes in molecular crystals which is difficult to be observed in usual molecular crystals because the crystal " suddenly " melts into liquid without exhibiting any kind of partially disordered or i.e. partially ordered states. The studies on the motional properties of the liquid crystalline compounds are thus expected to give us an insight into the melting phenomenon in relation to the various kinds of fluctuation and to the special kinds of order. It is the purpose of this study to investigate the dynamical nature of the various phases which are exhibited by a series of compounds, by utilizing the NMR (nuclear magnetic resonance) technique. The effects of rotational, trans-

lational, and orientational fluctuations of molecules on the NMR spectra and relaxation are discussed.

The mesogen compounds which are taken in this work exhibit two different kinds of liquid crystalline states: the nematic state and the smectic state. The nematic liquid crystal is a fluid state with partial orientational order in one-dimension. The centers of gravity of molecules have no long-range order. There is some order, however, in the direction of the long molecular axis; they tend to be parallel to a common axis (the unit vector parallel to this axis is defined as the director, \vec{n}). The system is optically uniaxial with the local optical axis parallel to \vec{n} . Most of the NMR works have been done on this mesophase.³⁾

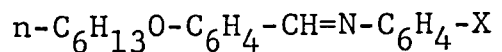
The smectic liquid crystal is a system of layered structure with well-defined interlayer spacing and with some orientational order within a layer, but it lacks three dimensional long-range order with regard to the centers of gravity of molecules. The smectic state has many variations Within this category, and the nomenclature and the classification of them are still in progress.^{4,5)} Very little is known about the dynamical nature of the smectic liquid crystal.

The sample we have chosen are the three p'-substituents of p-n-hexyloxybenzylideneaniline (HBA), the chemical formulae and the names of which are given in Table I-1 together with their acronyms. Their thermal behavior studied by Tsuji is represented in Table I-2 and Fig. I-1. The following features should be appreciated. (1) These compounds exhibit various

kinds of liquid crystalline polymorphisms depending on the terminal atom or group. Hence one can examine the motional modes in relation to various phase transitions without altering the possible degrees of freedom of molecular motion. (2) HBAC and HBT are ones of the smallest (or simplest) molecules which exhibit smectic liquid crystalline state, the dynamical nature of which has not been well understood yet. (3) Thermodynamical data of these compounds have been obtained by Tsuji,⁶⁾ which will help us to understand the motional states of each phase and the nature of the phase transitions.

After a brief review on the physical properties of the three compounds in this chapter, a theory of spin-lattice relaxation due to orientational fluctuation in smectic liquid crystal based on elastic continuum theory is developed in chapter II. Chapter III describes the experimental setup. The phase relations revealed by the differential thermal analyses (DTA) and the microscopic texture observations are given in chapter IV. The NMR results and discussion are presented in chapters V, VI, and VII. A phenomenological theory of viscosity and translational self-diffusion in nematic liquid crystal is developed in chapter VIII. The last chapter summarizes this work. An appendix is given for the kinetics study of the intercrystalline phase transition in HBAB.

Table I-1. The three compounds under study.



X	names of the compounds	acronyms
CN	p-n-hexyloxybenzylideneamino- p'-benzonitrile	HBAB
Cl	p-n-hexyloxybenzylideneamino- p'-chlorobenzene	HBAC
CH ₃	p-n-hexyloxybenzylidene- p'-toluidine	HBT

Table I-2. Transition temperatures and the entropies of transitions measured by Tsuji.⁶⁾

Compounds	T/K									
	S / J K ⁻¹ mol ⁻¹									
HBA	C	321.63	I							
		96.1								
HBAB	CII	306.98	CI	334.05	N	375.11	I			
		16.7		71.2		3.2				
HBAC	C	327.7	III	333.9	SB	362.98	SA	370.38	I	
		33.2		37.0		9.3		15.6		
HBT	CII	317.5	CI	334.26	N	346.90	I			
		15.9		74.9		4.0				

thermal behavior of
 $p-n-C_6H_{13}O-C_6H_4-CH=N-C_6H_4-X$

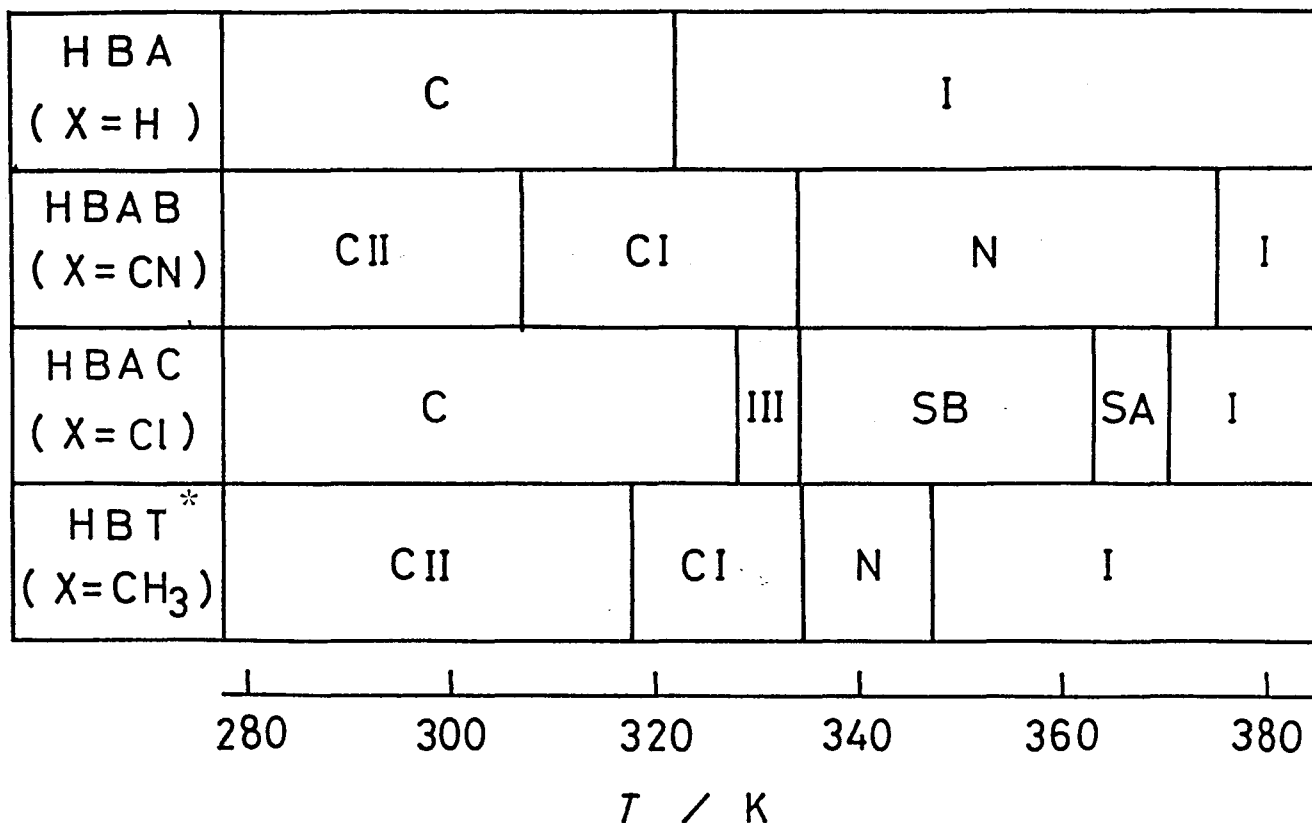


Fig. I-1. Thermal behavior of the three mesogen compounds together with the unsubstituted HBA.⁶⁾ The symbols C, CI, and CII represent the crystalline phases. N, SA, and SB represent the nematic, smectic A, and smectic B mesophases. The symbol I is for the isotropic liquid. The phase III in HBAC has not been identified.

* Although not shown in this figure, HBT is known to have two metastable phases⁷⁾ when cooled from N, which are identified as SB and CIII (see chapter IV).

§ I-2. Survey of the Studies on the Physical Properties of the Three Compounds

I-2-1. HBAB

The most noticeable feature of HBAB among the homologous series from the viewpoint of molecular structure is that it has a large dipole moment along the long molecular axis due to the large group-dipole of the cyano substituent (~ 4 D). On the other hand its thermal behavior stands out in that it has a nematic phase ^{of} a wide temperature range and that it has a high-temperature crystalline phase in stead of having smectic meso-phase.

The nematic liquid crystal HBAB is one of the typical compounds which have been extensively studied by various experimental methods. In the early 1970's, dielectric constant and relaxation⁸⁾ in the nematic phase, and the Keer effect⁹⁾ in the isotropic phase were measured with special interest in its very strong positive dielectric anisotropy. HBAB also attracted the interest of many scientists because of the G hwiller's dicoverly (1972) of hydrodynamic instability under shear flow.¹⁰⁾ Some experimental as well as theoretical efforts¹¹⁻¹⁴⁾ have been dedicated to this point, and it is now conceived phenomenologically that flow instability occurs because the Leslie viscosity coefficient α_3 changes its sign at about 365 K. But the origin of this phenomenon on the molecular level has not been clarified. G hwiller suggested that the dimerization of the molecules side by side and in an antiparallel manner due to the strong parmanent dipole may have partially occured in nematic

mesophase, hindering the uniform alignment along the shear flow. He suggested that measurements of the temperature-dependence of the orientational order parameter or low frequency dielectric relaxation will give a clue to solve this problem. Schadt⁸⁾ measured the low frequency dielectric relaxation and insisted that the static dipolar coupling between the molecules is weak in contradiction to Gähwiller's suggestion. The orientational order parameter of bulk HBAB has not been reported until now. Some other physical quantities such as density,¹⁴⁾ viscosity coefficients,^{11,14,15)} elastic constants,¹⁶⁾ magnetic anisotropy,¹⁵⁾ transition temperatures^{17,18)} were measured for nematic HBAB. Recently temperature-dependence of IR spectra¹⁹⁾ of thin film HBAB aligned on a solid surface was obtained with special interest in the molecular motion in the nematic phase.

Finally, let us pay some attention on the nature of the high temperature crystalline phase (CI) of HBAB in relation to smectic mesophase. HBAB is the only compound which does not exhibit any kind of smectic mesophase among the p'-substituents of HBA (Fig. I-1). The two compounds, HBAB and HBT, have CI in stead of having thermodynamically stable smectic mesophase. Arora and Ferguson²⁰⁾ discussed such a terminal effect on mesophase-forming tendency. Tsuji^{21,6)} further studied this problem and found the high temperature crystalline phases in HBAB and HBT. Nothing but thermodynamical data is known about the nature of this crystalline phase, CI.

I-2-2. HBAC

Liquid crystallinity of HBAC was first reported by Arora and Ferguson.²⁰⁾ They found two smectic mesophases using DTA and polarizing microscope. They assigned the high-temperature mesophase as SA because of its optical uniaxiality and its texture. The phase transition to the low-temperature mesophase was difficult to be detected optically but was evidenced by a large qualitative change in viscosity. They assumed this low-temperature mesophase to be SB. Billard et al.¹⁷⁾ carried out DSC (differential scanning calorimetry) and miscibility experiment and confirmed the characterization by Arora and Ferguson.

Tsuji et al.²²⁾ carried out a heat capacity measurement and found another phase, SIII, between SB and the crystalline phase. They supposed, from the data of transition entropies, that this new phase is a kind of smectic mesophase (SE or SH). But the name phase III in stead of SIII will be used in this thesis because this new phase has not been well identified yet.

I-2-3. HBT

Before 1977, HBT was known as a mesogen compound having only a nematic mesophase.²³⁻²⁶⁾ In 1977 Bahadur²⁷⁾ found a metastable SB phase and another crystalline phase which is different from the room-temperature phase, while decreasing the temperature. The melting behavior of HBT was soon revealed to be quite complex.⁷⁾ Bhide et al.⁷⁾ examined this problem

by utilizing DTA, DSC, X-ray, and polarizing microscope, but there remained some questions in the phase relations. Tsuji, in his heat capacity measurement,⁶⁾ found an intercrystalline phase transition at 317.5 K. The complex thermal behavior of HBT will be analyzed in chapter IV of this thesis.

Almost all the works on the physical properties of HBT were carried out by Indian scientists. The specific volume,²⁴⁾ molar compressibility,²⁵⁾ and ultrasonic velocity and absorption²⁶⁾ were measured in the nematic and the isotropic liquid phases with special interest in the N/I phase transition. The orientational order in N and SB phases were discussed by utilizing various methods: The magnetic susceptibility,⁷⁾ Mössbauer study using ⁵⁷Fe-bearing impurity,²⁸⁾ the refractive indices,²⁹⁾ and the positron annihilation studies.³⁰⁾

References to chapter I

- 1) P. G. de Gennes: " The Physics of Liquid Crystals " (Clarendon Press, Oxford, 1974).
- 2) G. W. Smith: " Advances in Liquid Crystals " vol. 1 (ed. G. H. Brown, Academic Press, 1975), p. 189.
- 3) C. W. Wade: Ann. Rev. Phys. Chem. 28 (1977) 47.
- 4) G.W. Gray: " The Molecular Physics of Liquid Crystals " (ed. G. W. Luckhurst & G. W. Gray, 1977, Academic Press), chapter 12.
- 5) A. de Vries: Mol. Cryst. Liq. Cryst. 63 (1981) 215.
- 6) K. Tsuji: Thesis, Osaka Univ. (1979).
- 7) V. G. Bhide, B. D. Malhotra, V. K. Kondawar, and P. C. Jain: Phys. Lett. 64A (1977) 111.
- 8) M. Schadt: J. Chem. Phys. 56 (1972) 1494.
- 9) M. Schadt and W. Helfrich: Mol. Cr[^]yst. Liq. Cryst. 17 (1972) 355.
- 10) Ch. G^hwiller: Phys. Rev. Lett. 28 (1972) 1554.
- 11) S. Meiboom and R. C. Hewitt: Phys. Rev. Lett. 30 (1973) 261.
- 12) P. Pieranski and E. Guyon: Phys. Rev. Lett. 32 (1974) 924.
- 13) P. E. Cladis and S. Torza: Phys. Rev. Lett. 35 (1975) 1283.
- 14) A. E. White, P. E. Cladis, and S. Torza: Mol. Cryst. Liq. Cryst. 43 (1977) 13.
- 15) Ch. G^hwiller: Mol. Cryst. Liq. Cryst. 20 (1973) 301.
- 16) P. Simova, N. Kirov, H. Ratajczak, G. Vergoten, and G. Fleury : Mol. Cryst. Liq. Cryst. 46 (1978) 137.

- 17) J. D. Billard and A. Zann: J. Phys. (Paris) 36 (1975) C1-355.
- 18) G. W. Smith: Mol. Cryst. Liq. Cryst. 41 (1977) 89.
- 19) N. Kirov, P. Simova, and H. Ratajczak: Mol. Cryst. Liq. Cryst. 58 (1980) 285.
- 20) S. L. Arora and J. L. Ferguson: Symp. Faraday Soc. 5 (1971) 97.
- 21) K. Tsuji, M. Sorai, H. Suga, and S. Seki: Mol. Cryst. Liq. Cryst. 55 (1979) 71.
- 22) K. Tsuji, M. Sorai, H. Suga, and S. Seki: Mol. Cryst. Liq. Cryst. 41 (1977) 81.
- 23) D. Coates and G. W. Gray: J. Chem. Soc. Perkin II (1976) 300.
- 24) B. Bahadur: Z. Naturforsch. 30a (1975) 1094.
- 25) B. Bahadur and S. Chandra: J. Phys. Soc. Japan 41 (1976) 237.
- 26) B. Bahadur: J. Phys. C: Sol. St. Phys. 9 (1976) 11.
- 27) B. Bahadur: J. Chem. Phys. 67 (1977) 3272.
- 28) V. G. Bhide, M. C. Kandpal, and S. Chandra: Solid State Commun. 23 (1977) 459.
- 29) R. K. Sarna, B. Bahadur, and V. G. Bhide: Mol. Cryst. Liq. Cryst. 51 (1979) 117.
- 30) V. G. Bhide, B. D. Malhotra, and P. C. Jain: Phys. Lett. 71A (1979) 99.

Chapter II Theory of Nuclear Spin-Lattice Relaxation
due to Orientational Fluctuation in Smectic Liquid Crystals

§ II-1. Description of Order

It is well known that in nematic liquid crystals the director $\vec{n}(\vec{r})$ is defined as a unit vector parallel to the average direction of the molecules within a certain volume (i.e., \vec{n} is parallel to the local optical axis). This idea is still valid in smectic systems, and so the orientational order parameters are defined by the averaged Legendre polynomials $\langle P_n(\cos \theta) \rangle$ where θ is the angle between $\vec{n}(\vec{r})$ and the instantaneous axis of a molecule. In the present thesis, practically only the second rank order parameter

$$\langle P_2(\cos \theta) \rangle = \frac{1}{2} \langle 3 \cos^2 \theta - 1 \rangle \quad (\text{II-1})$$

is taken into account. Additional order parameter which describes biaxiality of the system will be needed for smectics such as SC or SH (tilted smectics). But in the present study only optically uniaxial smectics, SA and SB are treated, so the biaxial order parameter is not necessary.

Stacked lamellae structure which is the most essential feature of the smectics can be described as a one dimensional density wave. de Gennes¹⁾ and McMillan²⁾ developed a Landau theory of N/SA transition, in which they used a complex order parameter

$$\psi(\vec{r}) = \psi_0 \exp[iq_0 u(\vec{r})], \quad (\text{II-2})$$

and described the one-dimensional density wave,

$$\begin{aligned} \rho(\vec{r}) &= \rho_0 \left[1 + \text{Re} \left\{ \psi(\vec{r}) \exp(iq_0 z) \right\} \right] \\ &= \rho_0 \left[1 + \psi_0 \text{Re} \left\{ \exp(iq_0 [u(\vec{r}) + z]) \right\} \right] \end{aligned} \quad (\text{II-3})$$

Here ψ_0 is the scalar order parameter which describes the amplitude of the 1-D density fluctuation, $u(\vec{r})$ is the displacement of the layer in z -direction from its unperturbed position (plane layer), ρ_0 is the average density, $q_0 = 2\pi/a$, a is the layer thickness which is essentially constant in smectic systems. The z -axis is defined as the direction parallel to

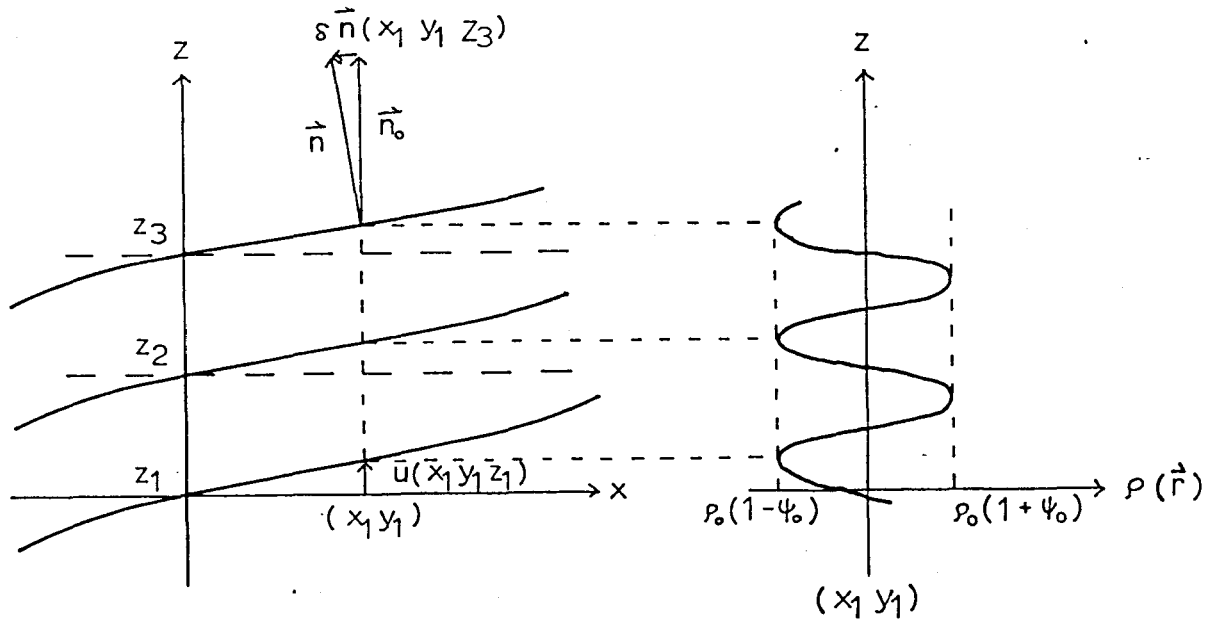


Fig. II-1. Description of the smectic system.

$\vec{n}(\vec{r})$ in the unperturbed system (Fig. II-1). Fluctuating part of the director

$$\delta \vec{n}(\vec{r}, t) = \vec{n}(\vec{r}, t) - \vec{n}_0 \quad (\text{II-4})$$

is connected with $u(\vec{r})$ by the relations

$$\begin{aligned} n_x &= - \frac{\partial u}{\partial x} , \\ n_y &= - \frac{\partial u}{\partial y} . \end{aligned} \quad (\text{II-5})$$

When one-dimensional stacking order is nearly complete (i.e. $\psi_0 \simeq 1$), the condition $|\partial u / \partial z| \ll |\partial u / \partial x|$, $|\partial u / \partial y|$ is satisfied. It is such a case that is discussed in the sections 2 to 4 in this chapter. In this picture orientational fluctuation is restricted effectively in two-dimension. Whereas in section II-5, the case of imperfect stacking order is treated where three-dimensional fluctuation of the director is discussed.

§ II-2 Elastic Continuum Theory of the Smectic System — a simplified review of the theory^{3,4)} —

In orthogonal smectic systems, the director $\vec{n}(\vec{r})$ is perpendicular to the smectic layer in every place of the system. Going from point P to Q along the path C in Fig. II-2, we obtain the equation,

$$\int_C \frac{\vec{n}(\vec{r})}{a(\vec{r})} d\vec{r} = \nu_C, \quad (\text{II-6})$$

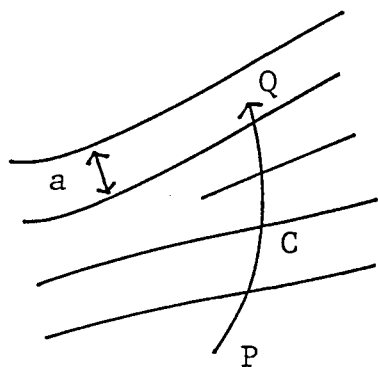
which gives the number of the layers crossed by the path C. Here, $a(\vec{r})$ is the interlayer spacing. If $a(\vec{r})$ does not depend on \vec{r} , and also if the system does not contain edge dislocations (stacking defect of the layers), the closed integral of $\vec{n}(\vec{r})/a(\vec{r})$ should vanish, i.e.,

$$\frac{1}{a} \oint \vec{n}(\vec{r}) d\vec{r} = 0, \quad (\text{II-7})$$

regardless of the path taken. This condition is equivalent to

$$\text{rot } \vec{n}(\vec{r}) = \vec{0}. \quad (\text{II-8})$$

In the elastic free energy expression of nematic liquid crystals developed by Oseen, Zöcher, and Frank,⁵⁾



$$F_d = \frac{1}{2} K_1 (\text{div } \vec{n})^2 + \frac{1}{2} K_2 (\vec{n} \cdot \text{rot } \vec{n})^2 + \frac{1}{2} K_3 (\vec{n} \times \text{rot } \vec{n})^2,$$

(II-9)

Fig. II-2. Smectic system including an edge dislocation.

the second (twist deformation) and the third (bend deformation) terms drop off leaving only the splay deformation term. This kind of elastic deformation is called " undulation " of the layers.

The basic idea of the expression of elastic free energy of the smectic system was first given by de Gennes³⁾ in the form,

$$\begin{aligned}
 F - F_0 = & \frac{1}{2} B \left(\frac{\partial u}{\partial z} \right)^2 + \frac{1}{2} K_1 \left(\frac{\partial^2 u}{\partial x^2} + \frac{\partial^2 u}{\partial y^2} \right)^2 \\
 & + \frac{1}{2} \chi_a H^2 \left[\left(\frac{\partial u}{\partial x} \right)^2 + \left(\frac{\partial u}{\partial y} \right)^2 \right] \\
 & + \frac{1}{2} K' \left(\frac{\partial^2 u}{\partial z^2} \right)^2 \\
 & + \frac{1}{2} K'' \frac{\partial^2 u}{\partial z^2} \left(\frac{\partial^2 u}{\partial x^2} + \frac{\partial^2 u}{\partial y^2} \right). \quad (\text{II-10})
 \end{aligned}$$

Here, the first two terms represent layer compression and splay deformation terms, respectively, and the coefficients B and K_1 are the corresponding elastic constants. The third term is the magnetic interaction with the external field due to the anisotropy of the diamagnetic susceptibility of the system. The last two terms can, in practice, be neglected compared with the first term because the interlayer spacing is essentially kept constant, i.e., $\partial u / \partial z \ll 1$. The Fourier transform,

$$u(\vec{r}) = V^{-1/2} \sum_{\vec{q}} u_{\vec{q}} \exp(-i\vec{q} \cdot \vec{r}) \quad (\text{II-11})$$

gives

$$\begin{aligned}
 F - F_0 &= \frac{1}{2} B V^{-1} \sum_{\vec{q}} q_z^2 |u_{\vec{q}}|^2 \\
 &+ \frac{1}{2} K_1 V^{-1} \sum_{\vec{q}} (q_x^2 + q_y^2) |u_{\vec{q}}|^2 \\
 &+ \frac{1}{2} \chi_a H^2 V^{-1} \sum_{\vec{q}} (q_x^2 + q_y^2) |u_{\vec{q}}|^2 .
 \end{aligned}
 \tag{II-12}$$

Transformation of the coordinates within x-y plane gives

$$\begin{aligned}
 F - F_0 &= V^{-1} \sum_{\vec{q}} \left[\frac{1}{2} B q_{\parallel}^2 + \frac{1}{2} K_1 (\xi^{-2} + q_{\perp}^2) \right. \\
 &\quad \left. q_{\perp}^2 \right] \cdot |u_{\vec{q}}|^2 ,
 \end{aligned}
 \tag{II-13}$$

where $q_{\perp}^2 = q_x^2 + q_y^2$, $q_{\parallel}^2 = q_z^2$, and ξ is called the magnetic coherence length defined by

$$\xi = \frac{1}{H} \left(\frac{K_1}{\chi_a} \right)^{1/2} .
 \tag{II-14}$$

Applying here the equipartition law of the energy in classical mechanics, we obtain the mean square amplitude of $u_{\vec{q}}$,

$$\langle |u_{\vec{q}}|^2 \rangle = \frac{k T}{B q_{\parallel}^2 + K_1 (\xi^{-2} + q_{\perp}^2) q_{\perp}^2} .
 \tag{II-15}$$

The mean square amplitude of the layer displacement in the real space can be calculated by integrating eq. (II-15) with respect to \vec{q} within $2\pi/L \leq |\vec{q}| \leq 2\pi/a$. The result for $H = 0$ is

$$\langle u^2(\vec{r}) \rangle = \frac{k T}{4 \pi \sqrt{B K_1}} \ln \left(\frac{L}{a} \right), \quad (\text{II-16})$$

which exhibits logarithmic divergence as L/a becomes large (here L is the macroscopic dimension of the sample). It was first discussed by Landau and Lifshitz⁶⁾ that a one-dimensional long-range stacking order and a two-dimensional complete disorder cannot be intervened (the problem of Peierls-Landau system). If the description we have taken are valid, the smectic (especially SA which is believed to be constructed by liquid-like layers) system can exhibit long-range order only under some restrictions: defects in 1-D periodicity (finite range of L) or large external field. We will not discuss more about this problem but only present a tentative calculation based on eq. (II-16). Typical values of B , K_1 , T , and a are taken to be 10^{10} J m^{-3} , $10^{-11} \text{ J m}^{-1}$, 300 K , and $2.0 \times 10^{-9} \text{ m}$, respectively. Then in order to make $\{ \langle u^2(\vec{r}) \rangle \}^{1/2}$ within $1 \times 10^{-10} \text{ m}$, L should be smaller than $4 \times 10^{-5} \text{ m}$ ($40 \mu\text{m}$). If the smectic A liquid crystal could be regarded as a genuine Peierls-Landau system, the spatial extent of one-dimensional periodicity would be restricted to within $\sim 100 \mu\text{m}$ under zero magnetic field. This value may give the order-of-magnitude estimate of the possible size of the monodomain smectic system.

§ II-3. Dynamics of Undulation

Dynamics of $u_{\vec{q}}$ were also discussed by de Gennes.³⁾ The character of the modes depends on the direction of propagation. If $q_{\parallel} \neq 0$ and $q_{\parallel} \simeq q_{\perp}$, two propagating modes and an overdamped shear mode (hydrodynamic mode) are found. If $q_{\parallel} = 0$, a longitudinal propagating mode, an overdamped shear mode, and a very slowly damped mode (pure undulation of the layers) are found. It is this last mode

$$\omega = i \tau_q^{-1} = i \frac{K_1}{\eta} q_{\perp}^2 \quad (\text{II-17})$$

which is characteristic of the smectic system and is expected to give significant effect on NMR relaxation. The symbol η denotes the effective viscosity of undulation. de Gennes discussed the dynamics of pure undulation ($q_{\parallel} = 0$), that is, the mode purely restricted within the layer, and conserving the interlayer spacing. It is, however, difficult to realize pure undulation in a real smectic system.

In 1974, Ribotta, Salin, and Durand⁷⁾ tried to detect " impure " undulation mode by quasielastic light scattering by utilizing a carefully prepared monodomain smectic A system of CBOOA (N-p-cyanobenzylidene-p'-n-octyloxylaniline). The size of the domain, L, was 200 ~ 800 μm . By developing de Gennes' theory to apply to the impure case, they used the relations,

$$\langle |\delta \vec{n}_{\vec{q}}|^2 \rangle = \frac{k T q_{\perp}^2}{B q_{\parallel}^2 + K_1 q_{\perp}^4} \quad (\text{II-18})$$

$$\tau_q^{-1} = \frac{B (q_{\parallel}^2 + \lambda^2 q_{\perp}^4)}{\gamma q_{\perp}^2}, \quad (\text{II-19})$$

with a boundary condition, $q_{\parallel} = m\pi/L$ (m is an integer). Scattered rays from the small numbers of m were observed and eqs. (II-18 & 19) were confirmed examining the q_{\perp} - and L - dependences of the intensities and the linewidths.

In the case of polydomain samples without special treatment, thermally excited impure undulations with various q_{\parallel} are expected to take place. In the next section, predictions are given for nuclear spin-lattice relaxation rate caused by undulation mode for three different cases: (1) de Gennes' pure undulation, (2) case of monodomain smectic systems under a boundary condition for q_{\parallel} , (3) case of polydomain smectics.

§ II-4. Nuclear Spin-Lattice Relaxation Rate due to Undulation Mode

Nuclear spin-lattice relaxation rate (T_1^{-1}) caused by fluctuating dipole interaction between a pair of spins is given by⁸⁾

$$T_1^{-1} = \frac{3}{2} \gamma^4 \hbar^2 I(I+1) \sum_{p=1,2} J'(p\omega_0). \quad (\text{II-20})$$

Here, $J'(p\omega_0)$ is the Fourier transform of the time correlation function of the fluctuating part of the dipole interaction

tensor, γ , I , \hbar are the gyromagnetic ratio of the spin, the spin quantum number, and the Planck constant divided by 2π , respectively. We now consider, as a spin pair under question, a pair of proton spins the interspin vector of which lie parallel to the molecular long axis, and the distance r of which is kept constant. Then the coordinate transfer technique gives⁹⁾

$$T_1^{-1} = \frac{3}{2} \gamma^4 \hbar^2 I(I+1) r^{-6} \langle P_2(\cos \theta) \rangle^2 \times \sum_{p=1,2} f_p(\theta_0) J(p \omega_0) \quad (\text{II-21})$$

$$f_1(\theta_0) = \frac{1}{2} (1 - 3 \cos^2 \theta_0 + 4 \cos^4 \theta_0), \quad (\text{II-22})$$

$$f_2(\theta_0) = 2 (1 - \cos^4 \theta_0), \quad (\text{II-23})$$

$$J(p \omega_0) = \int_{-a}^{+a} \langle \delta \vec{n}^*(\vec{r}, 0) \delta \vec{n}(\vec{r}, t) \rangle \times \exp(-ip \omega_0 t) dt. \quad (\text{II-24})$$

Here, θ is the angle between $\vec{n}(\vec{r})$ and an instantaneous molecular long axis, and θ_0 is the angle between \vec{n}_0 and the direction of the external magnetic field. Assuming an exponential time correlation function for $\delta \vec{n}(\vec{r}, t)$, T_1^{-1} can be expressed by a superposition of the modes with \vec{q} -dependent damping rates, i.e.,

$$J(p \omega_0) = \int_{-\infty}^{+\infty} V^{-1} \sum_{\vec{q}} \langle |\delta n_{\vec{q}}|^2 \rangle \exp(-t/\tau_{\vec{q}}) \times \exp(-ip \omega_0 t) dt. \quad (\text{II-25})$$

(1) case of pure undulation

In the case of pure undulation, q_{\parallel} is taken to be zero, and q_{\perp} -s are integrated up to the higher cutoff wavenumber, $q_H = 2\pi/a$ (a is taken to be the molecular length), eq.(II-24) is calculated to yield

$$J(p \omega_0) = \frac{k T}{2 \pi L K_1} \cdot \frac{1}{p \omega_0} \arctan\left(\frac{\omega_H}{p \omega_0}\right), \quad (\text{II-26})$$

where $\omega_H = K_1 q_H^2 / \eta$. Here L is the length of the ideal smectic system in the z -direction. The asymptotic behaviors under high and low frequency limits are given by

$$J(p \omega_0) \simeq \frac{k T \omega_H}{2 \pi L K_1} \cdot \frac{1}{(p \omega_0)^2}, \quad (\text{II-27})$$

when $p \omega_0 \gg \omega_H$,

$$J(p \omega_0) \simeq \frac{k T}{4 L K_1} \cdot \frac{1}{(p \omega_0)}, \quad (\text{II-28})$$

when $p \omega_0 \ll \omega_H$.

From the experimental point of view, however, this kind of pure undulation is lacking of reality. The smectic system is

subject to some boundary conditions which permits long wavelength distortions parallel to the z-direction.

(2) case of monodomain smectic system under a boundary condition on $q_{||}$.

When monodomain smectic liquid crystal is carefully prepared and put between glass plates distant by L in homeotropic arrangement, a boundary condition, $q_{||} = m\pi/L$, is imposed on the small displacement, u , along the z-axis. The spectral density function of the undulation mode is then given by

$$J(p\omega_0) = \frac{\eta k T}{4 m K_1^2 q_{||}} \times \frac{1}{\sqrt{\frac{4 B}{K_1 q_{||}^2} + \left(\frac{\eta}{K_1 q_{||}^2} p\omega_0\right)^2}} \quad (\text{II-29})$$

In deriving eq. (II-29), the cutoff effect is neglected for simplicity. The spectral density is a function of $p\omega_0/q_{||}$ (or of $L p\omega_0$), and the asymptotic behaviors are given by

$$J(p\omega_0) = \frac{k T}{8 m \pi K_1 \sqrt{K_1 B}} \quad (\text{II-30})$$

$$\text{when } p\omega_0 \ll \frac{2\sqrt{B K_1}}{\eta} q_{||} ,$$

$$\text{and } J(p\omega_0) = \frac{k T}{4 L K_1} \cdot \frac{1}{p\omega_0} \quad (\text{II-31})$$

$$\text{when } p\omega_0 \gg \frac{2\sqrt{B K_1}}{\eta} q_{||} .$$

Note that eq. (II-31) coincides ^(with) eq. (II-28).

The T_1^{-1} can be calculated by utilizing eq. (II-29) and eqs. (II-21~24) and the parameters listed in Table II-1.

Table II-1. Parameters for numerical calculations

$T = 350 \text{ K}$
$B = 10^{10} \text{ J m}^{-3}$
$K_1 = 10^{-11} \text{ J m}^{-1}$
$\eta = 1.0 \text{ Pa s}$
$\langle p_2 (\cos \theta) \rangle = 1.0$
$r = 2.45 \times 10^{-10} \text{ m}$

The results are represented in

Fig. II-3 & 4, and are summarized as follows.

(i) the frequency-dependence

If the ω_0 -dependence of T_1^{-1} is represented by $T_1^{-1} \propto \omega_0^\gamma$, the exponent γ varies from 0 (in the lower frequency limit) to -1 (in the higher frequency limit) as a function of $\omega_0 / (2 \sqrt{B K_1} q_0 / \eta)$.

(ii) the angular- (θ_0 -) dependence

The angular factor of T_1^{-1} is expressed by

$$T_1^{-1} \propto f(\theta_0) = f_1(\theta_0) + 2^\gamma f_2(\theta_0), \quad (\text{II-32})$$

and shown in Fig. II-4. It has a γ -dependence.

(iii) the temperature- (T-) dependence

The T-dependent factor of T_1^{-1} is $\langle p_2 \rangle^2 \eta k T / K_1 \sqrt{K_1 B}$. So the T-dependence of T_1^{-1} is expected to be small in the temperature region sufficiently far from the transition area. A strong T-dependence of T_1^{-1} would

appear when viscosity and elastic constants would exhibit a marked change associated with critical phenomena near the transition point.

(iv) The absolute value of T_1^{-1}

The value of T_1^{-1} in the low-frequency limit depends on $\langle P_2^2 \rangle \eta / K_1 \sqrt{K_1 B}$. By the present numerical calculation, it was calculated to be 0.36 s^{-1} in the orientation, $\theta_0 = \pi/2$. This value is of sufficient order of magnitude to be detected experimentally under some suitable conditions.

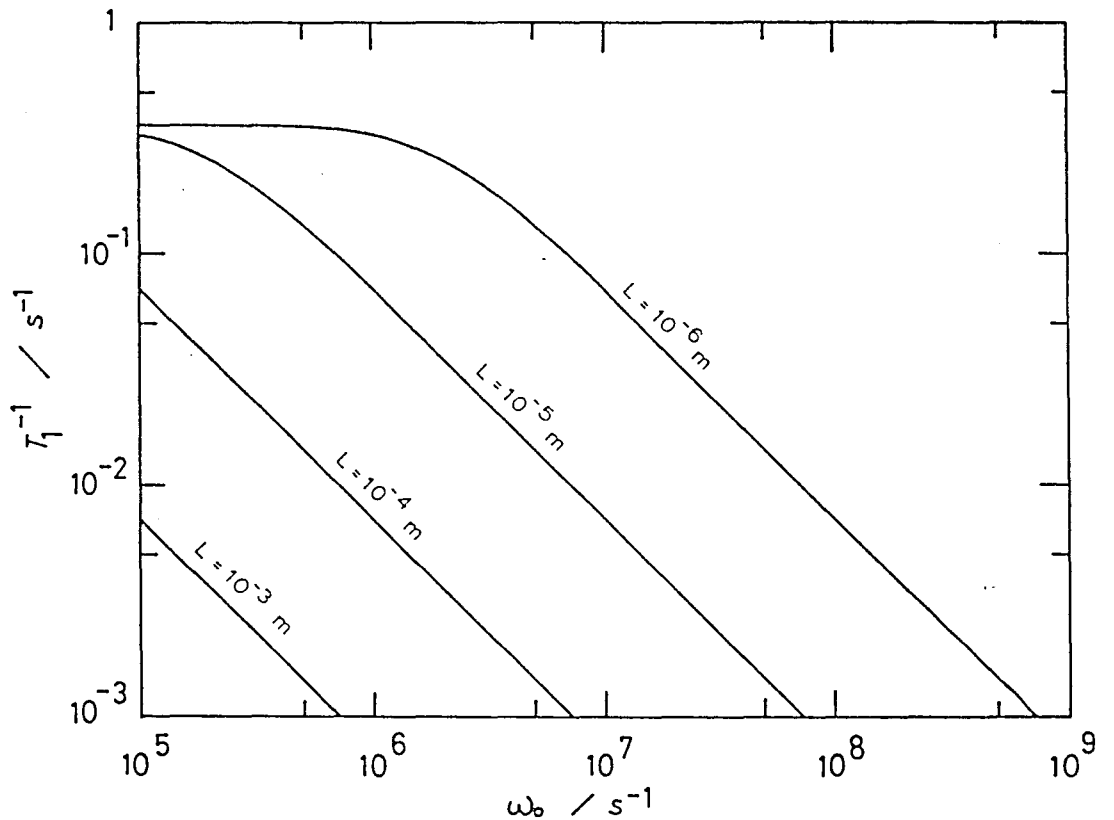


Fig. II-3. Spin-lattice relaxation rate due to undulation mode: case of mono-domain smectics. Theoretical curves are calculated by eqs. (II-21~24 & 29) and the parameters listed in Table II-1. The angle θ_0 was fixed to be $\pi/2$, and the " quantum number " m was fixed to unity for simplicity.

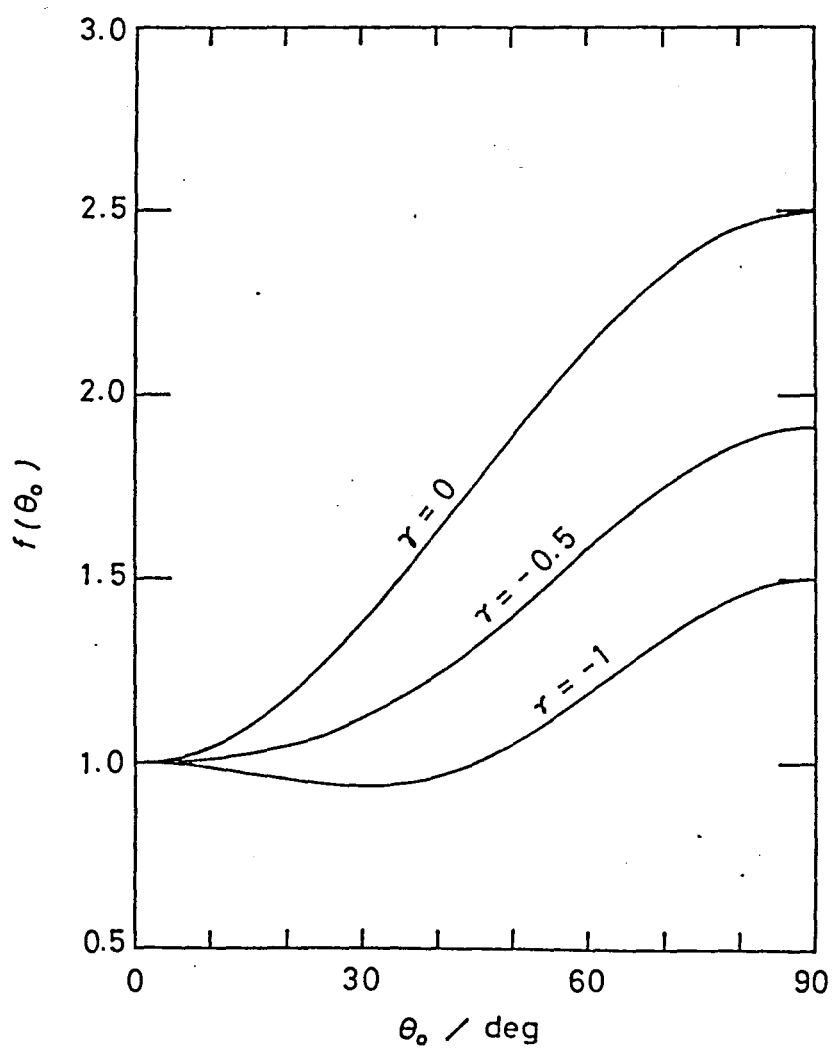


Fig. II-4. Orientation dependence of the angular factor $f(\theta_0)$. Theoretical curves are given for three different values of γ .

(3) case of polydomain smectic system

When the sample consists of domains with different dimensions, which is usually the case, a kind of distribution of L must be introduced. We assumed, for simplicity, a uniform distribution of L between L' and L_0 (the smaller and the larger cutoff of the domain size, respectively), and zero distribution for $L < L'$ and $L > L_0$. Then we obtain

$$J(p \omega_0) = \frac{k T}{4 K_1 (L_0 - L') p \omega_0} \times \ln \left| \frac{\frac{\eta p \omega_0}{K_1 \pi^2} L_0 + \sqrt{\left(\frac{\eta p \omega_0}{K_1 \pi}\right)^2 L_0^2 + \frac{4 B}{K_1 \pi^2}}}{\frac{\eta p \omega_0}{K_1 \pi^2} L' + \sqrt{\left(\frac{\eta p \omega_0}{K_1 \pi}\right)^2 L'^2 + \frac{4 B}{K_1 \pi^2}}} \right|.$$

(II-33)

In eq. (II-33), m was fixed to unity for simplicity. The temperature- and the angular-dependences of T_1^{-1} are identical with that in the case (2), whereas the crossover region ($-1 < \nu < 0$) in the ω_0 -dependence is widened if $L_0 - L'$ is taken large. A result of numerical calculation is presented in Fig. II-5.

In conclusion, it has been demonstrated that the spin-lattice relaxation due to undulation mode in smectic liquid crystal can be detected experimentally by its characteristic dependences on frequency, temperature, and orientational angle,

by a suitable choice and preparation of the sample. Results of numerical calculations were shown for monodomain and polydomain smectic systems.

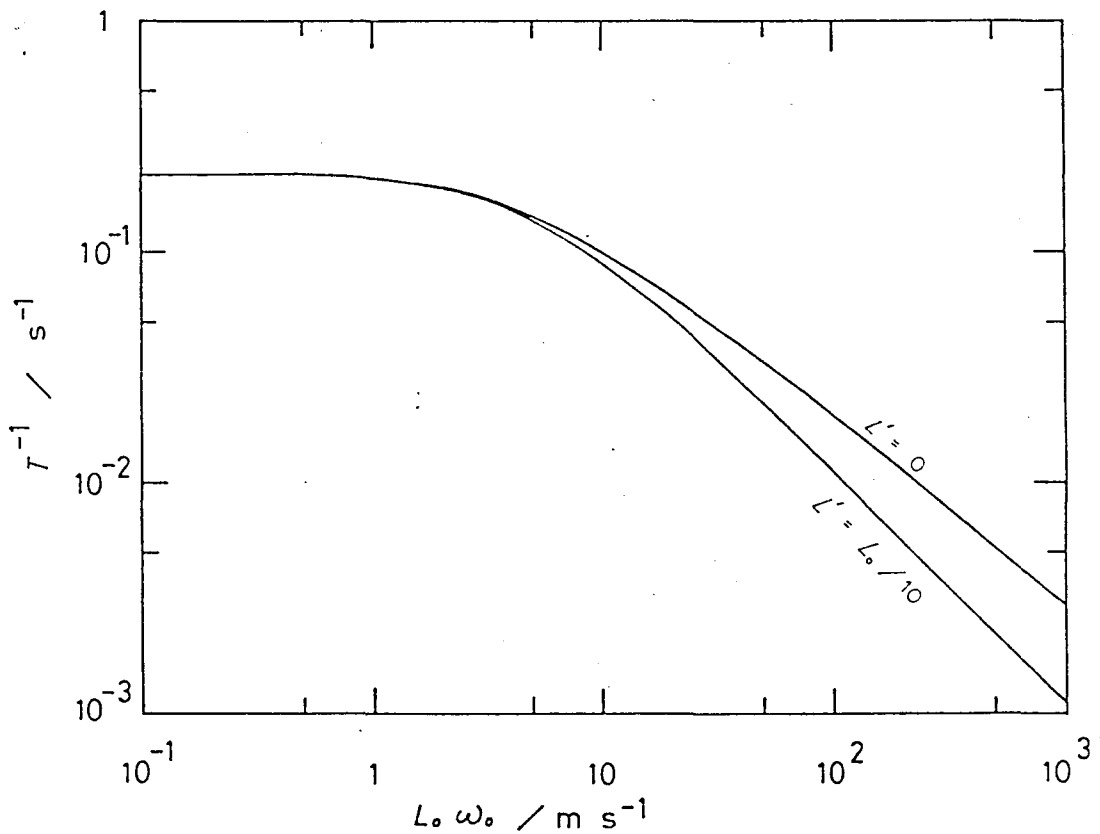


Fig. II-5. Spin-lattice relaxation rate due to undulation mode: case of polydomain smectics. Theoretical curves are calculated by eqs. (II-21~24 & 33). The angle θ_0 was assumed to be random in space to fit to the powder pattern. The curves corresponding to the cases $L' = 0$, and $L' = L_0/10$ were drawn. When L' is taken to be $L' \lesssim L_0/100$, the results revealed no significant differences from that for $L' = 0$.

§ II-5. Nuclear Spin-Lattice Relaxation due to Three-dimensional Director Fluctuation in Smectic A System

In the previous section, thermal fluctuation of the director was restricted to within two-dimensions. This has essentially come from the definition of the system given in section II-2, i.e., an ideal layer structure. On the other hand in 1973, Brochard¹⁰⁾ treated the dynamics of fluctuation near the SA/N transition, in which director fluctuation was treated in three-dimensions even below the transition point, by utilizing the complex order parameter as was defined by eq. (II-2).

The director fluctuation in SA phase has two normal modes and are given by

$$\langle |\delta n_{1q}|^2 \rangle = \frac{k T}{K_1 q_{\perp}^2 + \tilde{K}_3 q_{\parallel}^2 + \frac{\psi_0^2 q_s^2 q_{\parallel}^2}{M (q_{\perp}^2 + q_{\parallel}^2)}},$$

$$\tau_{1q}^{-1} = \frac{1}{\tilde{\eta}} \left(\tilde{K}_3 q_{\parallel}^2 + K_1 q_{\perp}^2 + \frac{\psi_0^2 q_s^2 q_{\parallel}^2}{M (q_{\parallel}^2 + q_{\perp}^2)} \right),$$

(II-34)

and

$$\langle |\delta n_{2q}|^2 \rangle = \frac{k T}{\frac{\psi_0^2 q_s^2}{M} + \tilde{K}_2 q_{\perp}^2 + \tilde{K}_3 q_{\parallel}^2},$$

$$\tau_{2q}^{-1} = \frac{1}{\tilde{\eta}} \left(\tilde{K}_3 q_{\parallel}^2 + \tilde{K}_2 q_{\perp}^2 + \frac{\psi_0^2 q_s^2}{M} \right). \quad (\text{II-35})$$

In eqs. (II-34 & 35), $\tilde{\eta}$, \tilde{K}_2 , and \tilde{K}_3 are the renormalized coefficients of the corresponding quantities, and $q_s = 2\pi/a$. Brochard predicted that the spin-lattice relaxation rate would be independent of frequency in the low-frequency limit and that $T_1^{-1} \propto \omega_0^{-0.5}$ would hold in the high-frequency limit. By our calculation, the analytical expression of the spectral density of the director fluctuation for the mode 2 is given by

$$J(p \omega_0) = \frac{k T}{2 \sqrt{2} \tilde{K}_2 \sqrt{\tilde{K}_3}} \cdot \frac{\tilde{\eta} \sqrt{M}}{\psi_0 q_s} g(x),$$

$$g(x) = \frac{1}{x} \sqrt{\sqrt{1+x^2} - 1},$$

$$x = \frac{\tilde{\eta} \psi_0^2 q_s^2}{M} p \omega_0. \quad (\text{II-36})$$

The mode 1 gives a more complicated spectre* The function $g(x)$ is drawn in Fig. II-6, in which

$$g(x) \rightarrow \frac{1}{x} = \left(\frac{M}{\tilde{\eta} \psi_0^2 q_s^2} \right)^{1/2} \cdot \frac{1}{\sqrt{p \omega_0}}$$

* Blinc et al. first gave an approximate expression of T_1^{-1} in ref. 11, which is different from ours (eq. (II-36)), but the essential feature of which is the same.

in the high frequency limit, and $g(x) \rightarrow 1/\sqrt{x}$ (independent of frequency) in the low frequency limit. A significant difference of the behavior of T_1^{-1} from that of two-dimensional undulation mode lies in its frequency-dependence.

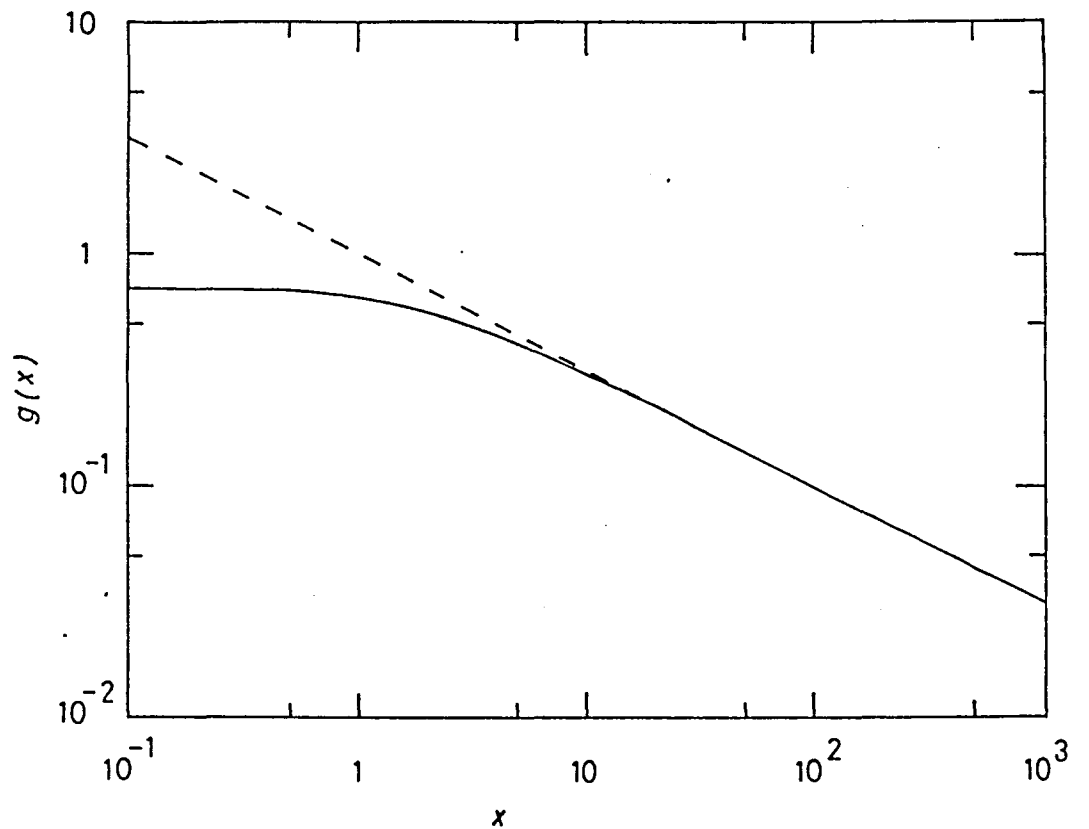


Fig. II-6. Spectral density function of the mode 2 of three-dimensional director fluctuation in smectic A system. The theoretical curve is based on eq. (II-36).

References to chapter II

- 1) P. G. de Gennes: Solid State Commun. 10 (1972) 753.
- 2) W. McMillan: Phys. Rev. A4 (1971) 1238.
- 3) P. G. de Gennes: J. Phys. (Paris) 30 (1969) C4-65.
- 4) P. G. de Gennes: " The Physics of Liquid Crystals " (Clarendon Press, Oxford, 1974), chapter 7.
- 5) C. W. Oseen: Trans. Faraday Soc. 29 (1933) 883.
F. C. Frank: Disc. Faraday Soc. 25 (1958) 1.
- 6) L. D. Landau and E. M. Lifshitz: " Statistical Physics ", 2nd edition (Pergamon Press, 1969), chapter 13.
- 7) R. Ribotta, D. Salin, and G. Durand: Phys. Rev. Lett. 32 (1974) 6.
- 8) A. Abragam: " The Principles of Nuclear Magnetism " (Clarendon Press, Oxford, 1961), chapter VIII.
- 9) P. Ukleja, J. Pirs, and J. W. Doane: Phys. Rev. A14 (1976) 414.
- 10) F. Brochard: J. Phys. (Paris) 34 (1973) 411.
- 11) R. Blinc, M. Luzar, M. Vilfan, and M. Burgar: J. Chem. Phys. 63 (1975) 3445.,
R. Blinc, M. Luzar, M. Mali, R. Osredkar, J. Seliger, and M. Vilfan: J. Phys. (Paris) 37 (1976) C3-73.

Chapter III. Experimental

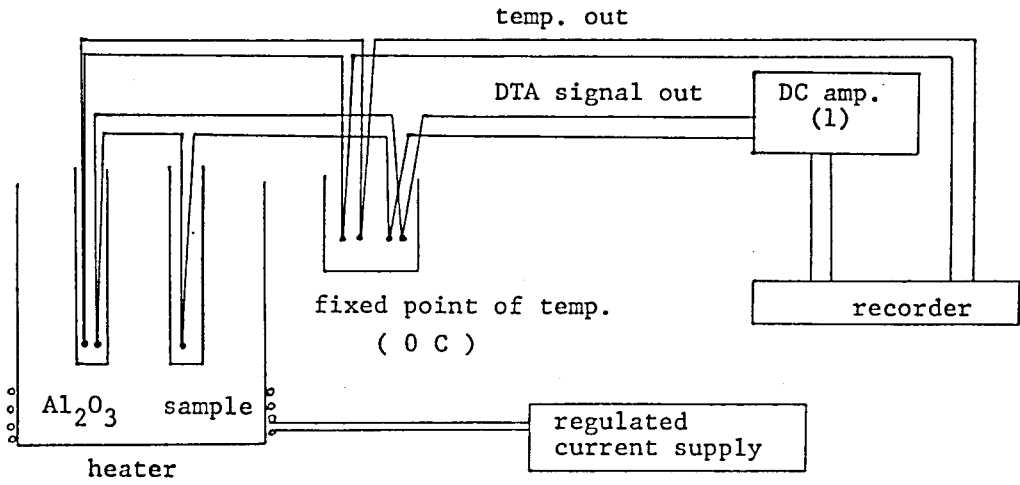
§ III-1. Samples

The samples HBAB, HBAC, and HBT were provided by Dr. K. Tsuji of Kwansai Gakuin University. Purities of the samples¹⁾ which had been determined by heat capacity measurements near their melting points are 99.90 % for HBAB, and 99.84 % for HBT. Purity of HBAC is not known. We further purified them by the molecular distillation method prior to the experiments. The samples for DTA and NMR experiments were sealed in a glass ampule under 2 ~ 4 kPa of helium exchange gas after evacuation for eight to ten hours with three freeze-and-thaw cycles.

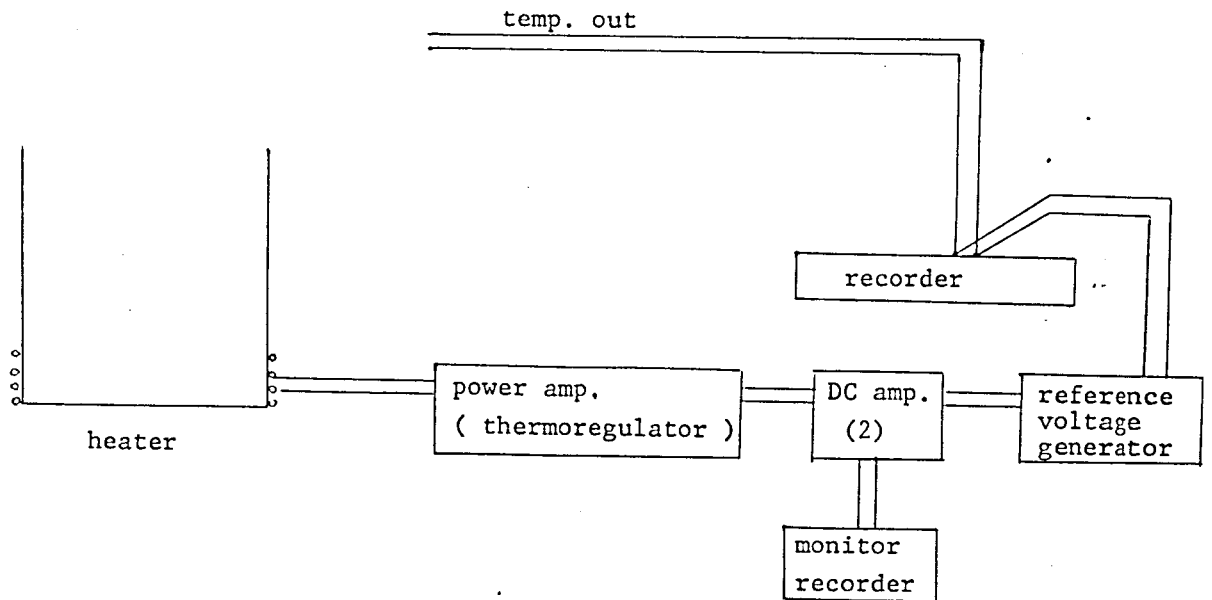
HBAC and HBT thus purified and evacuated were quite stable during our measurements, but in the case of HBAB, special precautions were necessary. No decomposition was observed during the experiments in the crystalline and the nematic phases of HBAB, but when put in the isotropic phase for more than five hours, decomposition took place to a small extent which was evidenced by a narrow central component in the proton NMR spectrum in the crystal. So we could not use the sample HBAB as donated for the experiment in the isotropic phase, without re-purification.

§ III-2 Differential Thermal Analysis (DTA)

DTA experiment was done by a conventional method accompanied by annealing of the sample when required. The block diagram of the system is shown in Fig. III-1.



(a) DTA system under measurement.



(b) DTA system under annealing experiment.

Fig. III-1. Block diagram of DTA system.

§ III-3. Texture Observations

Textures were observed by utilizing a polarizing microscope (OLYMPUS BHA-P) equipped with a camera (OLYMPUS PM-6) and an exposure meter (OLYMPUS EMM-7). Light source was a 30 watts wolfram lamp (LS 30), and the films used were daylight type color reversals (Kodak Ektachrome Daylight 64). Observations were made in a^w orthoscope mode, with crossed polarizers, and 100 or 400 magnifications, without using a sensitive-color plate (of 530 nm) except in some special cases.

Sample was put between glass plates and heated into its isotropic phase prior to each observation in order to obtain a flat and thin specimen widespread between the glass plates. Temperatures were monitored by a chromel-P-constantan thermocouple settled immediately under the sample. The schematic view of the total system is given in Fig. III-2.

§ III-4. NMR Lineshape Observations²⁾

Proton NMR lineshapes were observed by a continuous wave method by utilizing a Robinson-type spectrometer³⁾ working at 19.8 MHz. The external field was swept and calibrated by a signal of Cu^{2+} -doped H_2O at room temperature. Field modulation was applied by an audio frequency sine-wave generator of 147 Hz, and the signal was extracted via lock-in amplifier (Model LL-572B, NF Circuit Design Block Co. Ltd.) in an absorption derivative form. The block diagram of the cw-NMR system is shown in Fig. III-3.

Temperatures were controled by use of a proportionally

regulated heater system, and was measured by a calibrated chromel-P-constantan thermocouple.* Temperature was maintained within 0.1 K, and the NMR measurement was made after thermal equilibrium had been attained at each temperature. The description above concerning controlling and measurement of temperature holds as well for the spin-lattice relaxation measurements.

§ III-5. NMR spin-lattice relaxation measurements²⁾

Proton spin-lattice relaxation rates were measured by a pulse method. They were measured at three different Larmor frequencies ($\omega_0/2\pi$), 10.0, 20.5, and 40.5 MHz. In the crystalline states, only the experiments at 10.0 MHz were done. The block diagram of the spectrometers is given in Fig. III-4. Details of the 10.0 MHz spectrometer was reported elsewhere.⁴⁾ We used a new frequency-variable spectrometer for the experiments at 20.5 and 40.5 MHz, details of which will be reported elsewhere.⁵⁾

Measurements in the liquid crystalline phase were made for the sample cooled from the isotropic liquid phase.

The $\pi/2 - \tau - \pi/2$ (total duration about 100 μ s) pulse sequence was utilized in the crystalline phases, whereas $\pi/2 - \tau - \pi/2$ sequence was applied in the liquid crystalline

* This thermocouple was provided by the Chemical Thermodynamics Laboratory, Osaka University.

and the isotropic liquid phases. Free induction signals were observed by utilizing waveform recorders (Biomation Model 805 and Iwatsu Model DM 701). The magnetization recoveries were exponential in the crystalline and liquid crystalline phases, so well-defined T_1^{-1} were obtained from the experiments. In the isotropic liquid phase, however, the recovery was nonexponential and T_1^{-1} was defined by the inverse time to attain $1 - 1/e = 0.63$ recovery which reflects the fast (and which is the major) component of the recovery function. The typical experimental uncertainties of T_1^{-1} were 10 % for the crystalline phases, and 7 ~ 8 % for the liquid crystalline and the isotropic liquid phases.

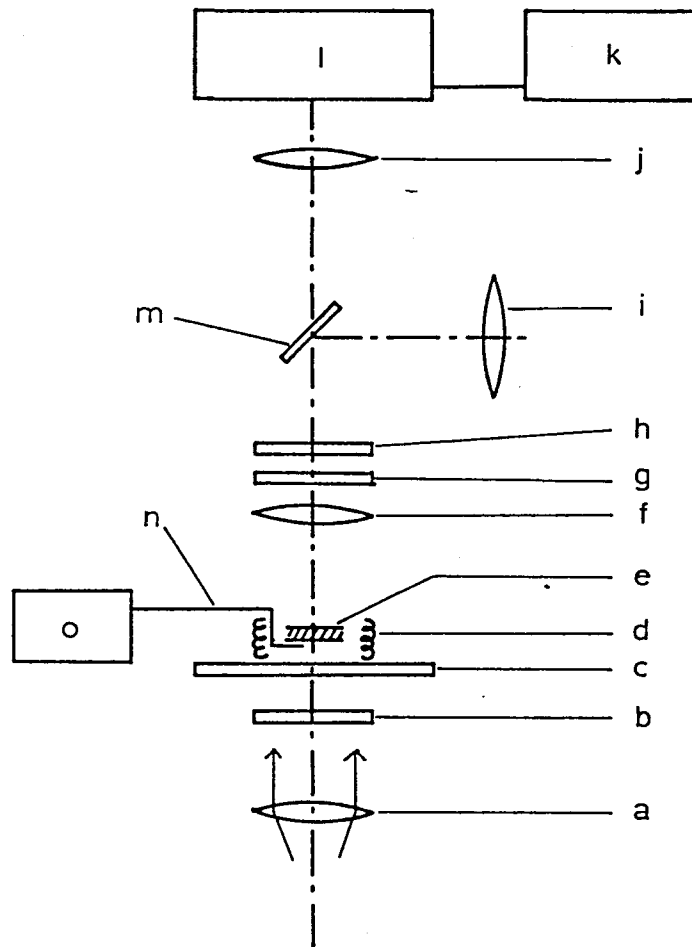


Fig. III-2. Schematic representation of the polarizing microscope and its attachments.

- | | |
|---|--------------------------|
| (a) lens | (h) analyzer (// Y) |
| (b) polarizer (// X) | (i) eye lens |
| (c) rotatable stage | (j) camera lens |
| (d) heater | (k) exposure meter |
| (e) sample | (l) camera |
| (f) field lens | (m) mirror |
| (g) sensitive color plate (530 nm)
(usually removed) | (n) thermocouple |
| | (o) digital multimeter |

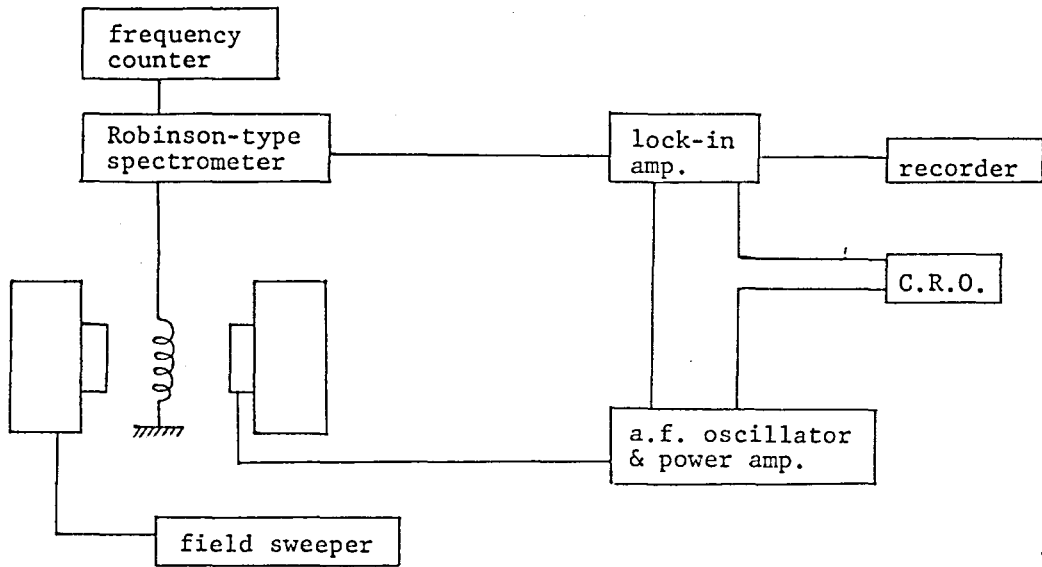


Fig. III-3. Block diagram of the CW-NMR spectrometer.

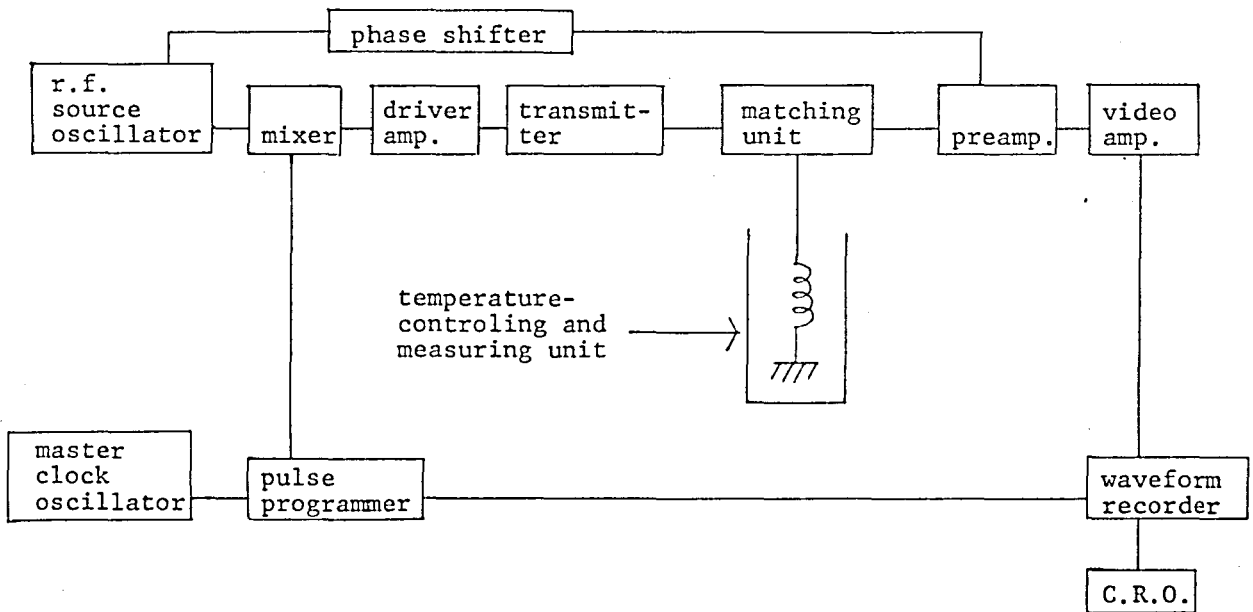


Fig. III-4. Block diagram of the pulse NMR spectrometer.

References to chapter III

- 1) K. Tsuji: Thesis, Osaka Univ. (1979).
- 2) for a general reference on NMR experimental technique, see for instance, " Techniques of Metals Research " (ed. R. F. Bunshah) vol. VI " Measurement of Physical Properties Pt. 2, Magnetic Properties and Mössbauer Effect " (ed. E. Passaglia, John Wiley & Sons, 1973).
- 3) F. N. H. Robinson: J. Sci. Instrum. 36 (1959) 481.
- 4) T. Tsuneyoshi, N. Nakamura, and H. Chihara: J. Magn. Reson. 27 (1977) 191.
- 5) K. Ichimura: private communications.

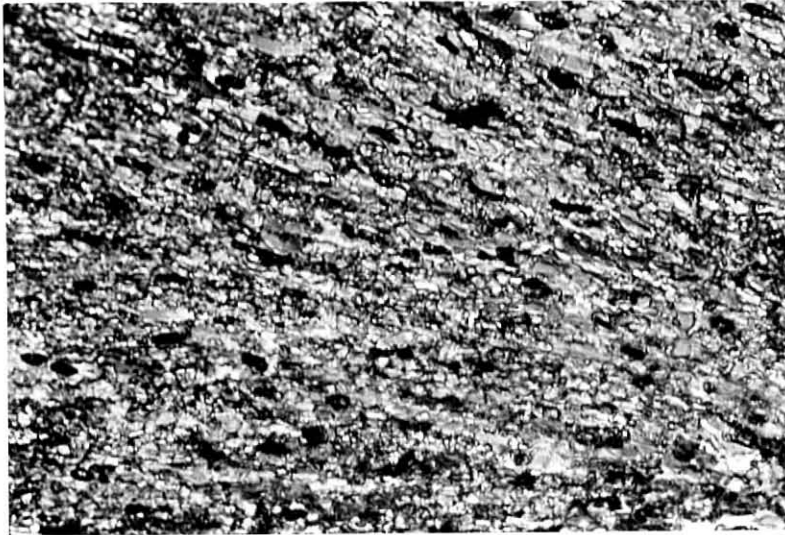
Chapter IV. Phase Relations and Textures

—— Results of DTA and Microscope Observations ——

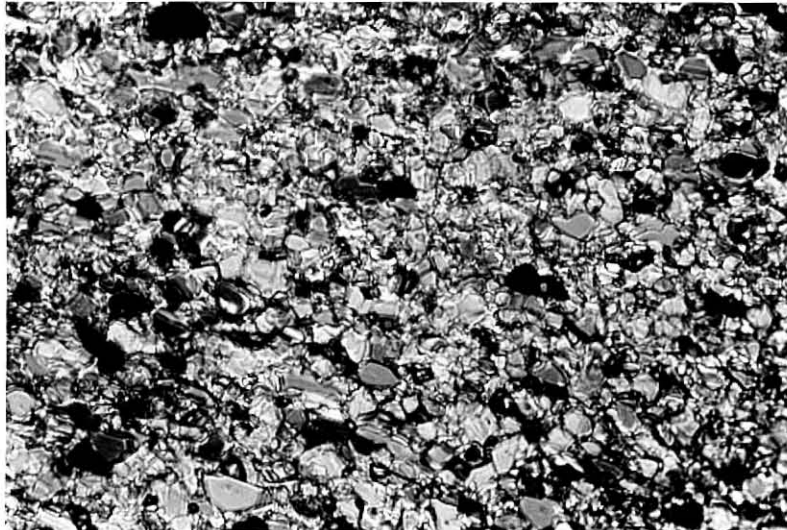
§ IV-1. HBAB

The phase relation of HBAB, CII \rightarrow CI \rightarrow N \rightarrow I, was established by Tsuji.^{1,2)} No metastable mesophase appears in this compound. So our DTA experiment was ^{done} only to ascertain this relation and the transition points. The results: CII $\xrightarrow{316.3\text{ K}}$ CI $\xrightarrow{333.3\text{ K}}$ N $\xrightarrow{375.6\text{ K}}$ I were obtained in good agreement with ref. 1, except that the superheating phenomenon CII \rightarrow CI was pronounced. CI was found to be undercooled to 77 K, and this fact became an advantageous point for the study of motional states in the two crystalline states. An NMR detection of the very sluggish phase transition from the undercooled CI to the stable CII was carried out, and the result is given in Appendix.

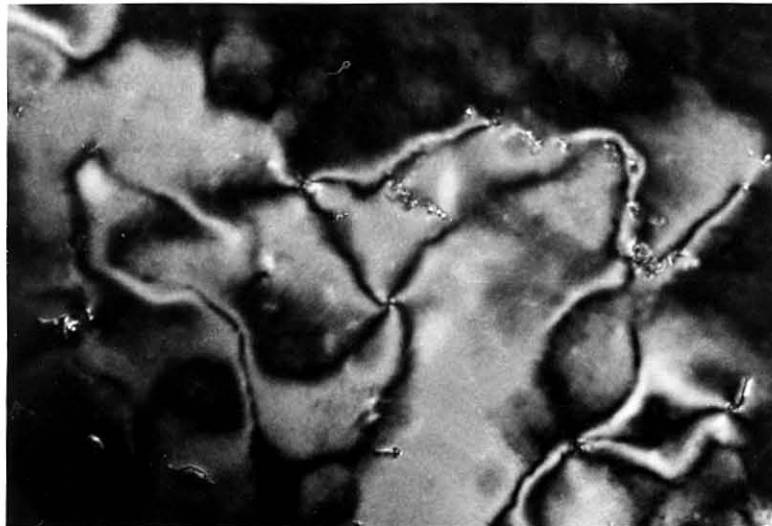
For the purpose of understanding motional disorder in CI, the change in textural appearance at the transition CII \rightarrow CI is quite interesting. Plate 1 shows this. The texture of CII (plate (a)) which is the typical one of the crystalline state disappears at the transition, and a new texture (plate (b)) is formed with irregular polygons resembling that of a kind of smectics. This observation is one of the evidences of high degree of motional disorder in this high-temperature crystalline phase. A typical schlieren texture ^{3,4)} (plate (c)) was observed in the nematic HBAB.



(a); CII at 298 K,
×400.



(b); CI at 328 K,
×400, the same section
as plate (a).



(c); Nematic schlieren
texture, ×400. Points
of singularity with
 $s = \pm 1$ can be seen
(s ; "strength" of
disclination).

§ IV-2. HBAC

The DTA of HBAC was first carried out by Tsuji¹⁾ in which the existence of the phase III was not recognized because of very sluggish nature of the C→III phase transition. They found this new phase later by an adiabatic calorimetry.⁵⁾ The purpose of our DTA experiment is to ascertain the existence of this new phase and to find the sufficient conditions under which this phase can be realized.

First, we carried out an ordinary DTA experiment (Fig. IV-1 (a)) which showed three phase transitions: 331.4 K (C→SB), 363.8 K (SB→SA), and 371.4 K (SA→I) in the heating run. The first transition undercooled to 306.2 K in the cooling run. In the next place we annealed the sample at 330.0 ± 0.1 K for 40 hours. After that, we found two phase transitions: 334.3 K (III→SB in the heating run, Fig. IV-1 (b)) and 312.8 K (III→C in the cooling run, Fig. IV-1 (c)) which provide us a clear evidence for the existence of the phase III. In the NMR experiment of the phase III, the annealing for 50 hours at 330.0 ± 0.1 K was carried out prior to the experiment.

SA mesophase exhibited a simple fan-shaped texture (Plate 2). Projections of Dupin cyclides⁶⁾ (hyperbola and the straight line connecting its foci) are seen in the plates. The transition SA→SB preserved the fan-shaped texture.

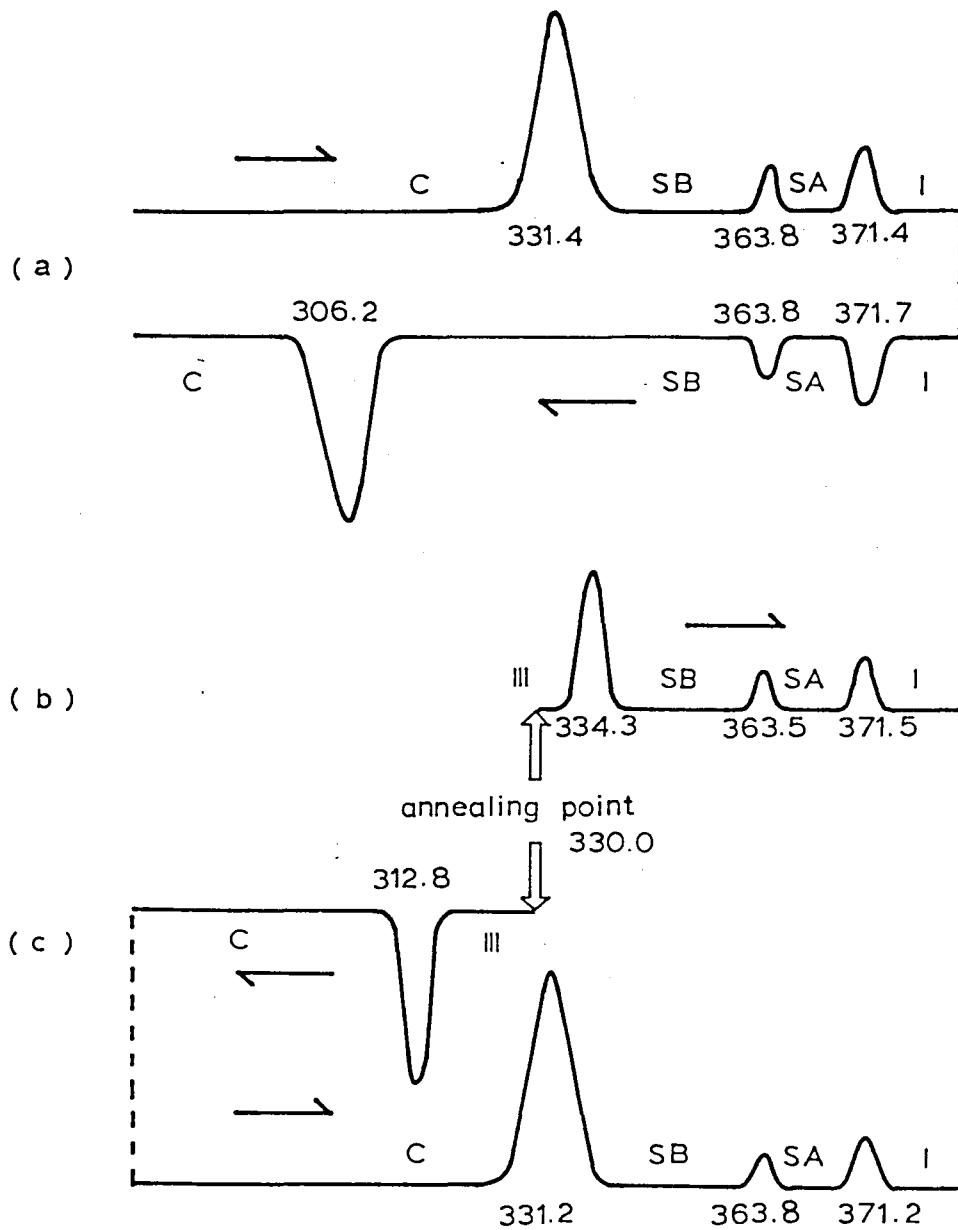
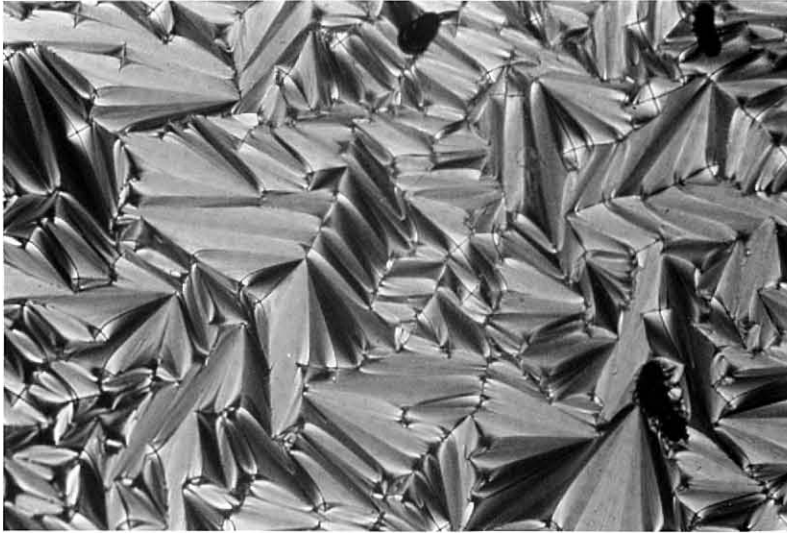
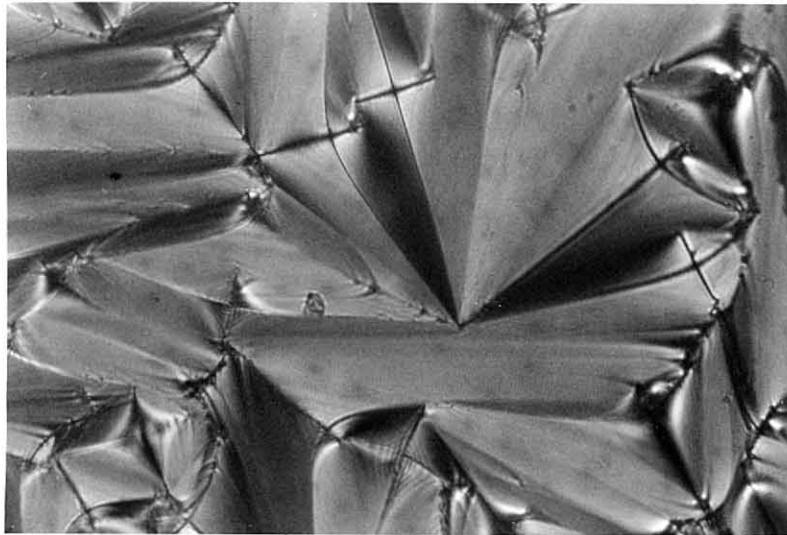


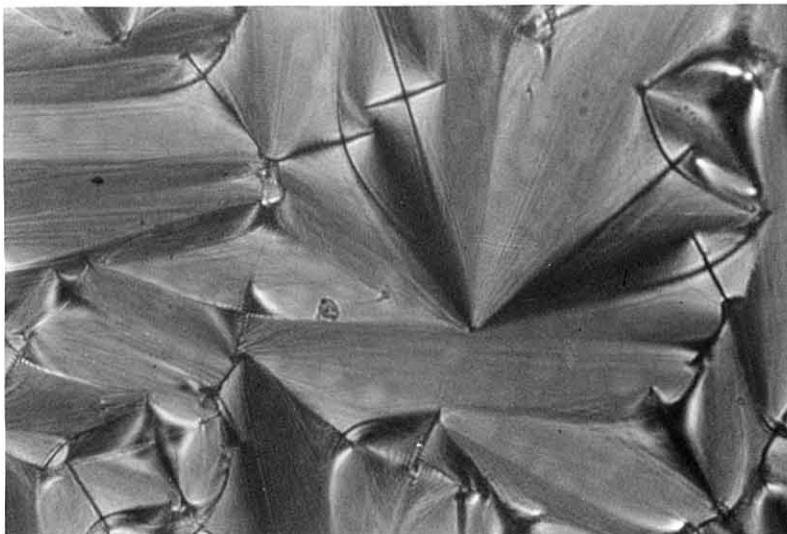
Fig. IV-1. Schematic representation of DTA thermogram of HBAC. (a); ordinary DTA experiment between 290 K and 385 K. (b) and (c); DTA of the sample annealed for 40 hours at 330.0 ± 0.1 K.



(a); Fan-shaped texture of SA at 345 K, $\times 100$.



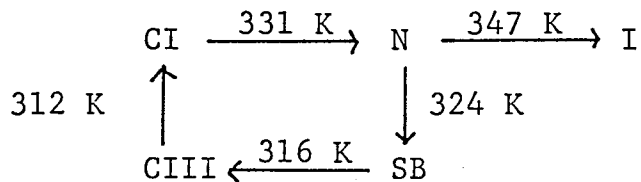
(b); Fan-shaped texture of SA at 345 K, $\times 400$. Projections of Dupin cyclides (Grandjean Boundaries) can be seen.



(c); Paramorphic fan-shaped texture of SB, $\times 400$, the same section as plate (b).

§ IV-3. HBT

Bhide et al.⁷⁾ proposed the following phase relation by the DTA and DSC experiment.



The crystalline phase which appear below SB in the cooling run was called solid II in their original report, but is replaced by CIII in the figure above because Tsuji¹⁾ discovered another stable crystalline phase by the adiabatic calorimetry (CII→CI at 317.5 K, see Table I-2).

The complexity of the thermal behavior is as follows. Bhide et al.⁷⁾ found another phase transition at 336 K in the heating run for the sample rapidly cooled from the isotropic phase. The relative intensity of the two peaks at 331 K and 336 K depends on the rate of cooling while the sum of the integrated intensities were nearly conserved. Annealing at room temperature (r.t.) had an effect on decreasing the intensity of the 336 K peak. They tried to interpret these phenomena by supposing the survival of the smectic B nuclei in the crystalline sample rapidly cooled from its isotropic phase. According to their explanation, the 336 K transition is the SB→N transition and the immiscible mixture of SB and N exists between 331 K and 336 K. This explanation is quite questionable. So we attempted to clarify the complex phase relation by DTA and

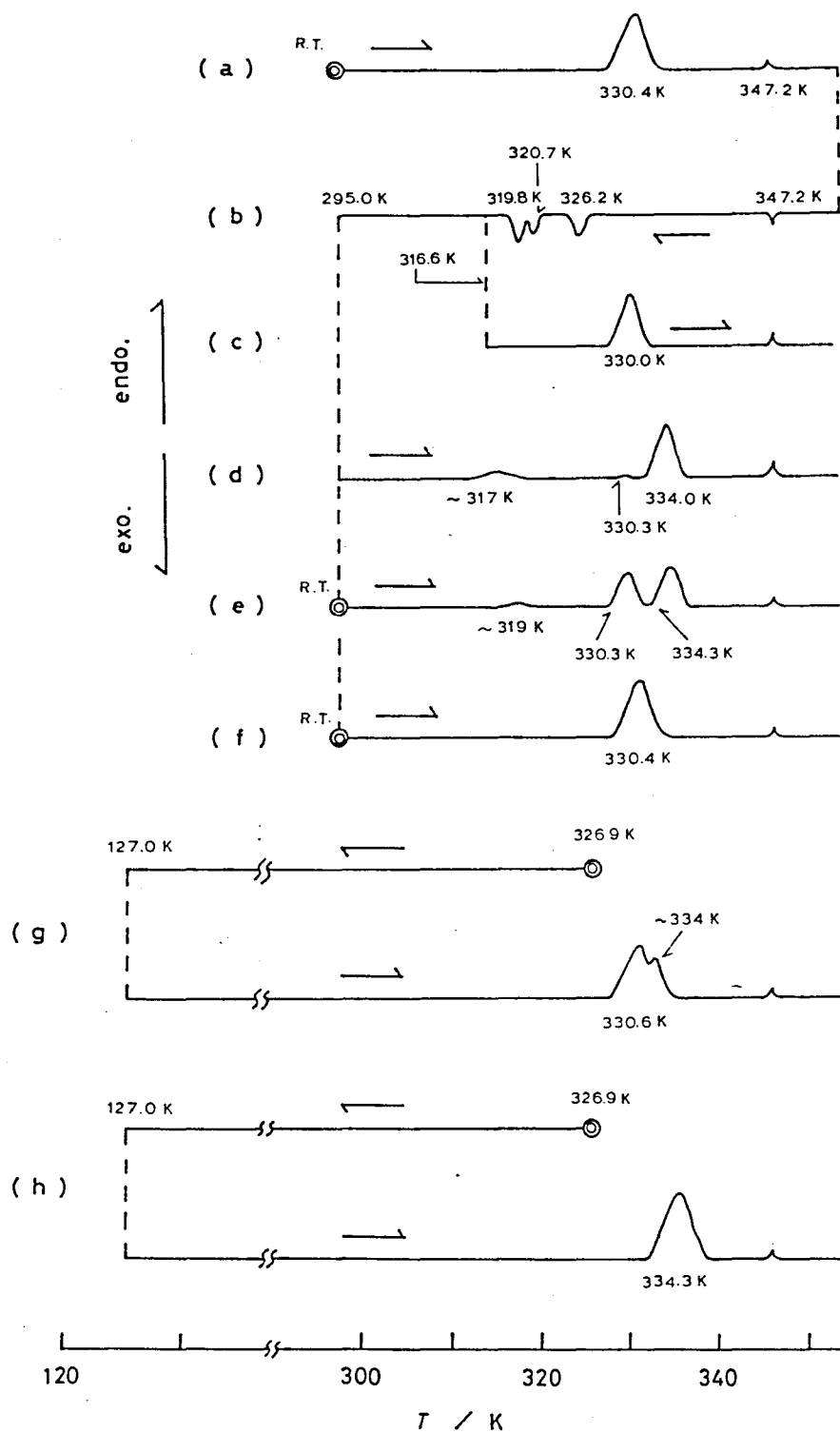


Fig. IV-2. Schematic DTA thermogram of HBT (Pt. 1)
 (The caption is given in the next page.)

texture observations.

The DTA experiment presented in Fig. IV-2 was carried out using the sample left at r. t. for thirteen months. In the first heating run (figure (a)), it melted at 330.4 K into nematic liquid crystal, and then transformed[✓]into isotropic liquid at 347.2 K. When the sample was cooled from the isotropic phase to 316.6 K and heated again, the crystal melted into the nematic phase at 330.0 K (c). On the other hand, when the sample was cooled to 295.0 K and heated again, the three transitions (\sim 317 K, 330.3 K, and 334.0 K) appeared (d). These three transitions were affected by annealing at r.t. The figures (e) and (f) represent the thermograms after the annealing at r.t. for 20 hours and three weeks, respectively. The figure (f) exhibited the same behavior as (a). It was clarified that the annealing at r.t. enhances the transition at 330 K.

captions to Fig. IV-2.

(a); initial heating run after the annealing for thirteen months at room temperature. The symbol \checkmark indicates annealing.

(b); cooling run from 350 K at the rate of 4.6 mK s^{-1} .

(c); heating run from 316.6 K after the cooling run (a) without annealing.

(d); heating run from 295.0 K after the cooling run (a) without annealing.

(e); heating run after the annealing for twenty hours at room temperature.

The thermograms (g) and (h) were obtained by the following procedure: (g); the sample was annealed at room temperature for fourteen months, then heated to 326.9 K and annealed there for four hours,

(h); the sample was annealed at 326.9 K for 44 hours after cooling from 350 K to 295 K.

The annealing at 326.9 K, on the other hand, enhanced the transition at 334 K as was evidenced by the figures (g) and (h). The annealing time is longer for (h) than for (g). Sum of the intensities of the two peaks were almost conserved for all the experiments.

The following conclusions can thus be deduced.

(1) From the annealing experiment at r.t. (f) and at 326.9 K (h), it is clarified that the stable phase at each temperature is different (CII and CI, respectively), the melting point for each of which being 330 K and 334 K, respectively.

(2) The thermogram having both of the transitions at 330 K and 334 K (figures (d), (e), and (g)) thus represent the coexistence of the two crystalline phases.

(3) So, between 330 K and 334 K in figures (d), (e), and (g), there exists a mixture of CI and N, contrary to the assumption by Bhide et al.⁷⁾ (mixture of N and SB).

(4) The intercrystalline phase transition CII→CI at ~316 K is very sluggish if the sample is pure CII without the nuclei of CI, and cannot be observed by DTA ((a) and (f)), but the transition is accelerated by the existence of CI nuclei enabling the observation by DTA ((d) and (e)). Enthalpy of the transition is far smaller than that of CII/CI transition in HBAB.

(5) The schematic diagram of Gibbs' free energies of the three phases, CII, CI, and N are given in Fig. IV-3. If the cooling of the sample from the isotropic melt is stopped at a temperature above 316 K and heated again without annealing, the

sample is in CII which is the metastable state at this temperature ((c) in Fig. IV-2), but falls into CI by annealing for sufficient time (h). If the cooling of the sample is stopped below 316 K, a mixture of CII and CI is obtained (d), and the annealing at r.t. assists the growth of CII ((e) and (f)).

We could solve the complex phase relation of HBT, which is summarized in Fig. IV-4.

Some further DTA experiments were carried out (Fig. IV-5) which revealed that N/SB phase transition temperature does not depend on cooling rate and is reversible in the cooling and heating runs. The transition temperature SB→CIII was dependent on cooling rate, which is characteristic of the transition from a metastable liquid crystalline phase to a crystalline phase.

Results of texture observations in HBT are presented in Plate 3. The plates (a) to (c) represent typical examples of the N/I transition, nematic schlieren texture, and smectic B mosaic texture,³⁾ respectively. The plates (d) and (e) represent the textures while the transition SB→CIII is proceeding. The star-like domains with orthogonal symmetry growing in the homeotropic (pseudoisotropic) area of SB mosaic texture can be seen clearly in the plate (d). The characteristic shape of the growing domain reflects the symmetry of this metastable phase. This phase CIII soon transformed into stable crystalline state even if the temperature is controlled well (see plate (f)).

The complex melting behavior was examined also by the microscope experiment. By the procedure described in the DTA

experiment, a mixture of CII and CI was prepared and its melting behavior was observed (plates (g) and (f)). The inter-crystalline phase transition CII \rightarrow CI caused no pronounced change in texture. But the texture at 332.5 K (plate (h)) was clearly different from that of both crystal and nematic liquid crystal. This is a strong evidence in support of the coexistence of CI and N at this temperature.

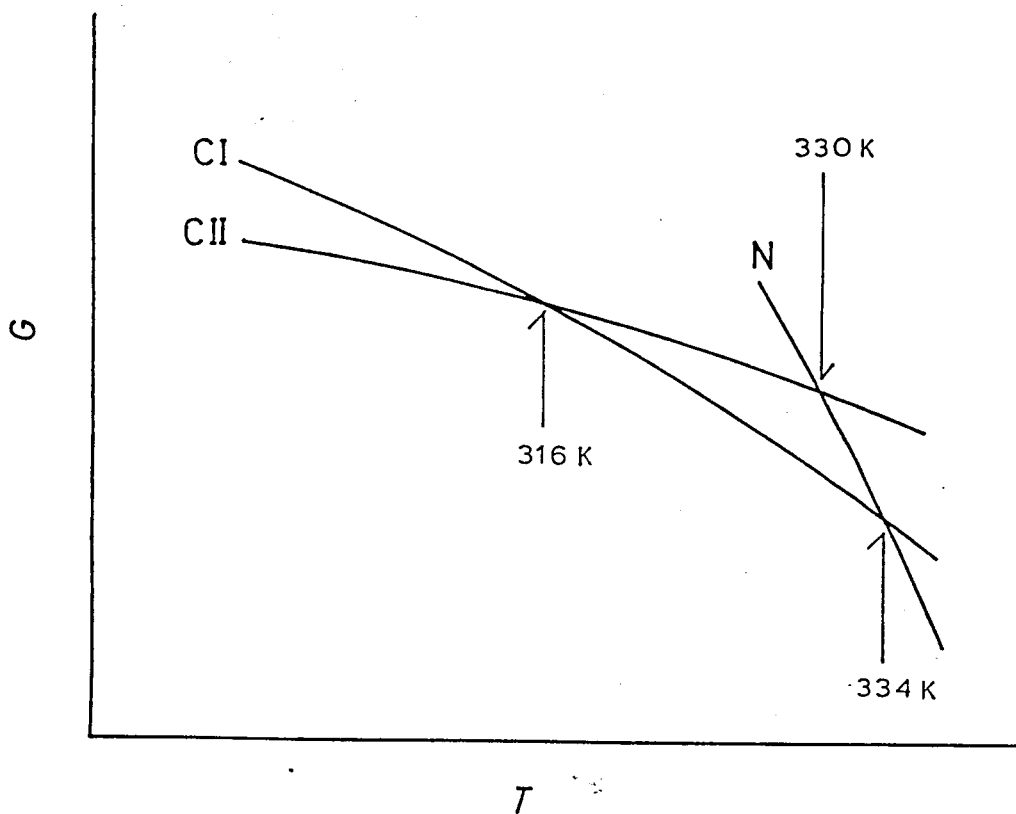


Fig. IV-3. Schematic representation of Gibbs' free energy of the three phases, CII, CI, and N of HBT.

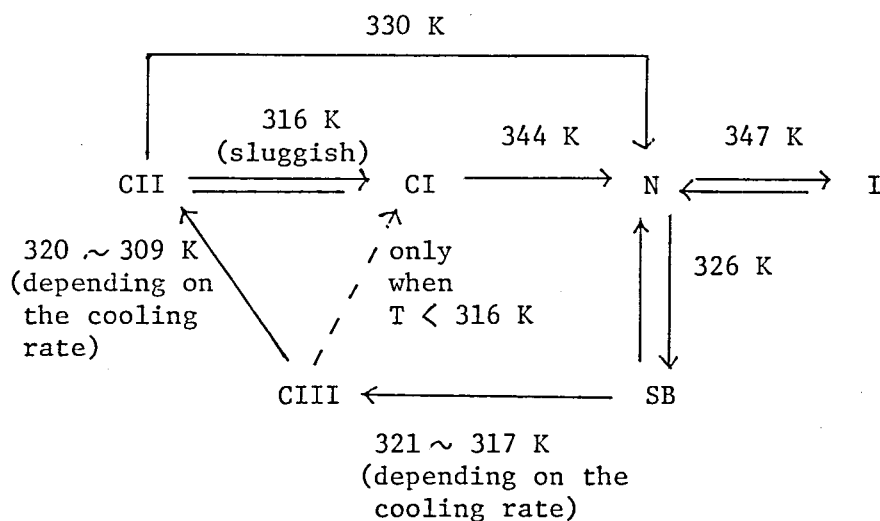


Fig. IV-4. Phase relation of HBT.
The phases SB and CIII are metastable.

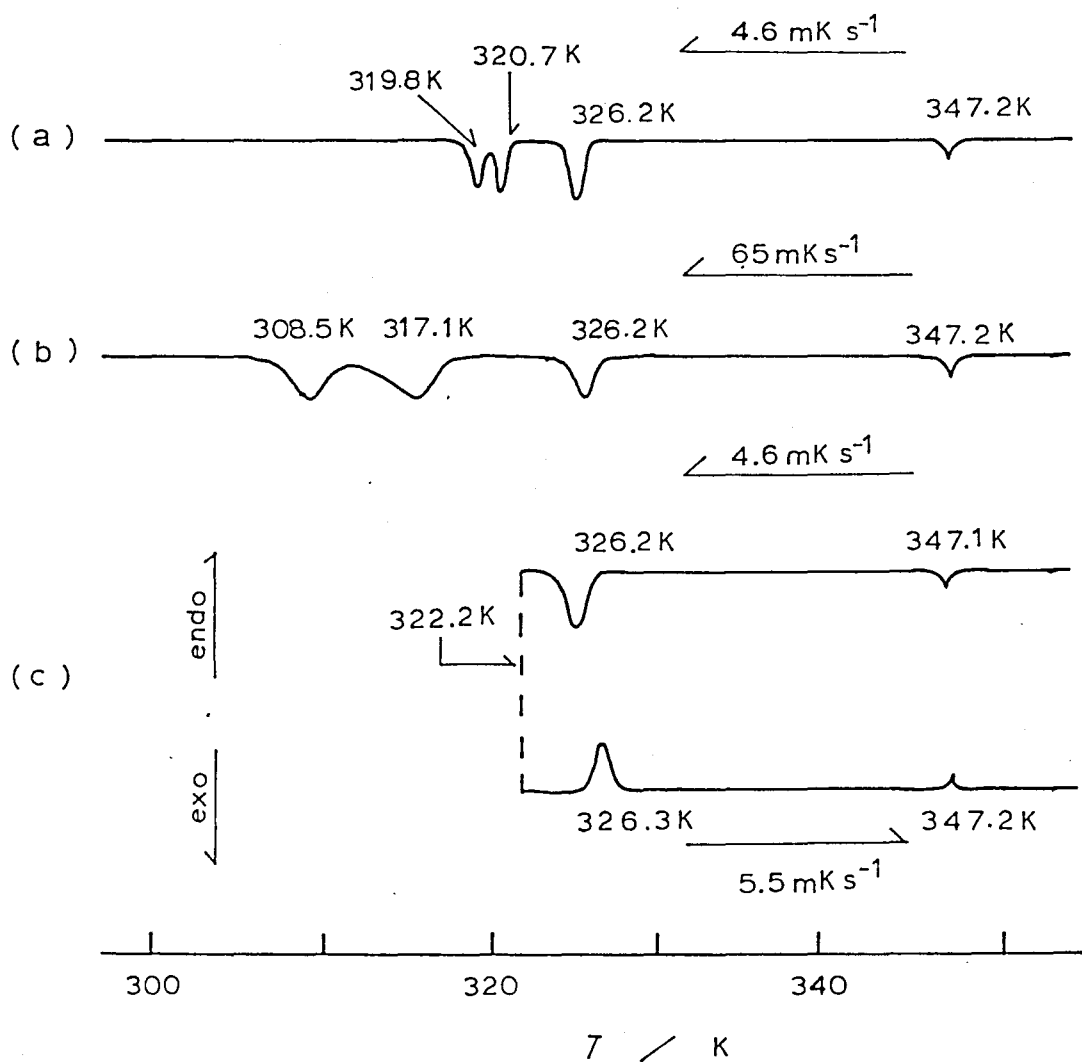
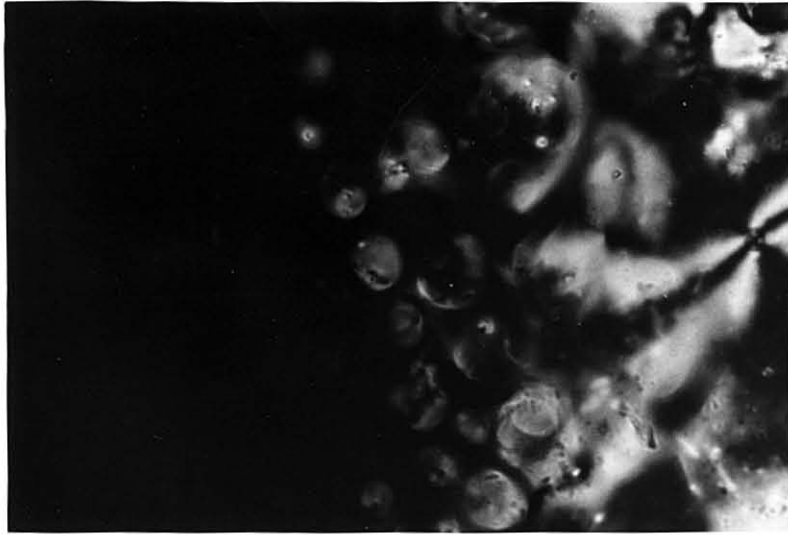
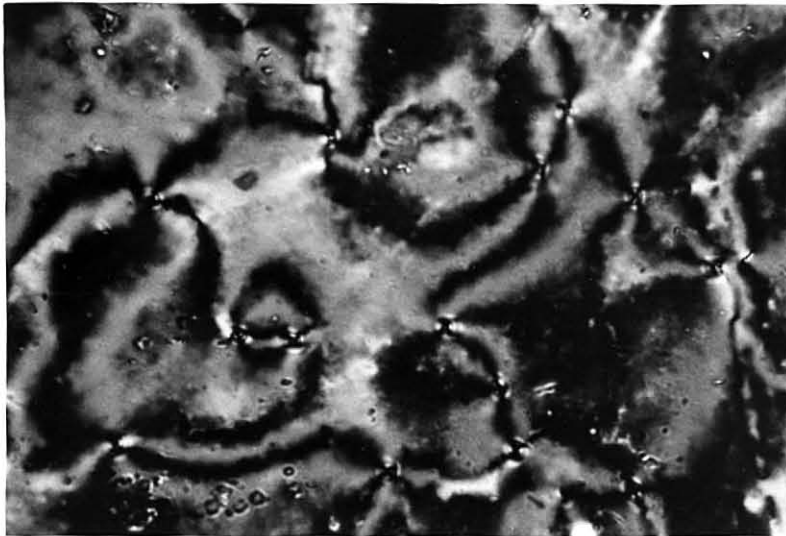


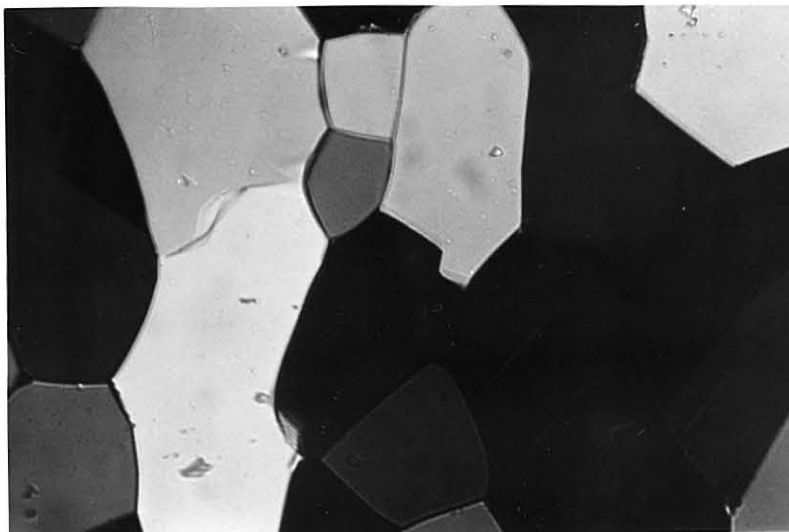
Fig. IV-5. Schematic DTA thermogram of HBT (Pt. 2)
(a); cooling run from the isotropic phase at the rate of 4.6 mK s⁻¹,
(b); at the rate of 65 mK s⁻¹, (c); test of reversibility of the
N/SB transition.



(a); Formation of nematic droplets in the isotropic media at the N/I transition point, $\times 400$. Nematic schlieren texture can be seen.



(b); Nematic schlieren texture, $\times 400$. Points of singularity with $s = +1$ are seen.



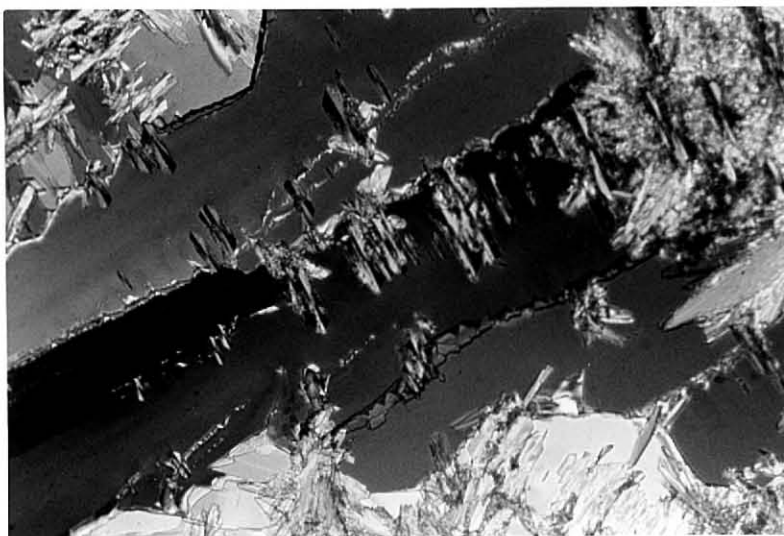
(c); SB mosaic texture, $\times 400$.



(d); Domains of CIII with the shape of orthogonal star growing in the homeotropic (pseudo-isotropic) area of SB mosaic texture, $\times 400$.



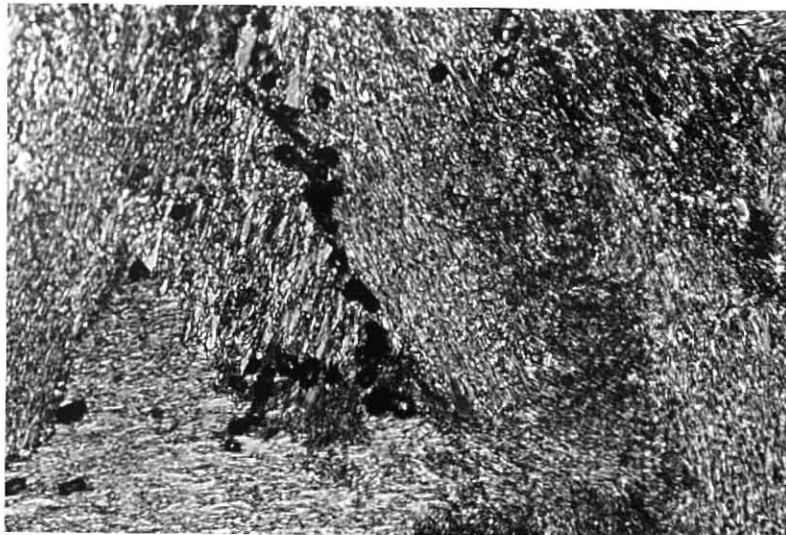
(e); Phase CIII growing (from left) in the SB mosaic texture, $\times 100$.



(f); Crystallites of stable crystalline phase growing in the CIII mosaic texture, $\times 100$.



(g); Crystalline state at 298 K, $\times 400$.



(h); Coexistence of CI and N at 332.5 K, $\times 400$, the same section as (g). Some of the crystalline texture has vanished, and the large-scale dislocations (black parts in plate (g)) have been smeared out or changed into holes of nearly spherical shape.

References to chapter IV

- 1) K. Tsuji: Thesis, Osaka Univ. (1979).
- 2) K. Tsuji, M. Sorai, H. Suga, and S. Seki: Mol. Cryst. Liq. Cryst. 55 (1979) 71.
- 3) D. Demus and L. Richter: " Textures of Liquid Crystals " (Verlag Chemie, Weinheim, New York, 1978).
- 4) J. Nehring and A. Saupe: J. Chem. Soc. Faraday II 68 (1972) 1.
- 5) K. Tsuji, M. Sorai, H. Suga, and S. Seki: Mol. Cryst. Liq. Cryst. 41 (1977) 81.
- 6) Y. Bouligand: J. Phys. (Paris) 33 (1972) 525.
- 7) V. G. Bhide, B. D. Malhotra, V. K. Kondawar, and P. C. Jain: Phys. Lett. 64A (1977) 111.

Chapter V Molecular Motion in the Nematic Liquid
Crystalline Compound, HBAB

§ V-1. Major Objectives of the NMR Study

The major objectives of this study are as follows:

(1) to make clear the differences of molecular motion in the two crystalline phases, and to find what kinds of disorder exists in CI, (2) to measure the temperature-dependence of orientational order in the nematic phase, and to examine the applicability of the mean field theories of nematic liquid crystal on the basis of intermolecular dispersion forces, to a system of molecules having strong electric dipole along its long axis as in HBAB, and (3) to examine what modes are responsible for nuclear spin-lattice relaxation in the nematic phase.

§ II-2. The Crystalline Phases

II-2-1. Second Moments

The proton NMR lines showed Gaussian envelopes without any fine structures in both crystalline states. The second moment M_2 in the two phases are shown in Fig. V-1 as a function of temperature. The second moment in CII showed a narrowing around 100 K, and held an almost constant value of 16 G^2 up to the transition point, $T_{\text{II-I}}$. On the other hand, while M_2 in CI showed a similar narrowing around 100 K, it then decreased gradually from 12 G^2 to 7 G^2 . In order to identify the motional modes responsible for these motional narrowings, we

attempted a model calculation of M_2 in the crystalline states. Since the structural data of HBAB was not available, we assumed that the molecular structure of HBAB can be represented by combining the reported data of benzylideneaniline¹⁾ and n-alkanes²⁾ as shown in Fig. V-2, in which the planes of the two benzene rings are twisted by 65.5° from each other. Taking

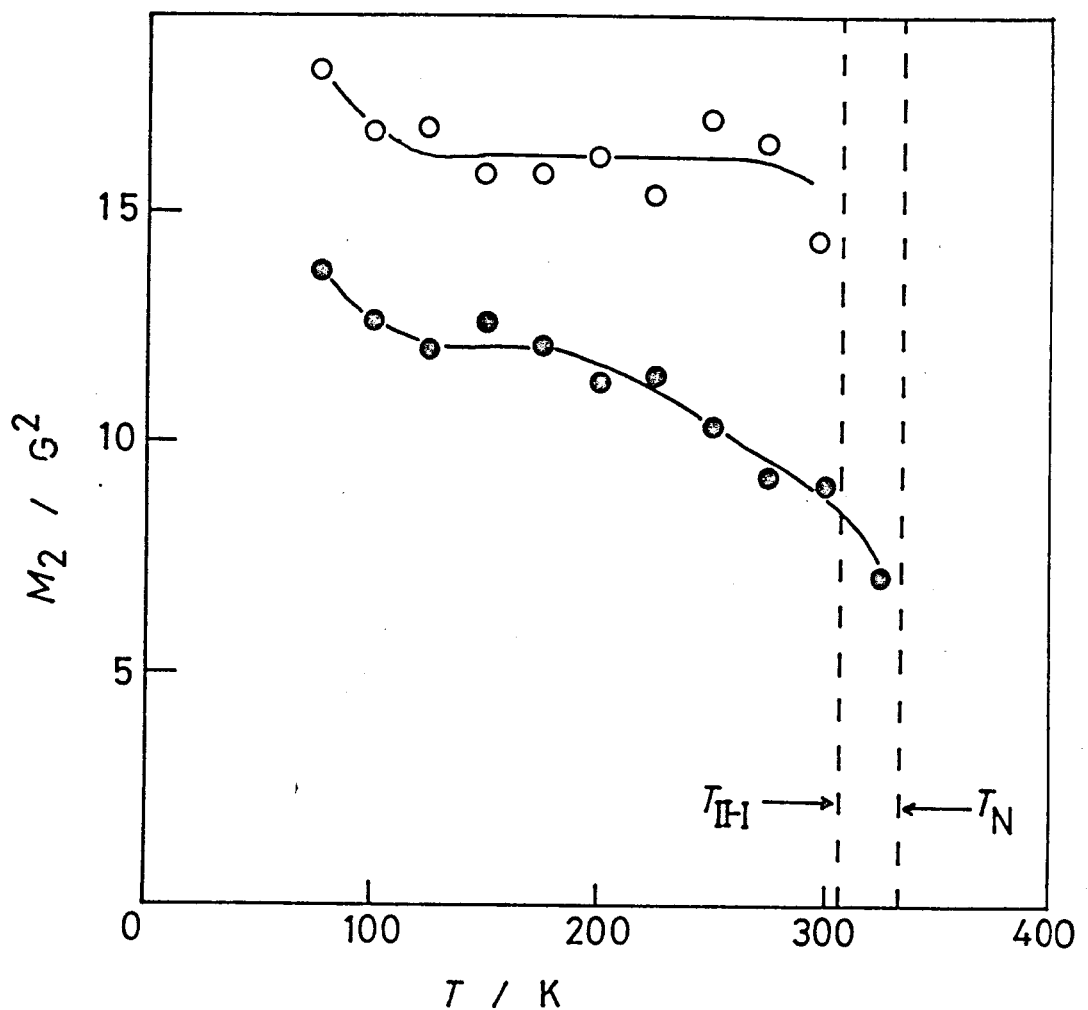


Fig. V-1. Second moments of proton NMR lines in the two crystalline phases of HBAB (● CII, and ○ CI). The solid lines are drawn only for the aid of the eyes.

into account all the pairwise dipole-dipole interactions between the twenty-two protons within a molecule, and ignoring small contributions from the other magnetic nuclei, the intramolecular contribution to M_2 in the rigid lattice was calculated to be 17.2 G^2 for a powdered sample. Motional narrowing was estimated^{3,4)} for three different types of internal rotation which is expected to take place in the crystalline states: (1) the terminal methyl reorientation, (2) the jump rotation of the C_2H_5 group about the next terminal C-C bond in addition to the methyl reorientation, and (3) the overall rotation of the hexyloxy chain about the the bond between the ring carbon and the oxygen. The results are summarized in Table V-1. In the case (3), we assumed that the hexyloxy

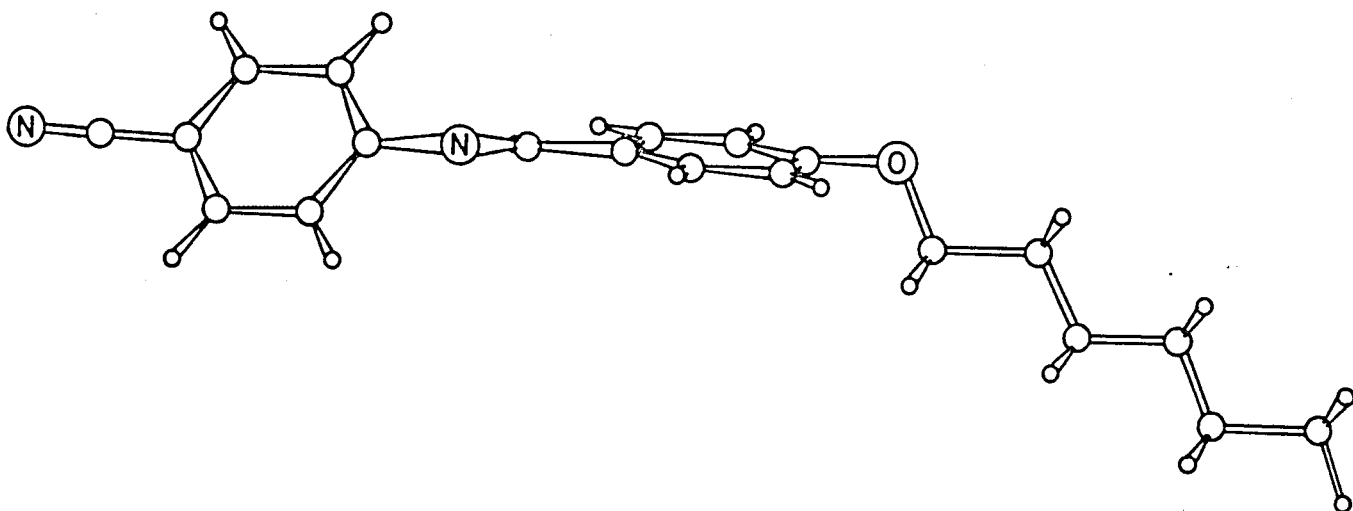


Fig. V-2. Assumed molecular structure of HBAB. Large and small circles represent carbon and hydrogen atoms, respectively. Nitrogen and oxygen atoms are indicated.

Table V-1. Calculated second moments of proton NMR lines (intramolecular contributions)

motional states	M_2 / G^2
rigid lattice	17.2
terminal CH_3 reorientation	13.9
CH_3-CH_2 rotation	11.4
overall chain rotation	less than 4.8

group is rigid, and rotates only about the $C_{ring}-O$ axis without any internal segmental motion except the methyl reorientation. Hence the value $4.8 G^2$ in Table V-1 will give an upper bound for model (3).

Comparing the experimental results of Fig. V-1 with the calculated values, the following assignments were made.

(1) In CII, the low-temperature narrowing is due to the methyl reorientation, and this is the only mode excited in this phase. It follows from this assignment that intermolecular contribution to M_2 in the plateau region is $2 G^2$ which is of reasonable magnitude. (2) In CI, the low-temperature narrowing is brought about by the rotation of the ethyl group. And the gradual decrease of M_2 in the higher~~X~~ temperature region suggests that several modes of segmental motion of the chain are excited successively, but that the overall rotation of the chain is not excited even in the vicinity of the melting point, T_N . The overall rotation of the chain is realized above T_N .

V-2-2. Spin-Lattice Relaxation Rates

The spin-lattice relaxation rates measured at 10.0 MHz in CII and CI are presented against reciprocal temperatures in Figs. V-3 & 4, respectively.

In CII, as was suggested in the analysis of the second moment, it is clearly seen that the terminal methyl reorientation is the only mechanism responsible for spin-lattice relaxation. The spin-lattice relaxation rate for a three-spin system

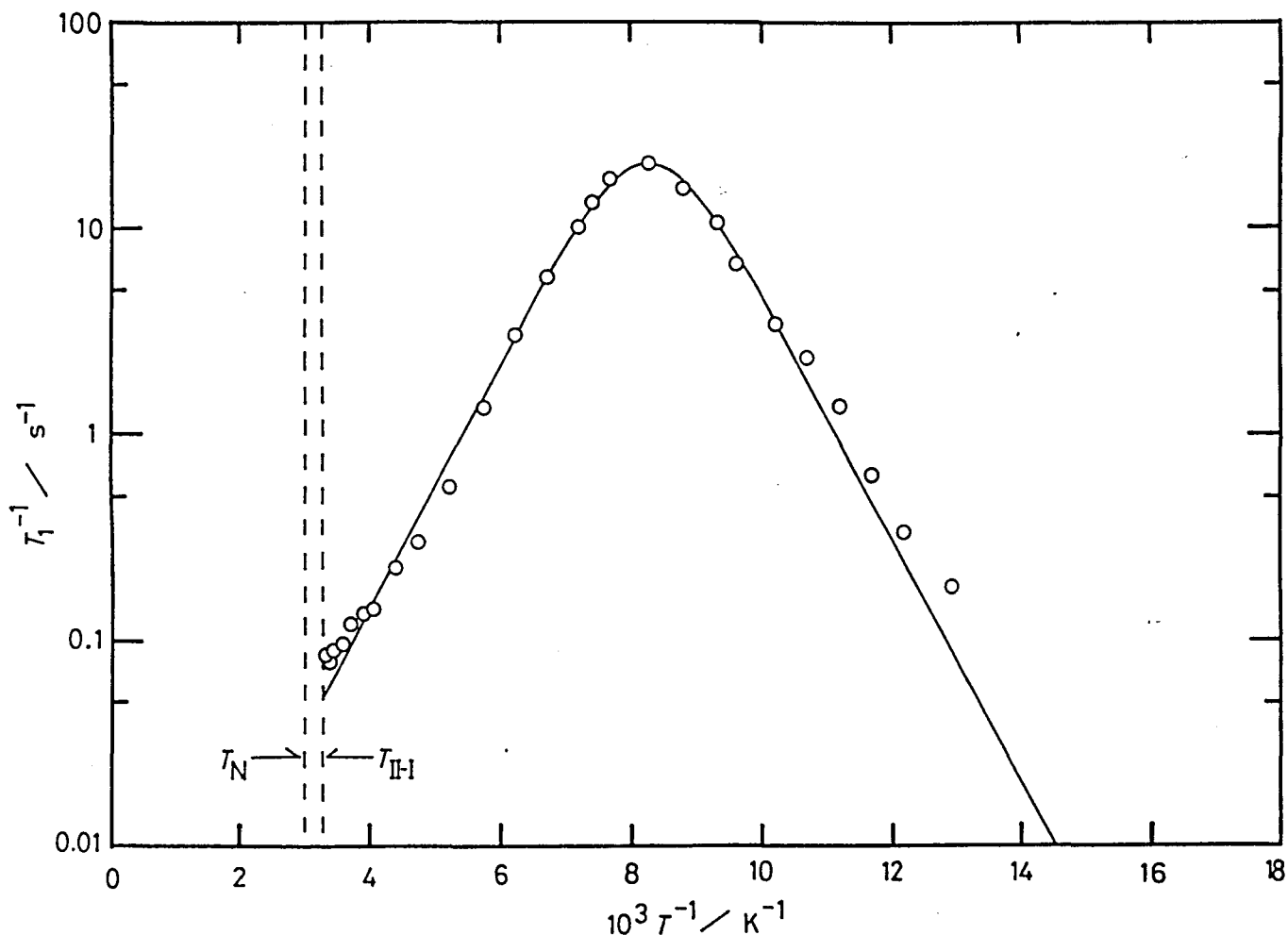


Fig. V-3. Proton spin-lattice relaxation rates at 10.0 MHz in CII. The solid line is the calculated one (see the text).

due to methyl reorientation can be expressed by³⁾

$$T_1^{-1} = A B(\omega_0 \tau_c) \omega_0^{-1} , \quad (V-1)$$

$$A = \frac{3}{5} \gamma^4 \hbar^2 r^{-6} I(I+1)$$

$$B(\omega_0 \tau_c) = \frac{\omega_0 \tau_c}{1 + \omega_0^2 \tau_c^2} + \frac{4 \omega_0 \tau_c}{1 + 4 \omega_0^2 \tau_c^2} ,$$

where ω_0 is the nuclear Larmor frequency, τ_c is the correlation time of reorientation, r is the interproton distance within the methyl group, and γ , \hbar , and I have their usual meanings (see section II-4). Now, using A as an adjustable parameter, and assuming an activation process of classical Arrhenius type,

$$\tau_c = \tau_0 \exp (\Delta H / RT) , \quad (V-2)$$

the T_1^{-1} can be reproduced and is shown in Fig. V-3. In this figure the parameters $A = 8.82 \times 10^8 \text{ s}^{-2}$,

$\tau_0 = 1.53 \times 10^{-13} \text{ s}$, and $\Delta H = 11.1 \text{ k J mol}^{-1}$ are used.

The agreement between the experiment and the calculation is good. Theoretical value of A was roughly estimated as follows. If we suppose that the spin temperature concept is valid in the whole system of protons, and that the methyl-protons are the only protons which can transfer the energy of spin system into lattice, the energy of the protons other than the methyl-protons will be transferred into lattice through methyl-protons via

nuclear spin diffusion to methyl-protons. Based on such a model, and by utilizing $r = 1.78 \times 10^{-10}$ m (from ref. 2), the value of A will be estimated at

$$A = 2 \left\{ \frac{3}{10} \gamma^4 \hbar^2 I(I+1) \right\} \times \frac{3}{22}$$

$$= 1.10 \times 10^9 \text{ s}^{-2} ,$$

which is not far from the value determined experimentally.

In CI, on the other hand, it can be seen that at least three relaxation processes (R_2 , R_3 , and the highest temperature branch) other than the methyl reorientation (R_1) are responsible for spin-lattice relaxation. As three of them (R_1 , R_2 , and R_3) have their relaxation maxima within this phase, semiquantitative analysis can be made. The first process R_1 is that of methyl-reorientation, so eqs. (V-1 & 2) can be used to analyze the data. We believe that the successive process R_2 and R_3 correspond to rotational motions of ethyl and propyl groups, respectively. In fact, the rigorous treatment of such a kind of segmental motion of the alkoxy chain needs a complicated calculation. For the present, let us assume an exponential time-correlation function of a pair of spins for each rotational mode (numbered j),

$$\langle F_p^*(\vec{r}, 0) F_p(\vec{r}, t) \rangle = \langle |F_p^*(\vec{r}, 0)|^2 \rangle$$

$$\times \exp(-t/\tau_{cj}) . \quad (\text{V-3})$$

Here, $F_p(\vec{r}, t)$ denotes the dipolar interaction tensor between a pair of spins under question. If eq. (V-3) is justified, T_1^{-1} can be described by a superposition of the relaxation modes formulated by $B(\omega_0 \tau_{cj})$,

$$T_1^{-1} = \sum_{j=1}^3 R_j = \omega_0^{-1} \sum_{j=1}^3 A_j B(\omega_0 \tau_{cj}) \quad (V-4)$$

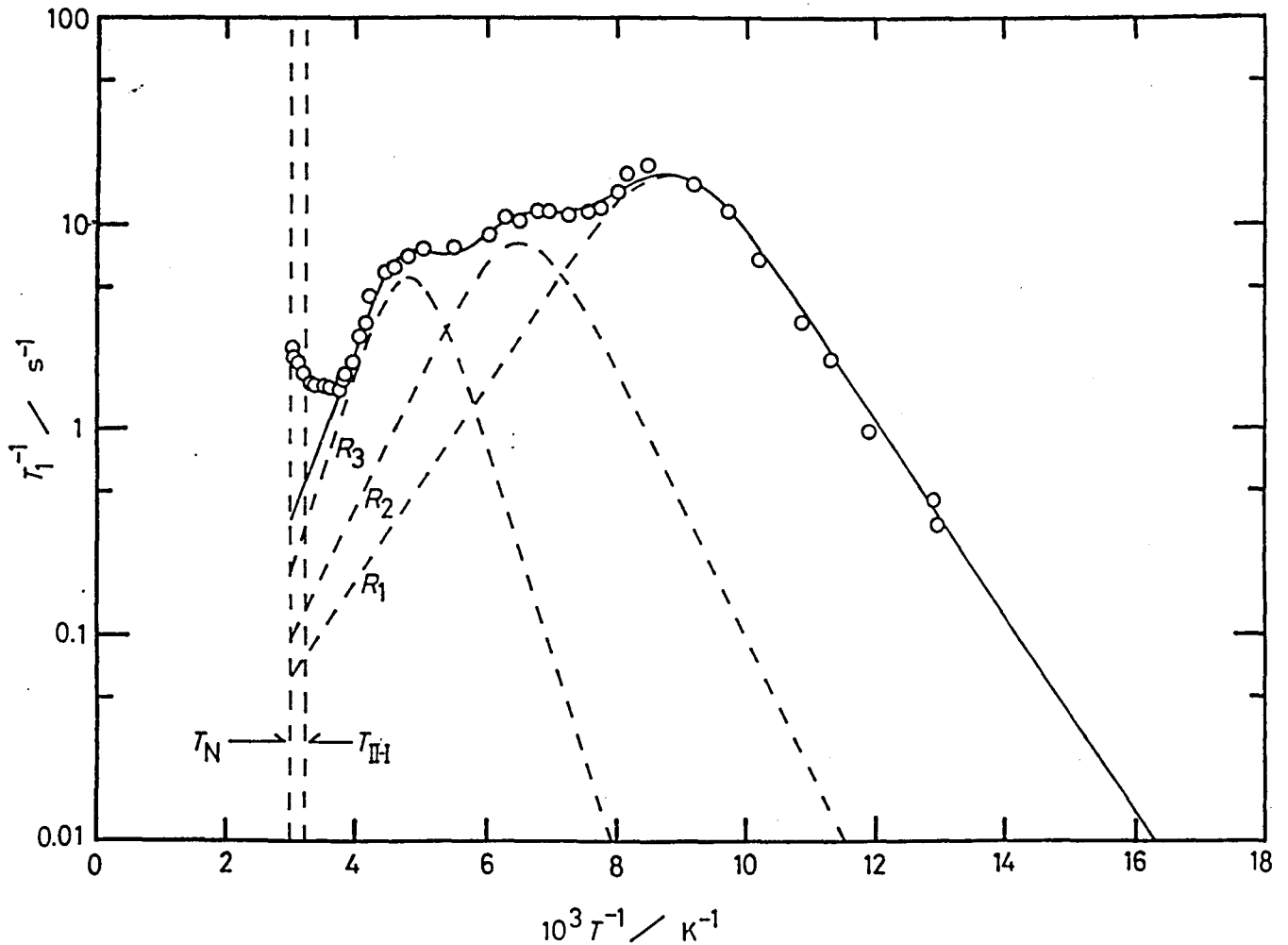


Fig. V-4. Proton spin-lattice relaxation rates at 10.0 MHz in CI. The broken lines R_1 , R_2 , and R_3 represent the contributions of the three relaxation modes (see the text and Table V-2). The solid line shows the sum of them, $R_1 + R_2 + R_3$.

Assuming again Arrhenius-type activation processes for τ_{cj} -s and using A_j -s for adjustable parameters, T_1^{-1} can be reproduced and drawn in Fig. V-4. The calculated curve explains the data fairly well except in the highest temperature region where a fourth process takes place. The parameters are summarized in Table V-2, at the end of this chapter.

§ V-3. Orientational Order in the Nematic Phase

The NMR line in the nematic phase has a triplet structure, the outer doublets of which come from the dipole interaction of the adjacent proton pairs within benzene rings which are not averaged to zero due to uniaxial orientational order. The width of the dipolar splitting is related to the orientational order by the equation⁵⁾

$$\Delta H = 3 \gamma \hbar r^{-3} \langle p_2(\cos \theta) \rangle p_2(\cos \Phi), \quad (V-5)$$

in which r is the distance of the adjacent protons within a benzene ring, $p_2(x)$ is the Legendre polynomial of the rank of two. Here, Φ is the angle between the interproton vector and the molecular long axis which is the axis of fast rotational diffusion in the nematic phase, and θ is the angle between the molecular axis and the nematic director. The bracket denotes the time- and ensemble-average, and $\langle p_2(\cos \theta) \rangle$ (hereafter abbreviated as $\langle p_2 \rangle$) is defined as the second rank orientational order parameter. If we assume that $\Phi = 10^\circ$ and $r = 0.245$ nm according to the data of molecular structure,¹⁾

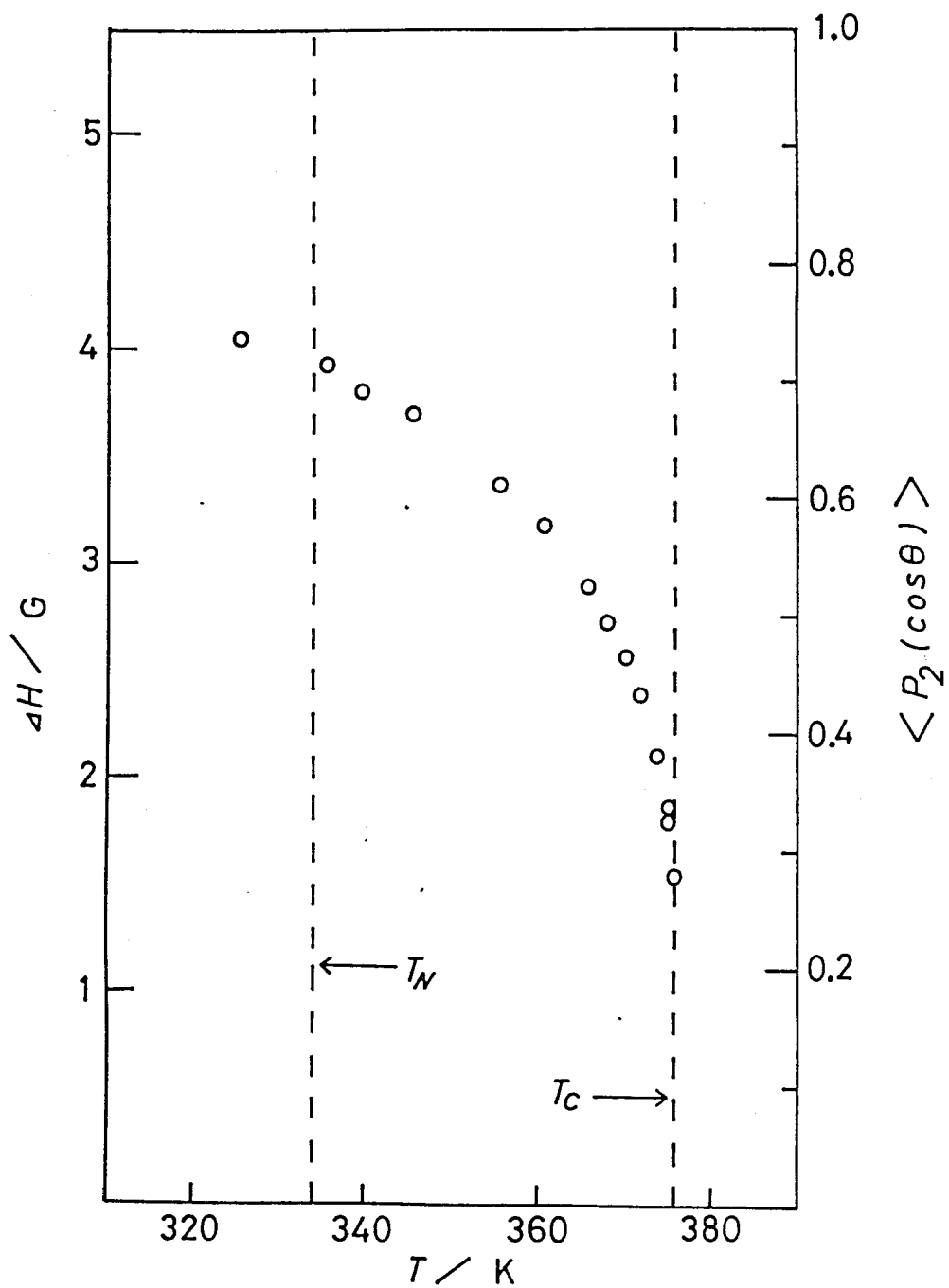


Fig. V-5. The peak width of the outer doublets of the proton NMR line in the nematic HBAB, and the corresponding orientational order parameter.

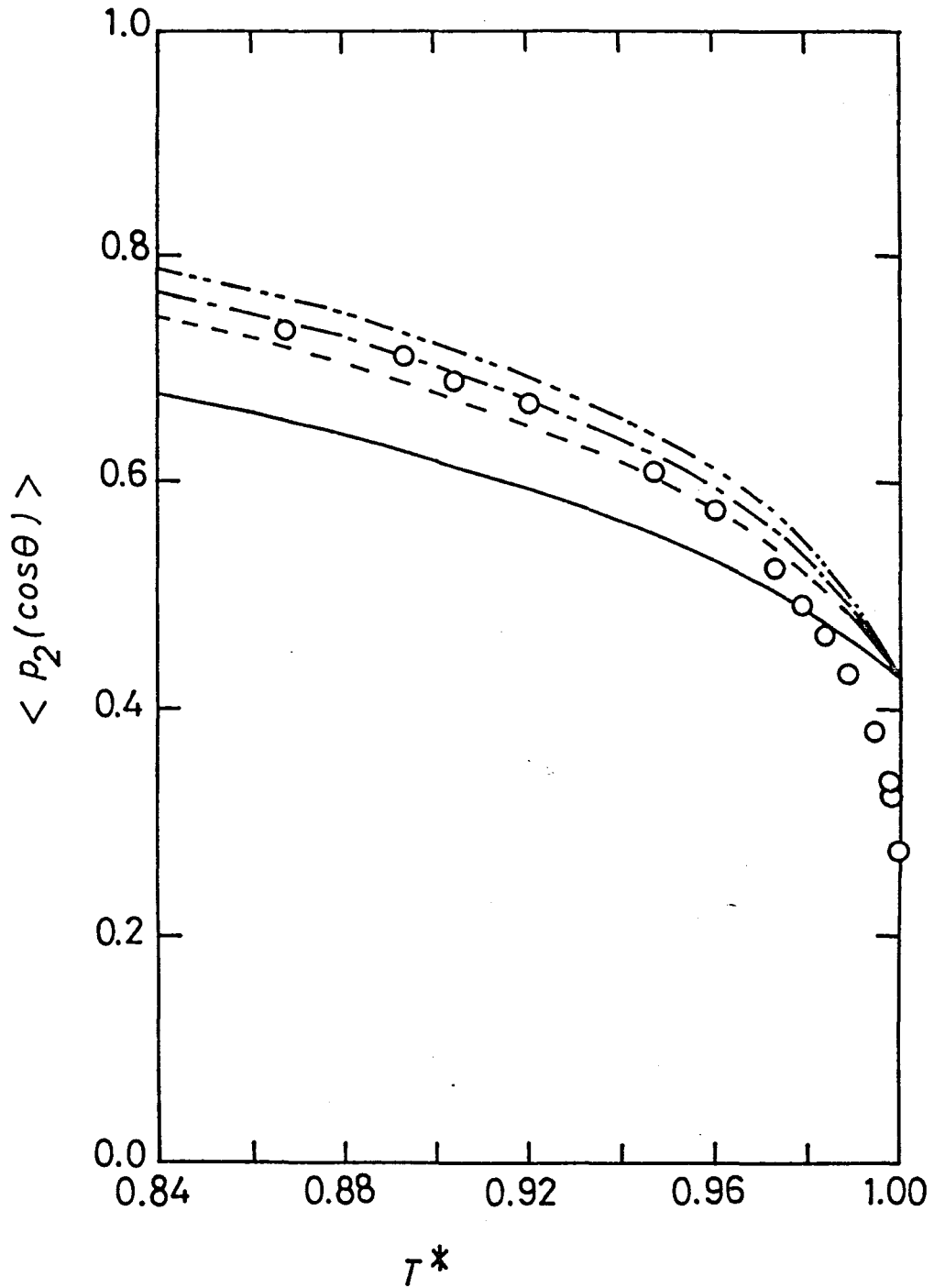


Fig. V-6. The second rank orientational order parameter plotted against reduced temperature ($T^* = T/T_c$). The theoretical curves are the solutions of the mean field theory, eq.(V-9), for different values of γ : — for $\gamma = 0$ (neglecting volume change), - - - for $\gamma = 2$ (Maier-Saupe), - · - · for $\gamma = 3$ (Chandrasekhar-Madhusudana), and - - - - for $\gamma = 4$ (Humphries-James-Luckhurst).

eq. (V-5) can be replaced by

$$\langle p_2 \rangle = 0.182 \times (\Delta H/G) .$$

The experimental values of ΔH and consequent $\langle p_2 \rangle$ are plotted in Fig. V-5 as a function of T . The order parameter exhibits a strong temperature-dependence, and the value at the clearing point is revealed to be $\langle p_2 \rangle_c = 0.28$ which is very small compared with those reported so far in other nematic systems. If the Gaussian angular distribution of the molecular axis around the director \vec{n} is assumed, the angular range of distribution, β is calculated by

$$\langle p_2 \rangle = \frac{\int_0^\pi p_2(\cos \theta) \exp(-\theta^2/2\beta^2) \sin \theta d\theta}{\int_0^\pi \exp(-\theta^2/2\beta^2) \sin \theta d\theta} .$$

(V-6)

The β amounts to 39° at T_c if $\langle p_2 \rangle_c = 0.28$. The $\langle p_2 \rangle$ is plotted again as a function of $T^* = T/T_c$ ($T_c = 375.6$ K) in Fig. V-6 for further discussion.

The first successful molecular theory for nematic order was developed by Maier and Saupe (M-S).⁷⁾ This famous theory is based upon the following major assumptions.

(1) Orientation-dependent intermolecular pairwise potential has a quite simple form,

$$\phi_{12}(\cos\theta_{12}) = -\frac{A}{N V^{\gamma}} P_2(\cos\theta_{12}), \quad (V-7)$$

where θ_{12} is the angle between the long axes of molecule 1 and 2, N and V are the number of molecules and the volume of the system, A is a constant, γ is an exponent defined later.

(2) Molecular field approximation is applicable: i.e. the potential which an individual molecule "feels" is assumed to be

$$\phi_1(\cos\theta_1) = -\frac{A}{V^{\gamma}} \langle P_2 \rangle P_2(\cos\theta_1). \quad (V-8)$$

Here θ_1 is the angle made by the long axis of the molecule 1 and the director.

(3) Molecular distribution function is assumed to be spherical, and the volume dependence of the strength of interaction is taken to be $\gamma = 2$ because the attractive term r^{-6} is thought to be dominant.

The orientational order parameter $\langle P_2 \rangle$ can be calculated in a self-consistent manner, i.e.,

$$\begin{aligned} \langle P_2 \rangle &= \frac{\int_0^1 P_2(\cos \theta_1) \exp \left[\frac{A}{V^{\gamma k T}} \langle P_2 \rangle P_2(\cos \theta_1) \right] d\cos \theta_1}{\int_0^1 \exp \left[\frac{A}{V^{\gamma k T}} \langle P_2 \rangle P_2(\cos \theta_1) \right] d\cos \theta_1} \\ &= \frac{\int_0^1 P_2(\cos \theta_1) \exp \left[\frac{4.541}{T^* V^{*\gamma}} \langle P_2 \rangle P_2(\cos \theta_1) \right] d\cos \theta_1}{\int_0^1 \exp \left[\frac{4.541}{T^* V^{*\gamma}} \langle P_2 \rangle P_2(\cos \theta_1) \right] d\cos \theta_1} \end{aligned}$$

(V-9)

Here T^* and V^* denote the quantities corresponding to T and V reduced by the values at the clearing point, $T^* = T/T_c$, and $V^* = V/V_c$.

After the pioneer work by M-S, some careful analyses were made using γ as an adjustable parameter. The values $\gamma = 3$ by Chandrasekhar and Madhusudana,⁶⁾ and $\gamma = 4$ by Humphries, James, and Luckhurst⁸⁾ were shown to explain the experimental results best. It was shown later by Cotter⁹⁾ that theoretical consistency of the mean field approximation requires that $\gamma = 1$.

In the case of HBAB, a precise density measurement[✓] was made by White et al.¹⁰⁾ By utilizing their data as well as eq. (V-9), $\langle p_2 \rangle$ could be calculated in a self-consistent manner as a function of T^* , and shown in Fig. V-6 for different γ -values. At a glance it seems that using the values $2 \lesssim \gamma \lesssim 4$, the mean field theory can reproduce the data well in the region $T^* \lesssim 0.94$. But where $T^* \gtrsim 0.94$, our experimental data significantly deviates from the theory i.e., a sharp descent of $\langle p_2 \rangle$ takes place towards 0.28 at T_c , whereas the theory predicts that $\langle p_2 \rangle_c = 0.43$ irrespective of γ . The failure of the mean field theory near the clearing temperature is now evident.

The value of $\langle p_2 \rangle_c$ can be lowered to some extent by applying some other statistical methods to eq. (V-7), the M-S potential. For example, Sheng and Wojtowicz¹¹⁾ found the value 0.38 by applying the cluster variation method and assuming the

number of nearest neighbors to be $z = 6$. Lebwohl and Lasher¹²⁾ and Jansen, Vertogen, and Ypma¹³⁾ found that $\langle p_2 \rangle_c = 0.33$ by the Monte-Carlo " experiments. " On the other hand, Humphries, James, and Luckhurst⁸⁾ made a quite different approach to reform the M-S theory. They used the general form of the intermolecular potential first developed by Pople,¹⁴⁾ and taking the first two terms in the expansion, assumed a mean field potential,

$$\begin{aligned} \phi_1(\cos \theta_1) = -A_2 [\langle p_2 \rangle p_2(\cos \theta_1) \\ + \mathcal{E} \langle p_4 \rangle p_4(\cos \theta_1)] . \end{aligned} \quad (V-10)$$

They showed that if the coefficient \mathcal{E} is taken to be negative, $\langle p_2 \rangle$ is lowered in the entire temperature range of interest. But considering that the series, p_n , should converge rapidly, the effect of p_4 is to slide $\langle p_2 \rangle$ along the longitudinal axis to a small extent.

Although several theoretical attempts have been made to obtain lower $\langle p_2 \rangle_c$ values than 0.43,^{8,9,11~13)} any type of the extensions of M-S theory that have been proposed so far cannot explain the steep descent of $\langle p_2 \rangle$ near T_c and the very small value of $\langle p_2 \rangle_c$ in the present substance. The molecular theories of nematic liquid crystal based on anisotropic dispersion force have yielded some successful results for systems having weak dielectric anisotropy such as PAA (p-azoxy-anisole)^{8,11)} etc. But it seems difficult to apply the same

type of theory to the quantitative understanding of molecular order in such a system of strong positive dielectric anisotropy as HBAB. It will be necessary to establish a theoretical treatment which involves strong dipole-dipole interaction between large molecules.

Before closing this section we will discuss the possibility of molecular association due to the strong dipole moment of cyano end group, suggested by Gähwiller¹⁵⁾ (cf. section I-2). It was shown by Sheng¹⁶⁾ that molecular association has an effect on decreasing $\langle p_2 \rangle_c$. The small value of $\langle p_2 \rangle_c$ in HBAB may be related to this effect because (as will be shown in chapter VII, this thesis) HBT, a homologue of HBAB which has small molecular dipole moment, exhibits $\langle p_2 \rangle$ values larger than that of HBAB in the entire T^* region studied. The difference of densities^{10,17)} in the two compounds also support this idea, i.e., HBAB is more closely packed than HBT in the nematic phase. It is interesting to note that Cladis^{18~21)} suggested that molecular association is closely related to the reentrant phenomenon which is one of the peculiar phenomena exhibited only by the nematogens having the cyano end group. HBAB is the constituent of the reentrant mixture first discovered in 1975.¹⁸⁾

§ V-4. Molecular Dynamics in the Nematic Phase

Spin-lattice relaxation rates T_1^{-1} in the nematic and isotropic liquid phases are plotted in Fig. V-7 against reciprocal temperatures. The figure includes the data taken in the under-cooled nematic region. The T_1^{-1} exhibited ω_0 -dependence in the entire nematic region studied, and this is attributable either to (i) order director fluctuation (ODF) or to (ii) translational self-diffusion of molecules (TSD).

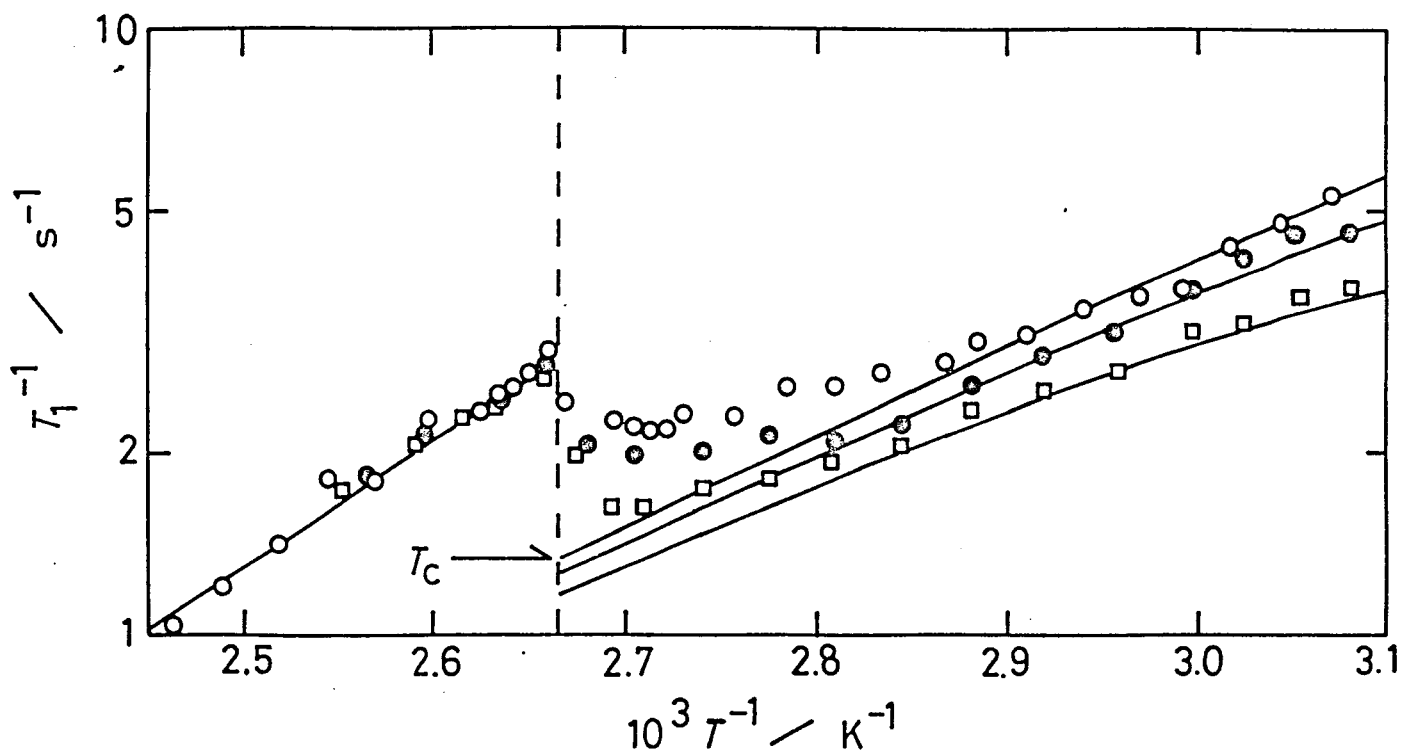


Fig. V-7. Proton spin-lattice relaxation rates in the N and I phases of HBAB. The experimental points \circ , \bullet , and \square represent the data taken at 10.0, 20.5, and 40.5 MHz, respectively. The three lines in the N phase represent the theoretical lines for the three Larmor frequencies, based on eqs. (V-15 & 16) and the parameters given in Table V-2.

ODF-assisted spin-lattice relaxation rate for a pair of proton spins with a fixed internuclear distance was given by Pincus²²⁾ and later modified by Ukleja, Pirs, and Doane²³⁾ in the form,

$$T_1^{-1} = \langle P_2 \rangle^2 B \omega_0^{-1/2} \left[1 - \frac{2\sqrt{2}}{\pi} \left(\frac{\omega_0}{\omega_c} \right)^{1/2} \right],$$

$$B = \frac{9}{8} \gamma^4 \hbar^2 r^{-6} \frac{1}{2\pi} \left(\frac{2\eta}{K^3} \right)^{1/2} k T. \quad (V-12)$$

Here, η is the apparent viscosity, K is the elastic constant under one-elastic-constant approximation (i.e., $K = K_1 = K_2 = K_3$ is assumed), and ω_c denotes the higher cutoff frequency of the director fluctuation. In eq. (V-12), only the sample aligned in the external field (i.e., $\theta_0 = 0$) is considered. As the second term in eq.(V-12) is usually small compared with unity especially in a low viscosity system, the relation $T_1^{-1} \propto \omega_0^{-0.5}$ follows: The temperature-dependence of T_1^{-1} is small except in the vicinity of T_c .

The theory of spin relaxation due to TSD was developed by Torrey²⁴⁾ and Harmon and Muller²⁵⁾ for isotropic liquids. An approximate solution in low but nonzero frequency limit for intermolecular spin-lattice relaxation rate was given by

$$T_1^{-1} = C \cdot D_{iso}^{-1} \left[1 - 0.555 \sigma_0 \left(\frac{\omega_0}{D_{iso}} \right)^{1/2} \right],$$

(V-13)

$$C = \frac{8 \pi n}{15 \sigma_0} \frac{4}{\hbar^2} I(I+1) .$$

Here, D_{iso} , σ_0 , and n denote the scalar diffusion constant, hard sphere diameter of the molecule, and the average number density, respectively. Recently Zumer and Vilfan²⁶⁾ modified this theory in order to apply it to the nematic liquid crystal system taking into account the effects of geometrical distribution of spins within a long molecule, anisotropy of the motion, and anisotropy of the molecular distribution in space. They found by numerical calculations that such effects could be reduced to well within a usual experimental uncertainty, and that eq. (V-13) could be utilized provided that the quantities D_{iso} and σ_0 are replaced by D_{\perp}^0 and d , and that $D_{\parallel}^0/D_{\perp}^0$ is put nearly equal to 2, provided the coupling constant C should be altered properly. The quantity d denotes the hard sphere diameter along the short axis of the molecule, and D_{\parallel}^0 and D_{\perp}^0 represent the components of the diffusion constant tensor parallel and perpendicular to \vec{n} , under the condition of perfect orientational order, and are related to the diffusion constant tensor in a real system by

$$D_{\parallel} = \frac{1}{3} (1 + 2 \langle p_2 \rangle) D_{\parallel}^0 + \frac{2}{3} (1 - \langle p_2 \rangle) D_{\perp}^0 ,$$

$$D_{\perp} = \frac{1}{3} (1 - \langle p_2 \rangle) D_{\parallel}^0 + \frac{1}{3} (2 + \langle p_2 \rangle) D_{\perp}^0 .$$

(V-14)

The relation $D_{\parallel}^0/D_{\perp}^0 \simeq 2$ was adopted to suit the experimental data available up to the present.²⁷⁻²⁹⁾ Now, let us apply eq. (V-13) in a modified form,

$$T_1^{-1}(\omega_0, D_{\perp}^0) = C' D_{\perp}^0^{-1} \left[1 - 0.555 d \left(\frac{\omega_0}{D_{\perp}^0} \right)^{1/2} \right],$$

(V-15)

to the nematic liquid crystal.

By analyzing the ω_0 - and T-dependences of the data by eqs. (V-12 & 15), we can conclude that TSD makes a dominant contribution to T_1^{-1} in the low temperature region of this mesophase. According to the X-ray analysis by Leadbetter et al.,³⁰⁾ d was evaluated to be 0.50 nm irrespective of the samples in such a Sciff base and biphenyl-type nematic systems. So we took this value $d = 0.50$ nm, and assuming that

$$D_{\perp}^0 = D_{\perp}^{00} \exp(-\Delta H_D / RT), \quad (V-16)$$

we can obtain informations on D_{\perp}^0 from the temperature- and frequency-dependences of the experimental T_1^{-1} by utilizing eq. (V-15). The following parameters were thus obtained: $D_{\perp}^{00} = 8.25 \times 10^{-6} \text{ m}^2 \text{ s}^{-1}$, $\Delta H_D = 31.3 \text{ kJ mol}^{-1}$, and $C' = 5.55 \times 10^{-10} \text{ m}^2 \text{ s}^{-1}$. The theoretical curves of eqs. (V-15 & 16) by using these parameters are given in Fig. V-7, demonstrating a good agreement with the data in the low temperature region.

The present stage of our research on self-diffusion is by no means sufficient on the point that the anisotropy of diffusion constant has not been determined experimentally. But according to the data available until now,^{27 ~ 29)} the relation $D_{\parallel}^0 / D_{\perp}^0 \simeq 2$ seems to hold and is not strongly dependent on samples provided that the shapes of the molecules are alike, therefore it is probably not far from truth to derive D_{\parallel} and D_{\perp} from eq.(V-14) assuming $D_{\parallel}^0 / D_{\perp}^0 = 2$. The following results were thus obtained: $D_{\parallel} = 2.7 \times 10^{-10} \text{ m}^2 \text{ s}^{-1}$, $D_{\perp} = 1.7 \times 10^{-10} \text{ m}^2 \text{ s}^{-1}$, and $D_{\parallel} / D_{\perp} = 1.6$ at 345 K.

The deviation of the data from the theory in the high temperature region will be due to ODF mechanism. The relaxation enhancement near T_c indicates the excitation of long-wavelength modes of director fluctuation related with the phase transition. Until now it has been accepted⁵⁾ that for high temperature nematics (which is less viscous) like PAA (p- azoxy-anisole), ODF governs nuclear spin-lattice relaxation and that for low temperature nematics (which is more viscous) like MBBA (p-methoxybenzylidene-p'-butylaniline), TSD governs it. HBAB stands in the intermediate position between PAA and MBBA from the viewpoints of both its temperature range and its rotational viscosity.³¹⁾ This point is consistent with our NMR observations.

§ V-5. Molecular Dynamics in the Isotropic Liquid Phase

The fast component of spin-lattice relaxation rate in the isotropic liquid phase exhibited no appreciable dependence on ω_0 . No effect of critical fluctuation due to short range order in this phase was observed as long as the dominant fast component was concerned. Assuming TSD dominates T_1^{-1} in this phase, we can roughly estimate the value of D_{iso} using eq.(V-13) and the parameter $\sigma_0 \simeq 1.0$ nm obtained from the density data.⁷⁾ The lower bound of D_{iso} , $D_{iso} > 3 \times 10^{-9} \text{ m}^2 \text{ s}^{-1}$ is deduced in order to make it reconcile with the fact that the T_1^{-1} observed at the three different Larmor frequencies should converge within 7 % of their values which is the limit of experimental certainty of our apparatus. This order-of-magnitude estimate will be correct even if contributions from other than TSD is involved in the experimental T_1^{-1} . The diffusion constant D thus increases when the sample passes through the N/I phase transition. But the apparent ΔH_b obtained from the temperature-dependence of T_1^{-1} is 40 kJ mol^{-1} which is greater than that in the nematic phase. In the isotropic phase in which the long range orientational order has vanished, it is expected that a large angle rotation of the molecule about its short axis or of the cluster of molecules is excited and is strongly correlated with TSD. If it is the case, such a motion will be quite effective on T_1^{-1} , and the apparent ΔH_b will indicate the potential barrier for such a correlated motion which can be larger than ΔH_b in the nematic phase.

§ V-6. Summary

Summary of the experimental results and discussion is as follows.

- (1) On the intercrystalline phase transition in HBAB, it was shown that one of the crystalline phases (CII) is the ordered phase and that the other (CI) is the phase with motional disorder with respect to hexyloxy chain. But even in CI, the " melting " of the hexyloxy chain does not take place until the transition to the nematic phase is brought about, where the translational self-diffusion of molecules is also excited.
- (2) The characteristic features^s of the nematic HBAB from the viewpoint of molecular motion are (i) a sharp decrease of orientational order near T_c , (ii) translational self-diffusion with the characteristic frequencies larger than but not far from NMR Larmor frequencies, and (iii) excitation of director fluctuation in the higher temperature region.
- (3) The temperature-dependence of the second rank orientational order parameter $\langle p_2 \rangle$ of nematic HBAB cannot be explained by the available statistical mechanical theories based on Maier-Saupe intermolecular potential. A molecular field treatment with modified potentials (including higher order terms of Legendre polynomials) seems to be insufficient, too. The role of permanent dipole-dipole interaction was suggested.
- (4) Molecular motion in the isotropic liquid phase was examined by the theory of translational self-diffusion in liquids. The diffusion constant increases when the substance is heated from nematic liquid crystal to isotropic liquid. But the

apparent activation enthalpy for self-diffusion also increases, suggesting that the slow rotational mode of a large angle rotation about molecular short axis or of cluster of molecules is excited in this phase and that it is strongly coupled with self-diffusion.

The motional data obtained are summarized in Table V-2.

Further discussion on self-diffusion in the nematic liquid crystal will be given in Chapter VIII.

Table V-2. Summary of motional data in HBAB.

phases	CII	CI		
		three rotational modes		
modes	CH ₃ -reorientation	R ₁ (C ₂ H ₅ ⁻)	R ₂ (C ₂ H ₅ ⁻)	R ₃ (C ₃ H ₇ ⁻)
$\Delta H_f / \text{kJ mol}^{-1}$	11.1	9.1	12.4	19.0
τ_c / s	1.53×10^{-13}	6.13×10^{-13}	6.04×10^{-13}	1.65×10^{-13}
A / s^{-2}	8.82×10^8	7.35×10^8	3.53×10^8	2.48×10^8
phases	nematic liquid crystal	isotropic liquid		
modes	translational self-diffusion	self-diffusion coupled with large angle rotation		
$\Delta H_D / \text{kJ mol}^{-1}$	31	40		
diffusion constants in the h.t. limit	$D_{\perp}^{\text{OO}} = 8.25 \times 10^{-6} \text{ m}^2 \text{ s}^{-1}$ $D_{\parallel}^{\text{OO}} = 1.65 \times 10^{-5} \text{ m}^2 \text{ s}^{-1}$	$D_{\text{iso}}^{\text{O}} > 1.1 \times 10^{-3} \text{ m}^2 \text{ s}^{-1}$ ($D_{\text{iso}} > 3.0 \times 10^{-9} \text{ m}^2 \text{ s}^{-1}$)		

References to chapter V

- 1) H. B. Bürgi and J. D. Dunitz: *Helvetica Chimica Acta* 53 (1970) 1747.
- 2) N. Norman and H. Mathisen: *Acta Chimica Scandinavica* 15 (1961) 1747.
- 3) A. Abragam: " *The Principles of Nuclear Magnetism* " (Clarendon Press, Oxford, 1961), chapters IV, VIII, and X.
- 4) J. G. Powles and H. S. Gutowsky: *J. Chem. Phys.* 21 (1953) 1695.
- 5) J. W. Doane: " *Magnetic Resonance of Phase Transitions* " (ed. F. J. Owens, C. P. Poole, Jr., and H. A. Farach, Academic Press, 1979), chapter 4.
- 6) S. Chandrasekhar and N. V. Madhusudana: *Acta Crystllogr.* A27 (1971) 303.
- 7) W. Maier and A. Saupe: *Z. Naturforsch.* 14a (1959) 882, *ibid.* 15a (1960) 287.
- 8) R. L. Humphries, P. G. James, and G. R. Luckhurst: *J. Chem. Soc. Faraday Trans. II* 68 (1972) 1031.
- 9) M. A. Cotter: *Mol. Cryst. Liq. Cryst.* 39 (1977) 173.
- 10) A. E. White, P. E. Cladis and S. Torza: *Mol. Cryst. Liq. Cryst.* 43 (1977) 13.
- 11) P. Sheng and P. J. Wojtowicz: *Phys. Rev.* A14 (1976) 1883.
- 12) P. A. Lebowhl and G. Lasher: *Phys. Rev.* A6 (1972) 426.
- 13) H. J. Jansen, G. Vertogen, and J. G. J. Ypma: *Mol. Cryst. Liq. Cryst.* 38 (1977) 87.

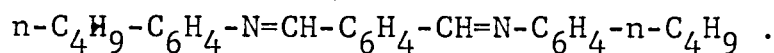
- 14) J. A. Pople: Proc. Roy. Soc. A221 (1954) 498.
- 15) Ch. Gahwiller: Phys. Rev. Lett. 28 (1972) 1554.
- 16) P. Sheng: J. Chem. Phys. 59 (1973) 1942.
- 17) B. Bahadur: Z. Naturforsch. 30a (1975) 1094.
- 18) P. E. Cladis: Phys. Rev. Lett. 35 (1975) 48.
- 19) P. E. Cladis, R. K. Bogardus, W. B. Daniels, and G. N. Tailor: Phys. Rev. Lett. 39 (1977) 720.
- 20) D. Guillon, P. E. Cladis, and J. Stamatoff: Phys. Rev. Lett. 41 (1978) 1598.
- 21) P. E. Cladis, R. K. Bogardus, and D. Aadsen: Phys. Rev. A18 (1978) 2292.
- 22) P. Pincus: Solid State Commun. 7 (1969) 415.
- 23) P. Ukleja, J. Pirs, and J. W. Doane: Phys. Rev. A14 (1976) 414.
- 24) H. C. Torrey: Phys. Rev. 92 (1953) 962.
- 25) J. F. Harmon and B. H. Muller: Phys. Rev. 182 (1969) 400.
- 26) S. Žumer and M. Vilfan: Phys. Rev. A17 (1978) 424.
- 27) C. K. Yun and A. G. Frederickson: Mol. Cryst. Liq. Cryst. 12 (1970) 73.
- 28) I. Zupančič, J. Pirš, M. Luzar, and R. Blinc: Solid State Commun. 15 (1974) 227.
- 29) G. J. Krüger and H. Spiesecke: Z. Naturforsch. 28a (1973) 964.
- 30) A. J. Leadbetter, R. M. Richardson, and C. N. Colling: J. Phys. (Paris) 36 (1975) C1-37.

Chapter VI. Molecular Motion in the Smectic Liquid
Crystalline Compound HBAC

§ VI-1. Purpose of this work

Recent studies on smectic liquid crystals have brought about considerable amount of new information especially on their static structures.¹⁾ But the well-established knowledge about the dynamical aspects of these mesophases is very little yet. In order to fully understand the properties of the various mesophases called " smectic, " and also to establish the idea which distinguishes the " three-dimensional smectic liquid crystal " from crystals, the knowledge about the dynamical properties of these mesophases are strongly desired. In 1970's TBBA²⁾ (terephthal-bis-p-butylaniline*) has been studied as a model compound of smectic liquid crystal by utilizing various experimental techniques, and some fundamental features of the smectic phases especially the orientational order of a few kind of smectic variations have been analyzed.²⁾ It is strongly desired to examine the successive excitation of modes of molecular motion from the crystalline state to the isotropic liquid state using a simpler molecule. HBAC is such a kind of compound. It is another objective of this work to try to detect the collective excitation of orientational fluctuation in the smectic phase by nuclear spin-lattice relaxation measurements.

*) The chemical formula of TBBA is



§ VI-2. The Crystalline State

The second moment of NMR lines in the temperature range studied is shown in Fig. VI-1. In the crystalline state, the lineshape showed no fine structure. The second moment decreased from 16.4 G² at 77 K to 9.0 G² at 326 K, suggesting a successive excitation of segmental motion in the hexyloxy chain. The trends of second moment reduction in the crystalline HBAC shows an intermediate feature between those of the ordered and the

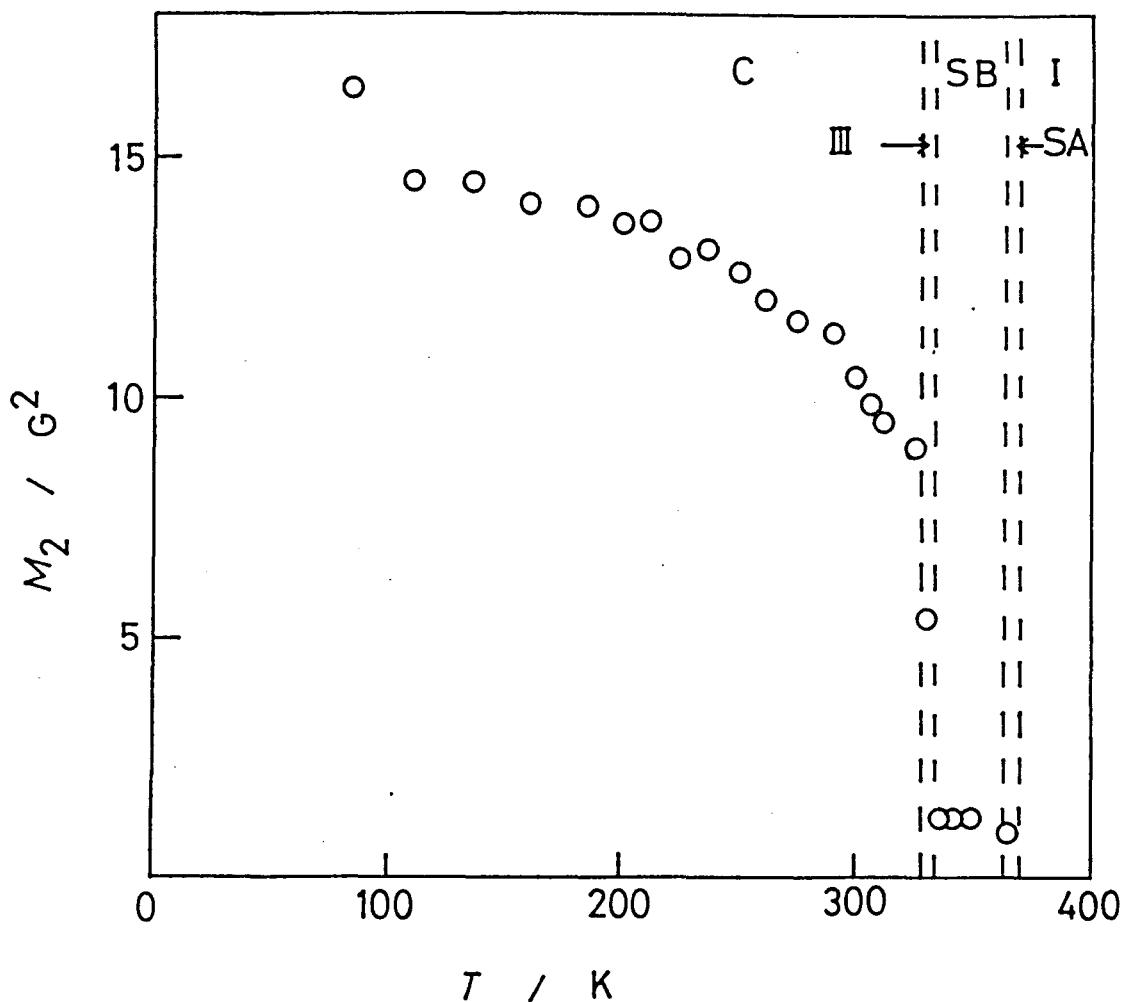


Fig. VI-1. Second moments of proton NMR lines in the C, III, SB and SA phases of HBAC.

disordered crystalline phases of HBAB, suggesting the existence of a small amount of disorder in this phase.

Fig. VI-2 shows the spin-lattice relaxation rates observed at 10.0 MHz in the crystalline HBAC. It is evident from the magnitude and the location of the relaxation maximum that the relaxation process below 170 K is the reorientational motion of the terminal methyl group of the hexyloxy chain. The solid

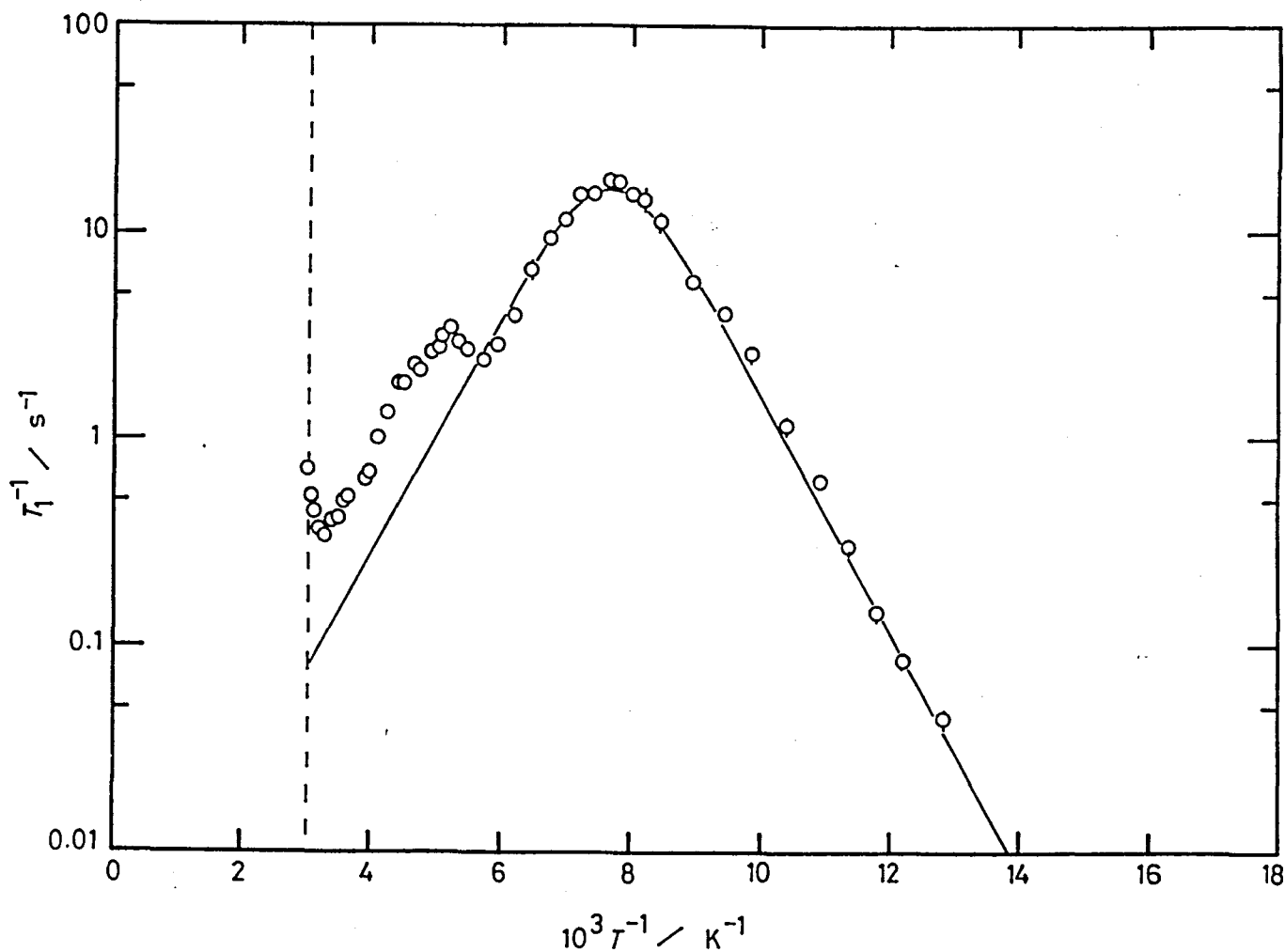


Fig. VI-2. Proton spin-lattice relaxation rates measured at 10.0 MHz in the crystalline HBAC.

line in Fig. VI-2 represents the calculated relaxation rates due to this mechanism assuming an Arrhenius type activation of the correlation frequency. The activation enthalpy and the preexponential factor were determined to be $\Delta H = 11 \text{ kJ mol}^{-1}$ and $\tau_0 = 4.01 \times 10^{-13} \text{ s}$. In the higher temperature region two other relaxation mechanisms were observed. Because the methyl group reorientation is the only motion possible without causing any kind of disorder in the crystal, the two relaxation mechanisms are related to some kind of motional disorder. But according to our calculation, the value of maximum relaxation rate at 192 K ($10^3 T^{-1} = 5.2 \text{ K}^{-1}$) and the corresponding second moment reduction are too small to be attributed to any kind of jump rotation of the chain segment (cf. section V-2). So we assign this mechanism to a kind of large angle oscillation of the chain segment. The apparent activation enthalpy was determined to be 13 kJ mol^{-1} . The origin of the third relaxation mechanism with the activation enthalpy of 31 kJ mol^{-1} near the melting temperature is another kind of segmental motion.

§ VI-3. The Phase III

A proton NMR absorption derivative in the phase III is presented in Fig. VI-3, which clearly fits to the calculated Gaussian derivative with the maximum-slope-width ($\mathcal{E}H_{\text{msw}}$) of 4.5 G and the second moment (M_2) of 5.1 G^2 . According to our calculation of intramolecular contribution to M_2 tabulated in Table V-1, it is concluded that the rotational motion of the

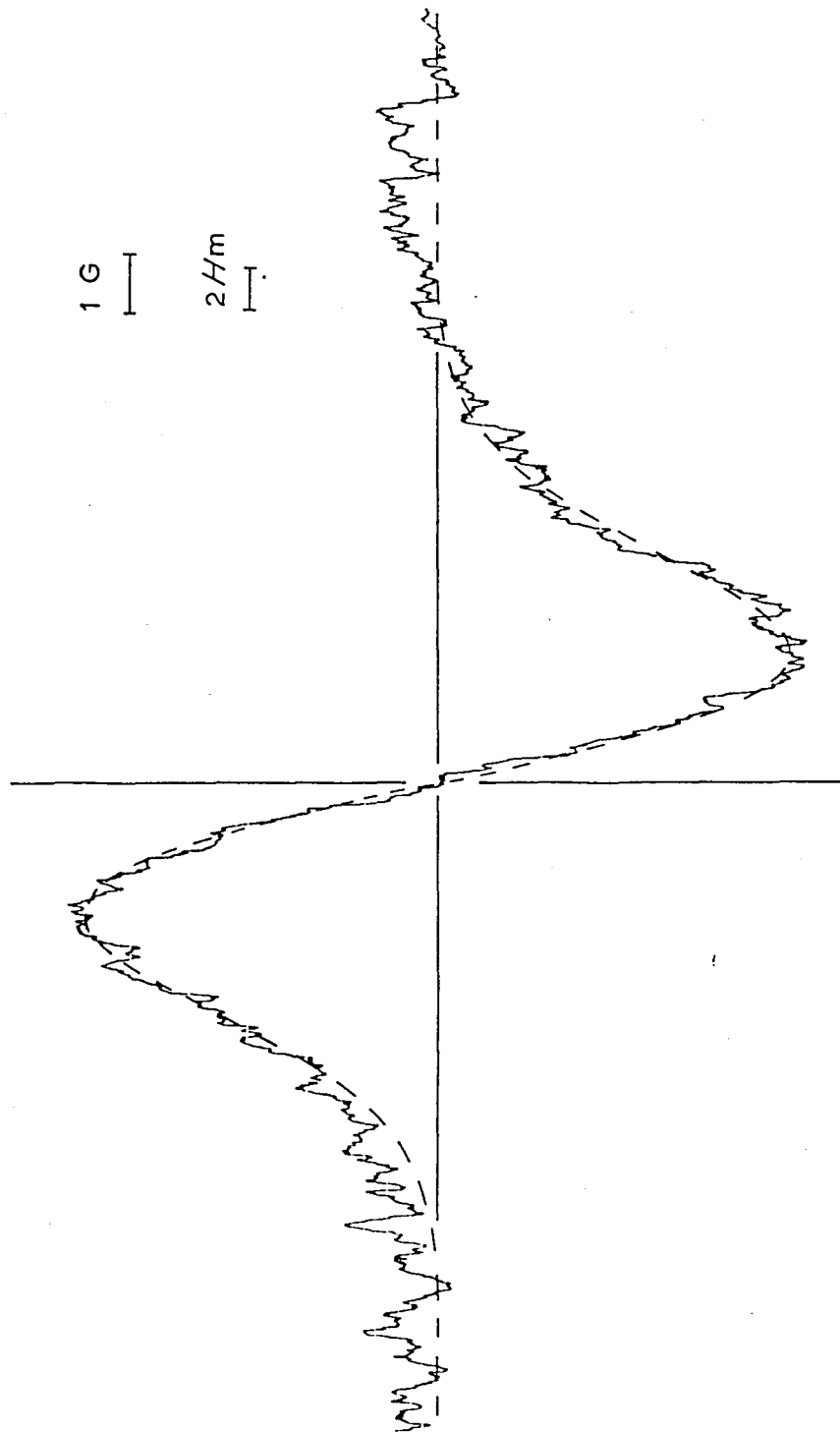


Fig. VI-3. Proton NMR absorption derivative in the phase III (330.5 K) of HBAC. The broken line is the calculated Gaussian derivative with the maximum-slope-width (δH_{msw}) of 4.5 G. The modulation width, $2H_m$, of the spectrometer is indicated.

hexyloxy chain is highly activated in this phase, but that the self-diffusion of the molecules is not activated enough.

Fig. VI-4 (a) shows the spin-lattice relaxation rates in the phase III measured at three different Larmor frequencies . The relaxation rates depend on the frequencies, ω_0 , and have negative gradients against T^{-1} . These facts suggest that a kind of slow motion (with the correlation frequency, $\tau_c^{-1} \ll \omega_0$) contributes to the relaxation rate. As it is evident from NMR lineshape that translational self-diffusion (TSD) does not contribute to T_1^{-1} , we can attribute this slow motion to a kind of random rotational motion. On such an assumption, the spin-lattice relaxation rate can be divided into two different types of contributions, i. e.,

$$T_1^{-1} = 2 A_s \omega_0^{-2} \tau_s^{-1} + 5 \sum_j A_j \tau_j . \quad (\text{VI-1})$$

The first term in eq. (VI-1) represents the contribution from the slow mode in question, whereas the second terms represent those from the other fast modes represented by j . The τ_s^{-1} and A_s are the correlation frequency of the slow mode and the dipolar coupling constant. We can selectively extract the information about the slow mode by taking the difference of T_1^{-1} measured at two different Larmor frequencies, ω_0 and ω_0' , at a fixed temperature, i. e. ,

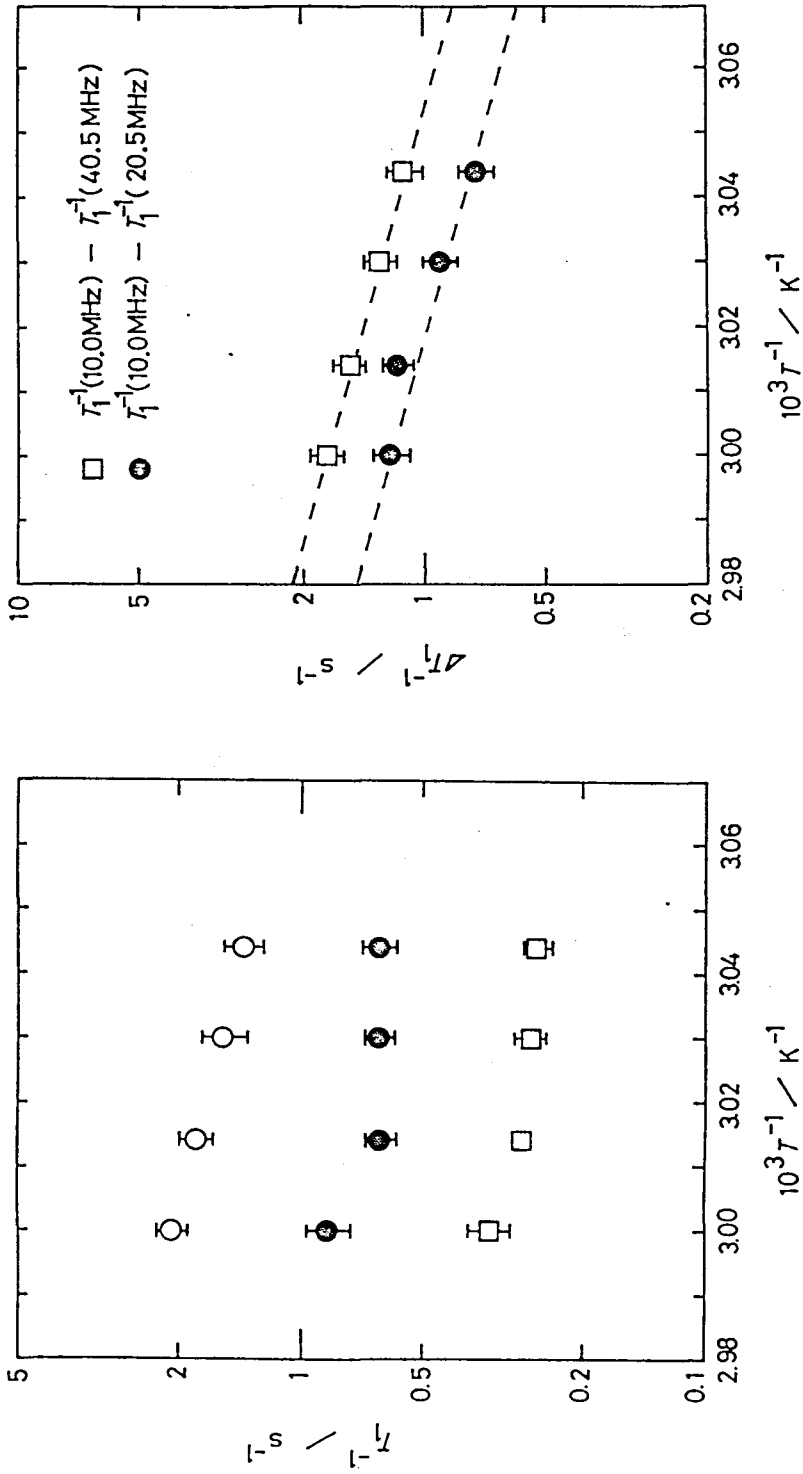


Fig. VI-4. (a); Proton spin-lattice relaxation rates in the phase III of HBAC measured at 10.0 (○), 20.5 (●), and 40.5 (□) MHz. (b); Differences of the spin-lattice relaxation rates measured at different Larmor frequencies.

$$\begin{aligned} \Delta T_1^{-1}(\omega_0, \omega_0', T) &\equiv T_1^{-1}(\omega_0, T) \\ &\quad - T_1^{-1}(\omega_0', T) \\ &= 2 A_s (\omega_0^{-2} - \omega_0'^{-2}) \tau_s^{-1} . \end{aligned}$$

(VI-2)

The temperature dependence of $\Delta T_1^{-1}(\omega_0, \omega_0', T)$ gives that of τ_s^{-1} . Two $\Delta T_1^{-1}(\omega_0, \omega_0', T)$ were deduced from the three experimental T_1^{-1} values corresponding to the three Larmor frequencies at each temperature, and are shown in Fig. VI-4 (b). They gave, when plotted against T^{-1} , straight lines with almost the same slope, yielding the activation enthalpy $\Delta H_s = 82 \pm 16 \text{ kJ mol}^{-1}$. This value means the existence of a considerably high potential barrier for the rotational motion of the hexyloxy chain.

The phase III has not been well identified either as a crystalline phase nor as a kind of smectic state until now. But the present analysis of modes of molecular motion and their time-scales showed that this phase has a character of a kind of crystalline state.

§ VI-4. The Smectic B mesophase

Fig. VI-5 (a) shows an absorption derivative of NMR line in the SB mesophase. The lineshape drastically changes at

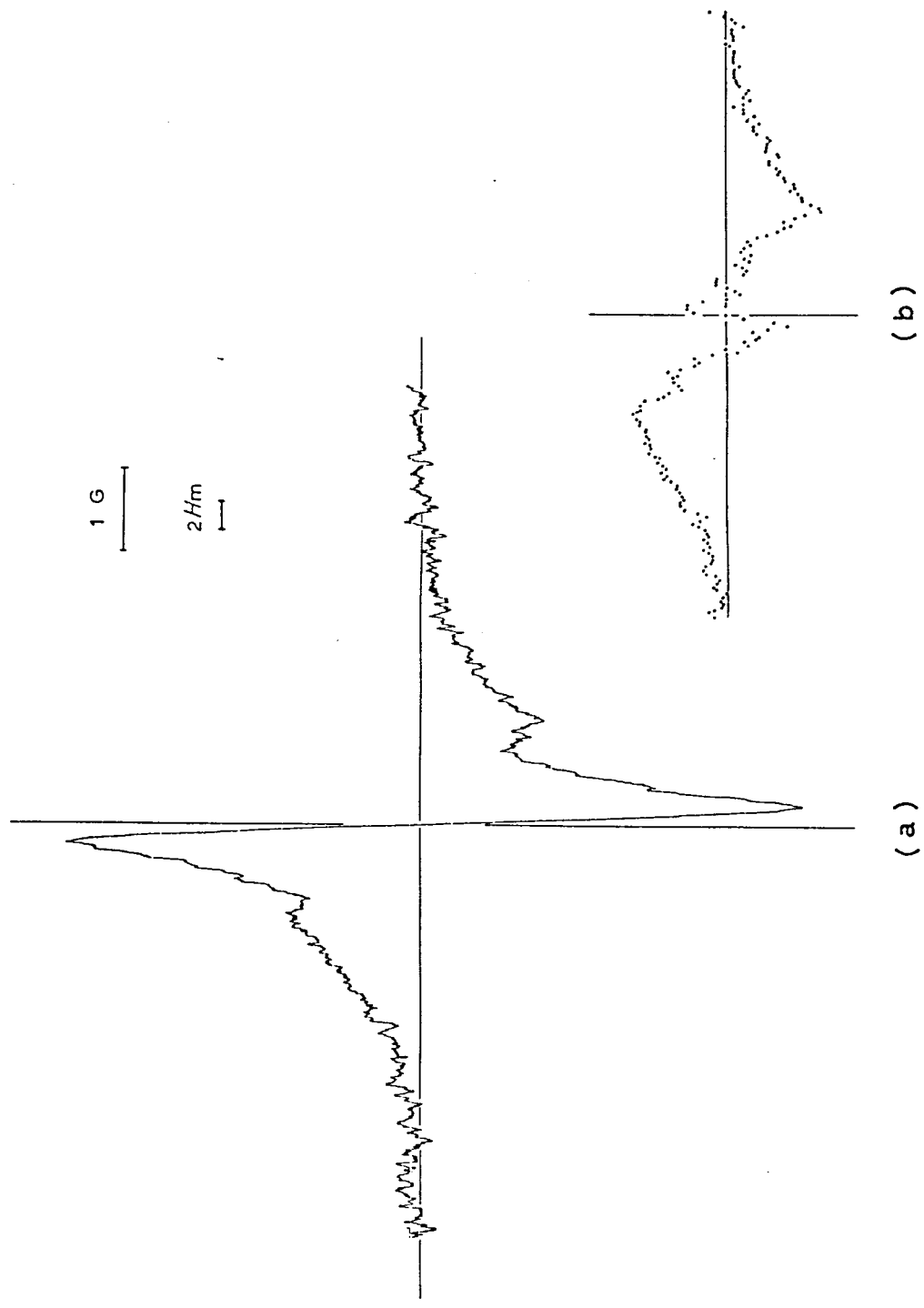


Fig. VI-5. (a); Proton NMR absorption derivative in the SB mesophase (349.7 K) of HBAC.
(b); Residual spectrum of (a) from which the calculated Lorentzian derivative with $\delta H_{msw} = 0.44$ G has been subtracted.

the transition III→SB. The spectrum in the SB mesophase consists of one narrow central component with $\delta H_{\text{msw}} = 0.44$ G and outer components with $\delta H_{\text{msw}} = 2.29$ G. The second moment value 1.25 G^2 of this line shows that the intermolecular dipole interactions have been reduced by the translational self-diffusion (the intermolecular contribution to M_2 in the crystalline state was estimated to be about 2 G^2 in section V-2), in addition to the strong reduction of intramolecular contribution by the highly excited rotational motion of the chain. Then the spectrum of the chain protons would be approximated by a Lorentzian line corresponding to the central component of the spectrum (a) in Fig. VI-5. Fig. VI-5 (b) shows the residual spectrum of (a) from which the calculated Lorentzian derivative with $\delta H_{\text{msw}} = 0.44$ G has been subtracted. This is a typical " powder pattern " of dipolar doublets.³⁾ In the present case, this doublets is formed by the adjacent proton pairs within a benzene ring.

Thus the NMR lineshape in the SB mesophase indicates the following facts.

(1) The rotational correlation frequency of the hexyloxy chain as a whole is faster than 10^5 s^{-1} which is the NMR linewidth in the solid state.

(2) The characteristic frequency of the translational self-diffusion is also faster than 10^5 s^{-1} . This point is the outstanding difference between the phases III and SB.

(3) The dipole-dipole interaction between the ring protons within a benzene ring are not reduced to a negligible amount

because of the existence of one-dimensional orientational order (parallel to the director). But the applied magnetic field (0.47 T) in our experiment is not sufficient to align the directors parallel to the external field. This is the origin of the " powder pattern " of the dipolar doublets.

The spin-lattice relaxation rates in SB (including the undercooled region), SA, and the isotropic liquid phases are presented in Fig. VI-6 as a function of temperature and frequency. The T_1^{-1} decreases with increasing temperature within each phase, but increases discontinuously at the phase transition, suggesting that several motional modes contribute in different ways in the three different kind of phases. We will now concentrate on the SB mesophase.

In order to analyse the T_1^{-1} data in the SB mesophase, let us divide T_1^{-1} into two parts, the ω_0 -dependent and the independent parts, i.e.,

$$T_1^{-1}(\omega_0, T) = A(T) \omega_0^\gamma + B(T) . \quad (\text{VI-3})$$

Some of the experimental data are extracted from Fig. VI-6, and plotted again in Fig. VI-7, showing that the exponent $\gamma = -0.5$ holds in the almost full temperature region of SB. It can also be recognized from Fig. VI-7 that $A(T)$ is a very weak function of T whereas $B(T)$ strongly depends on T . Now let us analyze the data to see what the origin of these terms are. Before discussing the motional modes, we will be reminded here

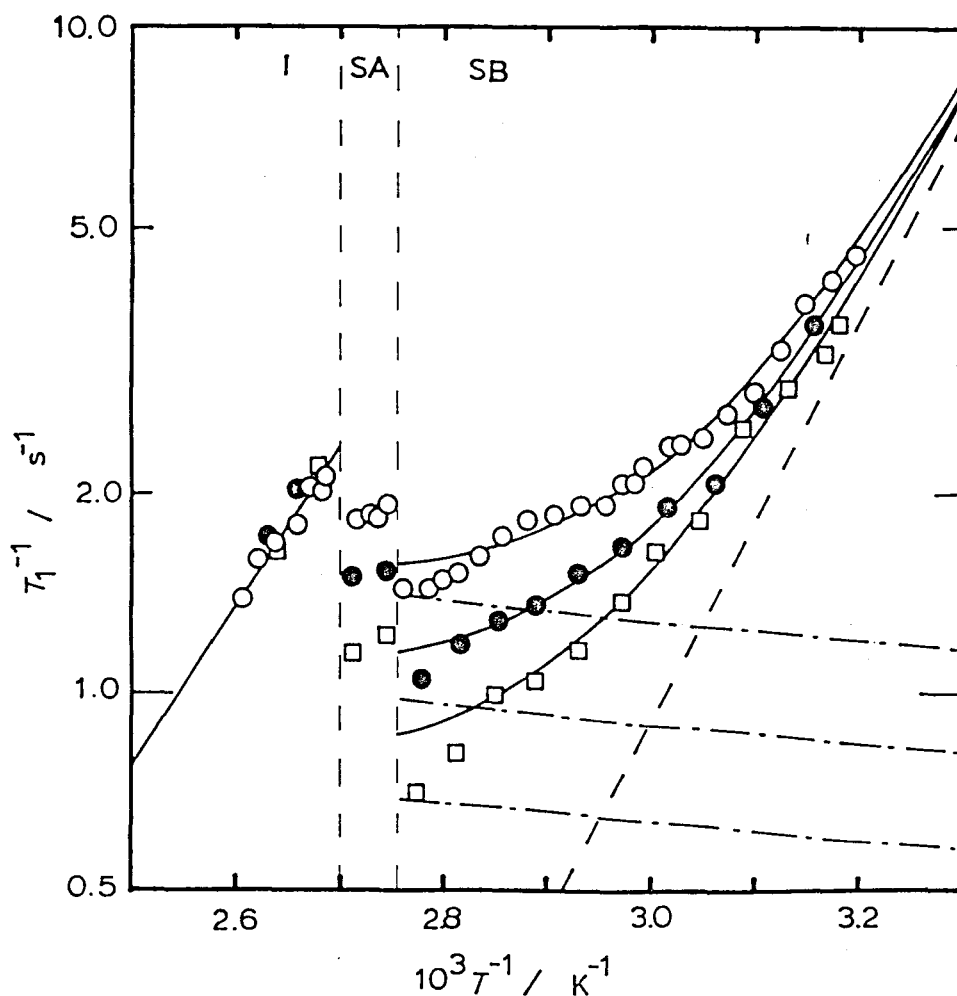


Fig. VI-6. Temperature-dependence of the proton spin-lattice relaxation rates in the SB, SA, and I phases of HBAC, measured at 10.0 (○), 20.5 (●), and 40.5 MHz (□). The solid lines in the SB region are the calculated ones using eqs. (VI-3,5, & 6) with $\gamma = -0.5$ for each Larmor frequency. The broken line represents $B(T)$, and the dashed broken lines represent $A(T)$. The parameters are given in the text. The solid line in the phase I shows $H = 46 \text{ kJ mol}^{-1}$.

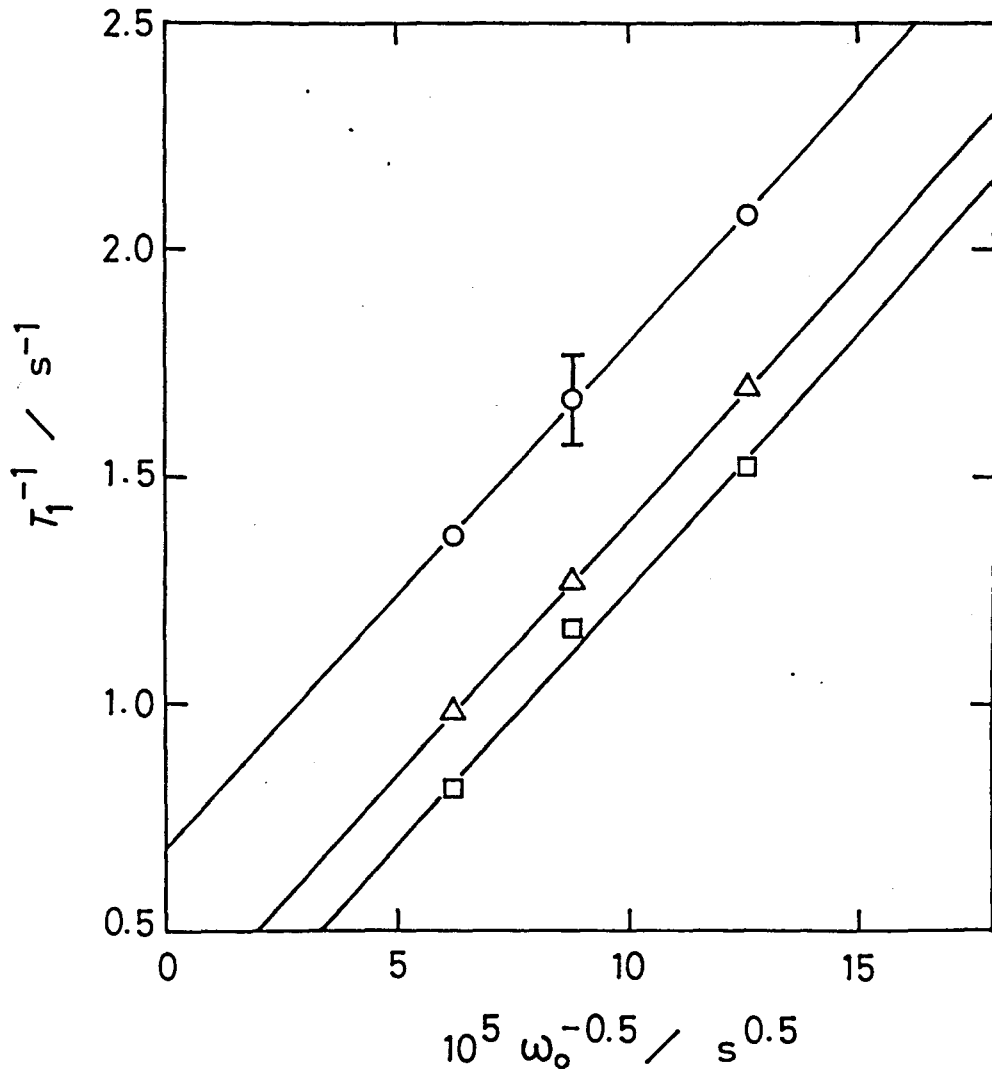


Fig. VI-7. Frequency-dependence of the proton spin-lattice relaxation rates in the SB mesophase of HBAC at some different temperatures: \circ at 336.4 K, \triangle at 350.9 K, and \square at 355.2 K. Typical experimental uncertainty is indicated.

that the spin-diffusion to paramagnetic impurities is ruled out from the possible mechanisms of spin-lattice relaxation as long as the relaxation rates faster than 0.045 s^{-1} are being discussed. It is because such a slow rate $T_1^{-1} = 0.045 \text{ s}^{-1}$ was observed at 77 K in the crystalline state, where no effect of paramagnetic impurity was evident.

The three different kinds of fluctuation are the candidates of spin-lattice relaxation mechanism in this phase.

(1) rotational fluctuation of the hexyloxy chain.

We have already recognized that the rotational correlation frequency τ_R^{-1} of this mode is faster than 10^5 s^{-1} . If τ_R^{-1} is in the order of $10^6 \sim 10^8 \text{ s}^{-1}$, T_1^{-1} due to this mode will be near its relaxation maximum. The frequency-dependent term with negative gradient against T^{-1} will be expected, and it will provide a very strong origin of T_1^{-1} . This temperature-dependence, however, is contrary to the experimental results. And so, it is concluded that this mode is in the extreme narrowing limit ($\tau_R^{-1} \gg \omega_0$) contributing to T_1^{-1} through ω_0 -independent term $B(T)$ with positive gradient against T^{-1} .

(2) translational fluctuation of the molecules.

Although the recent work by Vilfan and Žumer⁴⁾ revealed that T_1^{-1} due to translational self-diffusion (TSD) in the smectic liquid crystal cannot be expressed in a simple analytical form, the qualitative feature of it in the NMR frequency region is well expressed by the Harmon-Muller equation (eq. (V-13)) for the isotropic liquid,

$$T_1^{-1} = C \cdot D_{iso}^{-1} \left[1 - 0.555 \sigma_0 \left(\frac{\omega_0}{D_{iso}} \right)^{1/2} \right]. \quad (VI-4)$$

If this mode is one of the dominant mechanisms of T_1^{-1} , $A(T)$ in eq. (VI-3) becomes strongly dependent on temperature, and consequently, the ω_0 -dependent term becomes smaller as the temperature is raised, which is contrary to our experimental results. The contribution of TSD is thus small in this mesophase.

(3) orientational fluctuation.

As we have discussed in chapter II, T_1^{-1} due to undulation of the smectic layer will give the relation $T_1^{-1} \propto \omega_0^\gamma$ ($\gamma = -1$) in the present NMR time-scale. If the three-dimensional fluctuation of the director is introduced into the theory, the relation $\gamma = -1/2$ is predicted. The latter one is most favorable for the fitting to the data. Anyway, the ω_0 - and T-dependence of the observed T_1^{-1} in the SB mesophase can be interpreted only by introducing the mechanism of orientational fluctuation. By assuming

$$A(T) = A_0 T, \quad (VI-5)$$

and
$$B(T) = B_0 \exp(\Delta H_B / RT), \quad (VI-6)$$

and fitting the theory to the data, the T_1^{-1} were simulated for the three Larmor frequencies. The first term $A(T) \omega_0^\gamma$ represents the contribution from the orientational fluctuation.

The temperature-dependences of the elastic constants, viscosity, and the orientational order parameter are neglected when eq. (VI-5) is assumed. This will be justified in the SB mesophase except in the close vicinity of the transition point, SA/SB. The lines in Fig. VI-6 represent the calculated lines assuming $\gamma = -0.5$, whereas the lines in Fig. VI-8 represent those assuming $\gamma = -1$. The agreement with the experiment is more satisfactory in the former one ($\gamma = -0.5$) than the latter, but it is doubtful whether this theory based on the three-dimensional director fluctuation can justifiably applied to the smectic B mesophase which is more stiffly ordered mesophase than smectic A. Apparent disagreement in Fig. VI-8 will be improved by introducing a ω_0 -dependent term of TSD. Success of the work is thus imperfect at the present stage of investigation. But it has been shown that the orientational fluctuation in the smectic B phase was detected by nuclear spin-lattice relaxation, and has been explained at least qualitatively by the theory developed in chapter II, this thesis.

The frequency-independent contribution to T_1^{-1} comes mainly from the rotational mode of the hexyloxy chain. The effect of self-diffusion is small in this phase.

The parameters used in the calculations are as follows. Fig. VI-6; $A_0 = 30.6 \text{ s}^{-3/2}$, $B_0 = 8.68 \times 10^{-10} \text{ s}^{-1}$, and $\Delta H_B = 58 \text{ kJ mol}^{-1}$. Fig. VI-8; $A_0 = 1.51 \times 10^5 \text{ s}^{-2} \text{ K}^{-1}$, $B_0 = 1.31 \times 10^{-5} \text{ s}^{-1}$, and $\Delta H_B = 32 \text{ kJ mol}^{-1}$.

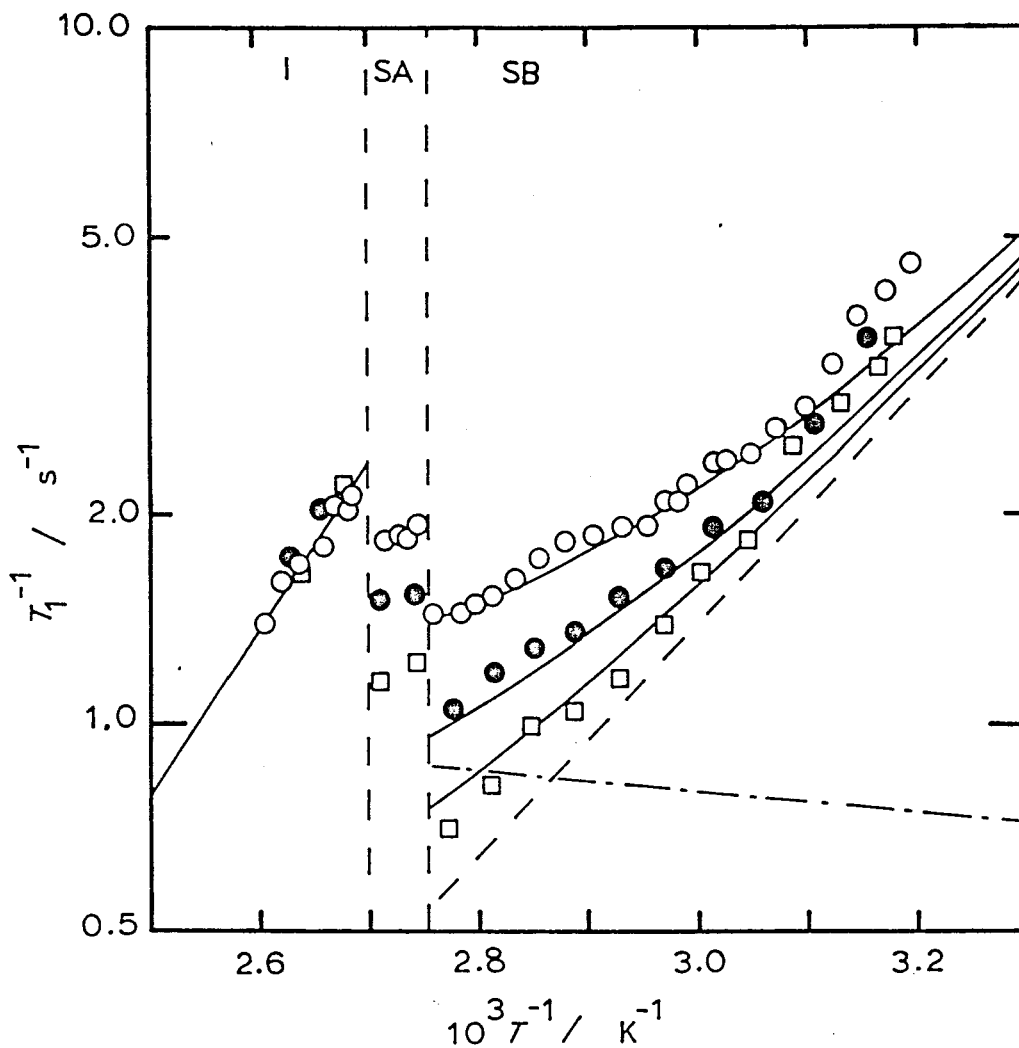


Fig. VI-8. Proton spin-lattice relaxation rates in HBAC. The solid lines in the SB region is calculated by utilizing eqs. (V-3, 5, & 6) with $\gamma = -1$, and with the parameters given in the text. The three lines corresponds to 10.0, 20.5, and 40.5 MHz. The broken line represents $B(T)$, and the dashed broken line represents $A(T)$ for 10.0 MHz. The experimental points are the same as those in Fig. VI-6.

§ VI-5. The Smectic A Mesophase and the Isotropic Liquid Phase

The NMR lineshape showed no qualitative change at the transition SB/SA. It can be seen from Fig. VI-6 that the increment of T_1^{-1} on going from SB to SA comes from the $B(T)$ term in eq. (VI-3), the ω_0 -independent term. This will indicate that the effect of TSD is more significant in SA mesophase than in SB mesophase. The T_1^{-1} in the isotropic phase exhibited no significant ω_0 -dependence. The activation enthalpy obtained from the T-dependence of T_1^{-1} is 46 kJ mol^{-1} , which is the activation barrier for self-diffusion coupled with large angle rotation.

§ VI-6. Summary

Various motional modes were examined in relation to their effects on NMR spectra and T_1^{-1} in HBAC. In the crystalline phase, large angle oscillatory modes related to chain segments were observed in addition to the methyl group reorientation. In the phase III, no effect of translational diffusion but a low-frequency rotational mode ($\tau_s^{-1} \ll 10^8 \text{ s}^{-1}$) of the chain was detected, and its activation enthalpy was $82 \pm 16 \text{ kJ mol}^{-1}$. These results reveal that this unidentified phase has a character of a crystalline state looked upon through the eyes of NMR. Molecular motion in the SB mesophase is characterized by the collective excitation of orientational fluctuation and the rotational motion ($\tau_R^{-1} \gg 10^8 \text{ s}^{-1}$) of the hexyloxy chain

with a lower activation enthalpy than that in the phase III. The effect of self-diffusion is more significant in SA than in SB. The activation enthalpy for self-diffusion coupled with rotation in the isotropic phase is 46 kJ mol^{-1} .

References to chapter VI

- 1) A. de Vries: Mol. Cryst. Liq. Cryst. 63 (1981) 215.
- 2) A. J. Dianoux and F. Volino: J. Phys. (Paris) 40 (1979) 181. and the references therein.
- 3) G. E. Pake: J. Chem. Phys. 16 (1948) 327.
- 4) M. Vilfan and S. Žumer: Phys. Rev. A21 (1980) 672.

Chapter VII Molecular Motion in HBT

§ VII-1. Purpose^{of} of This Work

The phase relations of HBT has a close resemblance to that of HBAB (Fig. I-1). So the comparative study of the motional states of these two compounds will throw some light on understanding of the effect of the terminal substituent. Another objective of this study is to develop the experimental study on the dynamical nature of the smectic mesophase.

§ VII-2. The Crystalline states

The proton spin-lattice relaxation rates measured at 10.0 MHz in the crystalline phases, CII and CI, are shown in Figs. VII-1 & 2, respectively.

As can be clearly seen from Fig. VII-1, the reorientation of the methyl group at the end of the chain is the only mechanism of spin-lattice relaxation in the phase CII. Although HBT has another methyl group bonded to the benzene ring, the relaxation maxima due to quantum mechanical tunnelling motion of this group is expected to take place at still lower temperatures,¹⁾ which is out of our interest at present. By utilizing eqs. (V-1 & 2) as usual, the empirical coupling constant and the activation parameters were determined to be $A = 6.61 \times 10^8 \text{ s}^{-2}$, $\tau_0 = 1.82 \times 10^{-12} \text{ s}$, and $\Delta H = 8.92 \text{ kJ mol}^{-1}$ for the classical reorientation of the chain methyl group.

The T_1^{-1} in the phase CI is shown in Fig. VII-2, in which two branches are seen. Fitting to the data gave two activation enthalpies, 10.0 kJ mol^{-1} and 58.2 kJ mol^{-1} , for the low

temperature and the high temperature branches, respectively. They can be assigned to the terminal methyl reorientation and a kind of segmental motion of the hexyloxy chain, respectively. The methyl reorientation branch obtained in CII is also represented in Fig. VII-2 for comparison.

It has been made clear that the extent of disorder in CI of HBT is far smaller than that in CI of HBAB. This is in accordance with our thermal analysis presented in chapter IV.

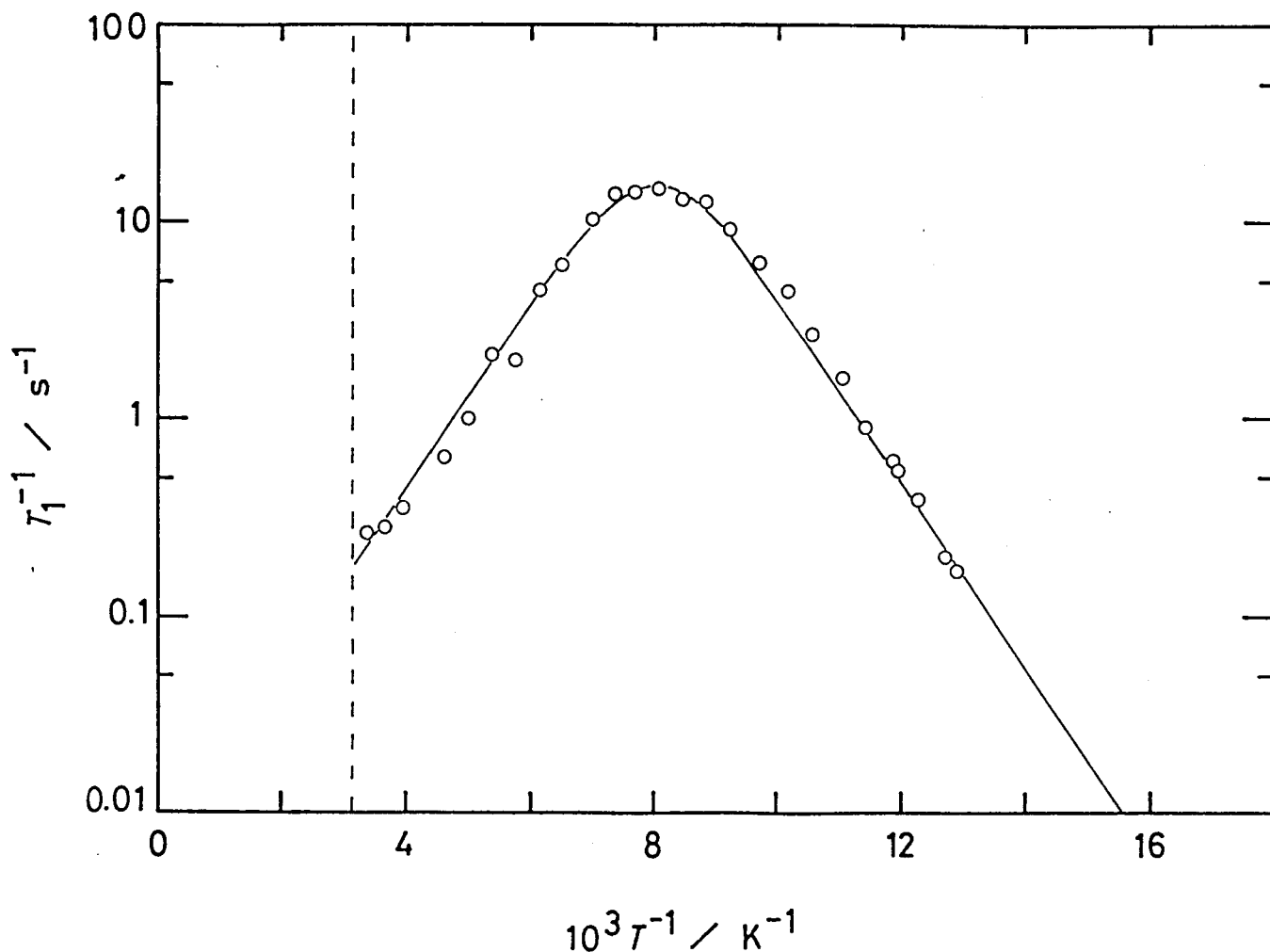


Fig. VII-1. Proton spin-lattice relaxation rate measured at 10.0 MHz in the crystalline phase CII of HBT. The solid line is the calculated line using the parameters given in the text.

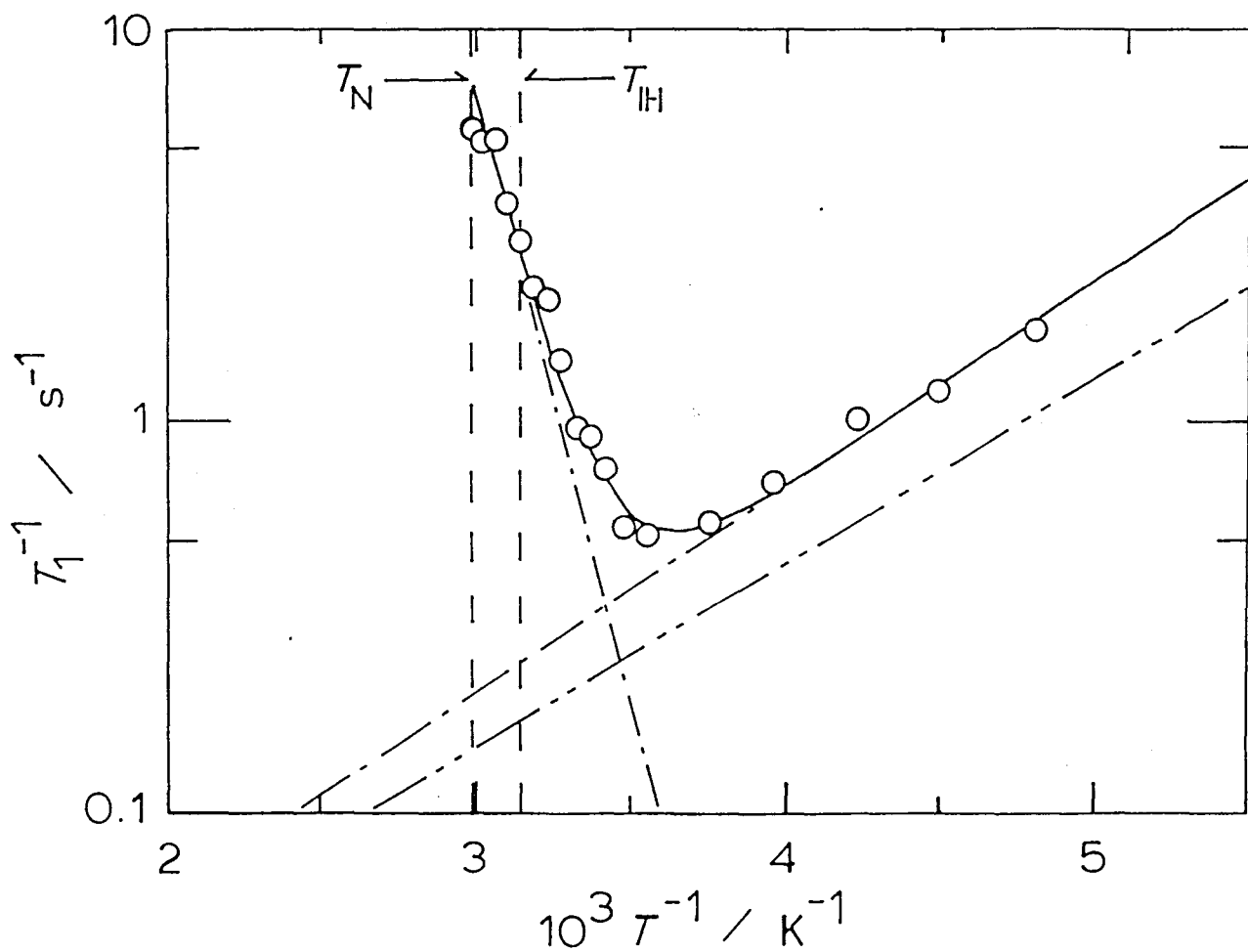


Fig. VII-2. Proton spin-lattice relaxation rate measured at 10.0 MHz in the crystalline phase CI of HBT. The two branches represented by $-\cdot-\cdot-$ show activation enthalpies of 10.0 kJ mol^{-1} (LT) and 58.2 kJ mol^{-1} (HT). The T_1^{-1} due to the methyl reorientation in CII is represented by $-\cdot-\cdot-$ for comparison.

§ VII-3. The nematic and the isotropic Liquid Phases

The orientational order parameter obtained by measuring the dipolar splitting width of NMR spectrum is presented in Fig. VII-3 as a function of T^* ($= T/T_c$). The results of self-consistent field calculations are also shown in the figure. The procedure of analysis was already given in chapter V, and the experimental data of the density of nematic HBT was taken from ref. 2. The experimental value of $\langle p_2 \rangle$ thus obtained at T_c was 0.39 which is close to the mean-field value 0.43, but the deviation from the theory becomes greater as the temperature is lowered.

It is informative to compare the results of the T^* -dependence of $\langle p_2 \rangle$ in nematic HBT and HBAB, both of which clearly show the failure of the mean-field theory. The outstanding difference between them is that the value of $\langle p_2 \rangle$ is larger for HBAB than for HBT in the entire T^* region. It is, however, quite interesting to recognize that the two compounds show some common features suggesting the existence of a kind of corresponding state: The value of $\langle p_2 \rangle$ was found to be 0.71 at the transition point CI/N in both compounds and was found to be about 0.78 at the limit of undercooling. If these facts suggest some general law, the fact that HBAB has a very wide temperature range of nematic phase is closely related to the low value of $\langle p_2 \rangle$. As has been discussed in chapter V, the very low value of $\langle p_2 \rangle$ in HBAB will at least partly be related to molecular association due to the strong dipole moment of the cyano end group.

In the discussion on the reentrant phenomena³⁾ in liquid crystals, Cladis⁴⁾ pointed out phenomenologically that association of molecules enhances the stability of the nematic state. Our comparative study of $\langle p_2 \rangle$ in HBT and HBAB presented here gives a clue to develop molecular theories of the stability of the nematic phase and the reentrant phenomena beyond mean-field approximation.

The results of proton spin-lattice relaxation rates in the nematic, isotropic, and the metastable smectic B phases are presented in Fig. VII-4.

In the nematic phase, the relaxation enhancements in the low and the high temperature regions will be due to translational self-diffusion and order director fluctuation. But the quantitative analysis of the data was not attempted because of the narrow nematic temperature range and overlapping of the modes.

The T_1^{-1} in the isotropic liquid phase exhibited no ω_0 -dependence. The activation enthalpy obtained from the T-dependence of T_1^{-1} is 43 ± 4 kJ mol⁻¹, which coincides with that of HBAB within the experimental accuracy.

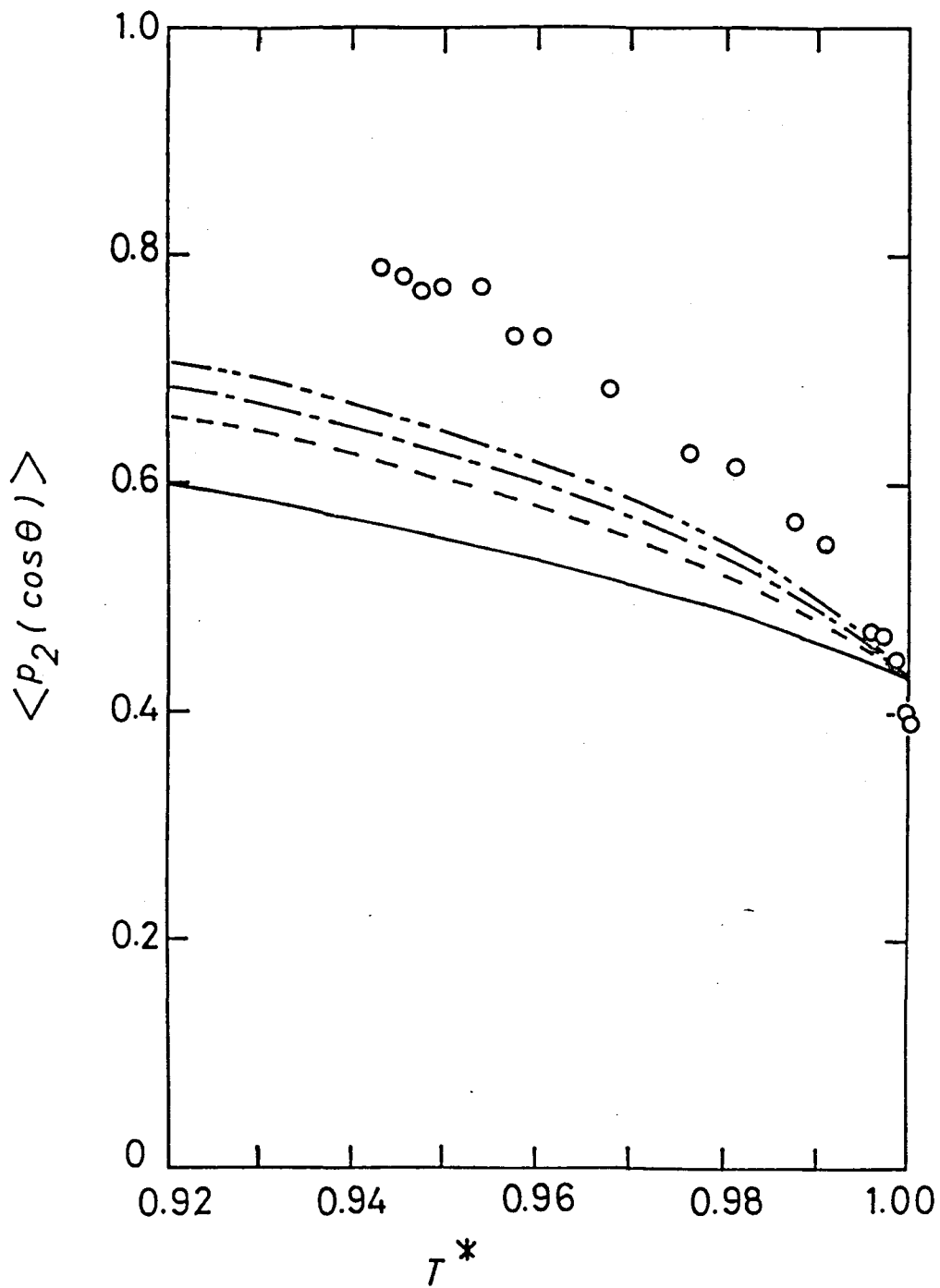


Fig. VII-3. The second rank order parameter in the nematic HBT. The theoretical curves are calculated by utilizing eq. (V-9): ——— for $\gamma = 0$ (neglecting volume change), — — — for $\gamma = 2$ (Maier-Saupe), — · — · — for $\gamma = 3$ (Chandrasekhar-Madhusudana), and — · · — · — $\gamma = 4$ (Humphries-James-Luckhurst).
 for

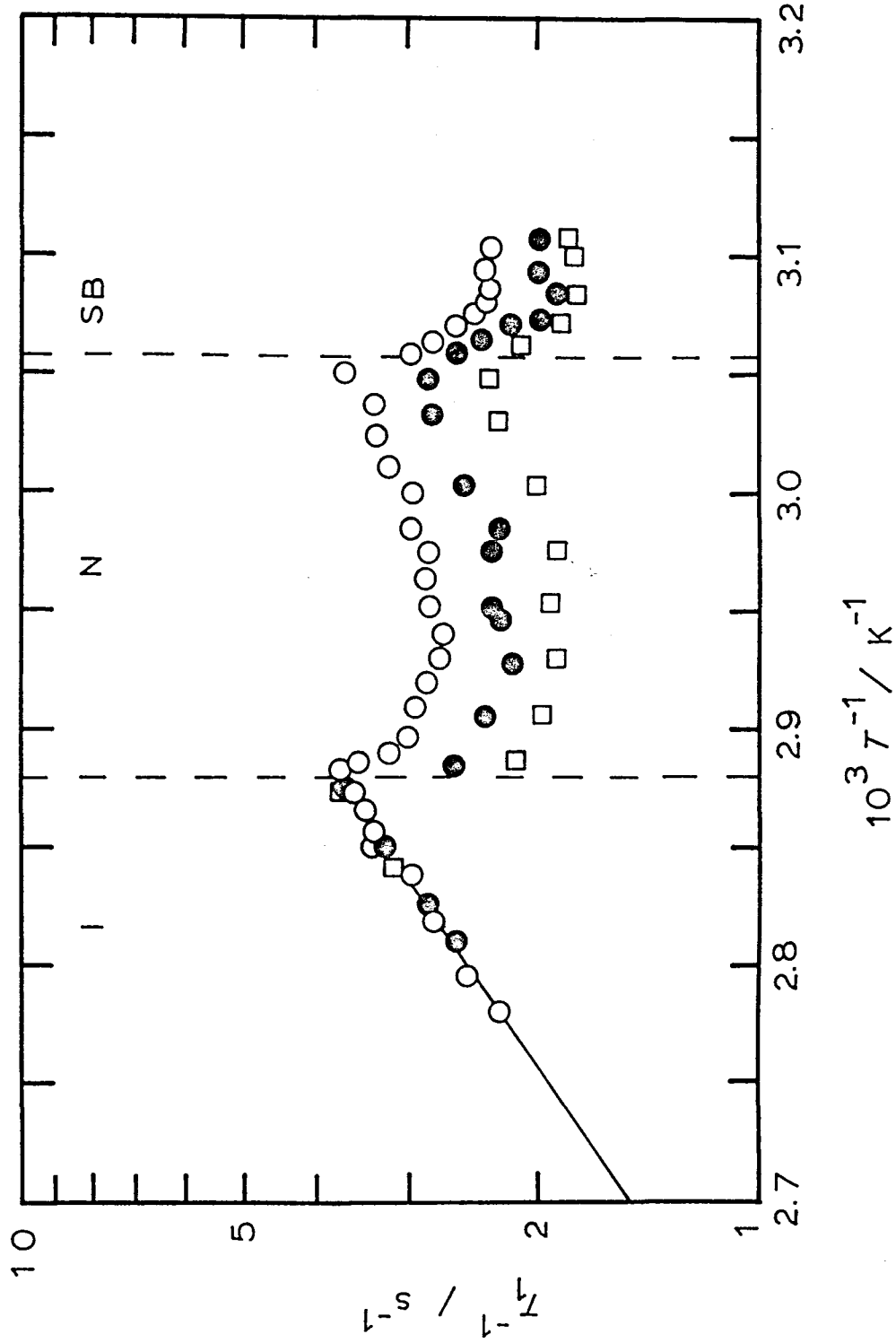


Fig. VII-4. Proton spin-lattice relaxation rates in I, N, and the metastable SB phases of HBT measured at 10.0 (O), 20.5 (●), and 40.5 (□) MHz. The solid line in the phase I represents the activation enthalpy of 43 kJ mol⁻¹.

§ VII-4. The Metastable Smectic B Mesophase

Proton NMR line in the SB mesophase consists of a narrow central peak and a pair of doublets. When cooled from the nematic phase, the spectrum exhibits a strong θ_0 -dependence because of the alignment of the director in the direction, $\theta_0 = 0$ (θ_0 is the angle between the director and the external field). The rotation patterns of the sample around the external field are represented in Figs. VII-5 & 6 at two different temperatures. In each experiment, all the conditions of the spectrometer were kept constant except the angle θ_0 . And in the experiment presented in Fig. VII-6, the gain of the detection amplifier was doubled compared with that in Fig. VII-5. As can be clearly recognized from Fig. VII-5, the width of the dipolar doublets varies with θ_0 . Theoretically the splitting width can be expressed by

$$\Delta H = 3 \gamma \hbar r^{-3} p_2(\cos \theta_0) \langle p_2(\cos \theta) \rangle p_2(\cos \Phi).$$

(VII-1)

Readers are referred to section V-3 for the details of this equation. When θ_0 is set at 54.7° (the magic angle), ΔH becomes zero and an infinite enhancement of the signal intensity is expected provided that initial alignment of the director along the external field is perfect. Fig. VII-5 & 6 represent such narrowing and strong enhancement of the signal. This is a clear evidence that this phase is a kind of orthogonal smectic

mesophase. After the experiment in Fig. VII-5, the sample was located in the magic angle orientation for two hours and the signal was recorded again, but nothing was changed in its line-shape. This fact evidences that this mesophase is smectic B (more stiff type of orthogonal smectics) but not smectic A. Another interesting discovery in the rotation pattern is its temperature-dependence. The spectra presented in Fig. VII-6 were taken at the temperature only 3.3 K lower than that in Fig. VII-5. Both central and outer components showed significant broadening. This fact suggests that the correlation frequencies of the molecular motion in this mesophase are around the scale of NMR linewidth, 10^5 s^{-1} , and strongly dependent on temperature.

The temperature (T)-, frequency (ω_0)-, and angular (θ_0)-dependences of T_1^{-1} were examined in the SB mesophase, the results of which are presented in Figs. VII-4, 7, & 8. According to the T -dependence of T_1^{-1} , this phase is divided into two regions: the high temperature region ($T \gtrsim 325 \text{ K}$) where T_1^{-1} is strongly enhanced as the transition point N/SB approaches, and the low temperature region ($T \lesssim 325 \text{ K}$) where T_1^{-1} is almost independent of temperature. The ω_0 -dependence is examined in Fig. VII-7. Although it is hardly possible to evaluate the value of τ (index of ω_0) quantitatively because of the experimental uncertainty, it can be seen that τ takes the value near $-0.5 \sim -1$. It can also be noticed that it is the ω_0 -dependent part of T_1^{-1} which is strongly enhanced in the vicinity of the N/SB transition. The T - and

ω_0 -dependences of T_1^{-1} can most reasonably be accounted for by assuming the collective excitation of orientational fluctuation in the smectic liquid crystal. Eqs. (II-29 & 23) predicts that T_1^{-1} is enhanced when the elastic constant K_1 becomes small in the vicinity of the N/SB transition. This point has been suggested by the strongly temperature-dependent motional narrowing (Fig. VII-5 & 6), and also by the unpublished result of ultrasonic velocity measurement⁵⁾ in our laboratory, in which anomalous decrease of the sound velocity near the N/SB transition was detected.

The θ_0 -dependence of T_1^{-1} was measured at 325.7 K and at the Larmor frequency of 10.0 MHz, and shown in Fig. VII-8. The result was analyzed by the theory given in chapter II and eqs. (II-22, 23, & 32). A qualitative but not quantitative agreement was obtained.

§ VII-5. Summary

The molecular motion in the phase CII is characterized by the reorientation of the terminal methyl group of the hexyloxy chain. The molecular motion in CI is not so different from that of CII, exhibiting a segmental motion of the chain only in the highest temperature region. The extent of disorder in CI of HBT is far smaller than that in the phase CI of HBAB.

The orientational order parameter in the nematic HBT is larger than that of HBAB in the entire T^* range, but some common features were discovered, i.e., $\langle p_2 \rangle = 0.71$ at the transition point N/CI, and $\langle p_2 \rangle \approx 0.78$ at the limit of undercooling.

The effect of terminal substituent was discussed in relation to molecular association and to stabilization of the nematic state.

The activation enthalpy for molecular diffusion coupled with large angle rotation in the isotropic phase was revealed to be $43 \pm 4 \text{ kJ mol}^{-1}$, coinciding with that in HBAB.

Strongly temperature-dependent motional narrowing and relaxation enhancement were observed in the high temperature region of the smectic B phase. The temperature-, frequency-, and angular-dependences of the experimental T_1^{-1} were explained qualitatively by the theory of spin-lattice relaxation due to collective excitation of orientational fluctuation developed in chapter II.

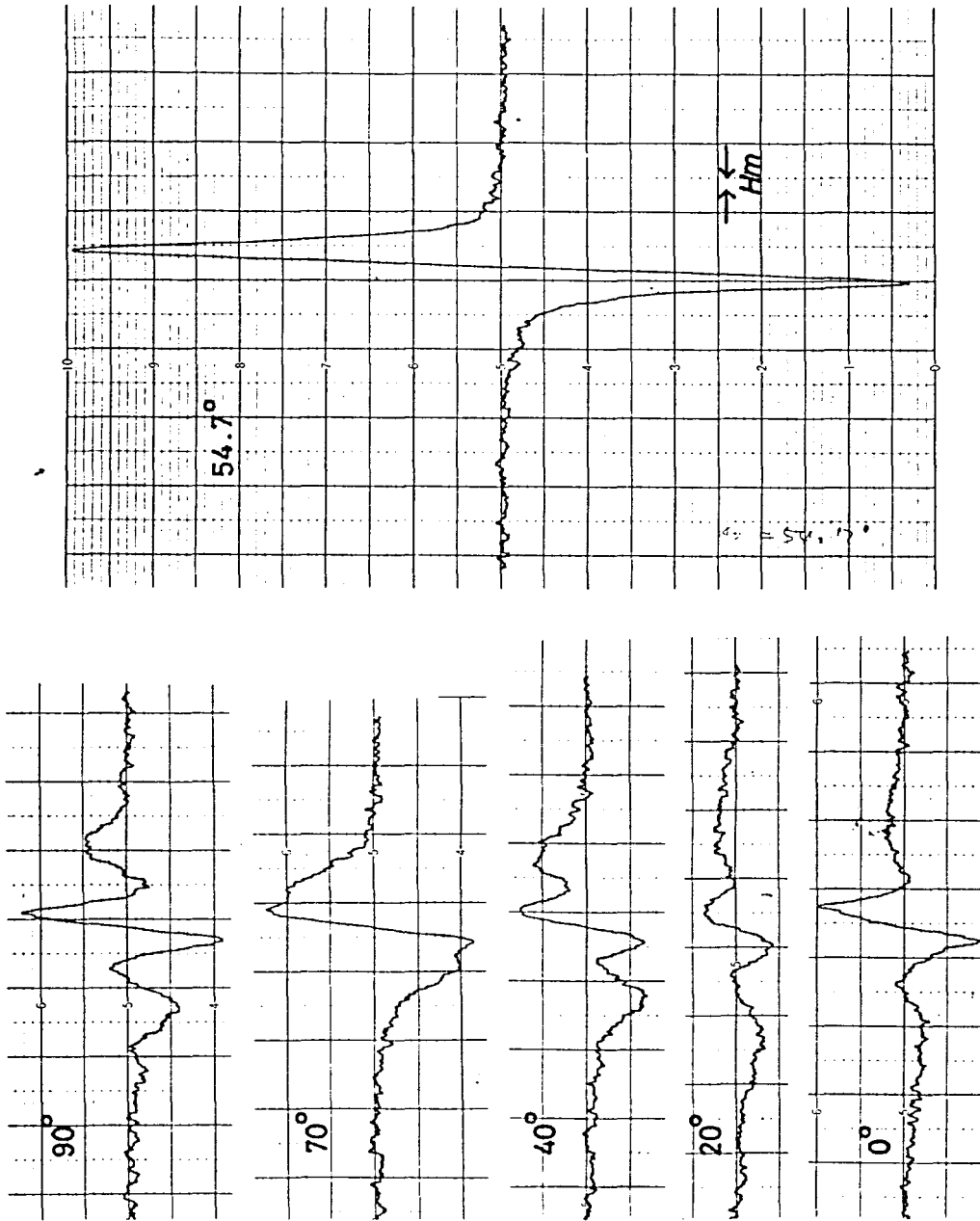


Fig. VII-5. Rotation pattern of the proton NMR spectrum (absorption derivative) in the SB mesophase (326.5 K) of HBT. The angle θ_0 and the modulation width are indicated. The conditions of the spectrometer are kept constant during the measurements. The horizontal one section corresponds to 0.8 G.

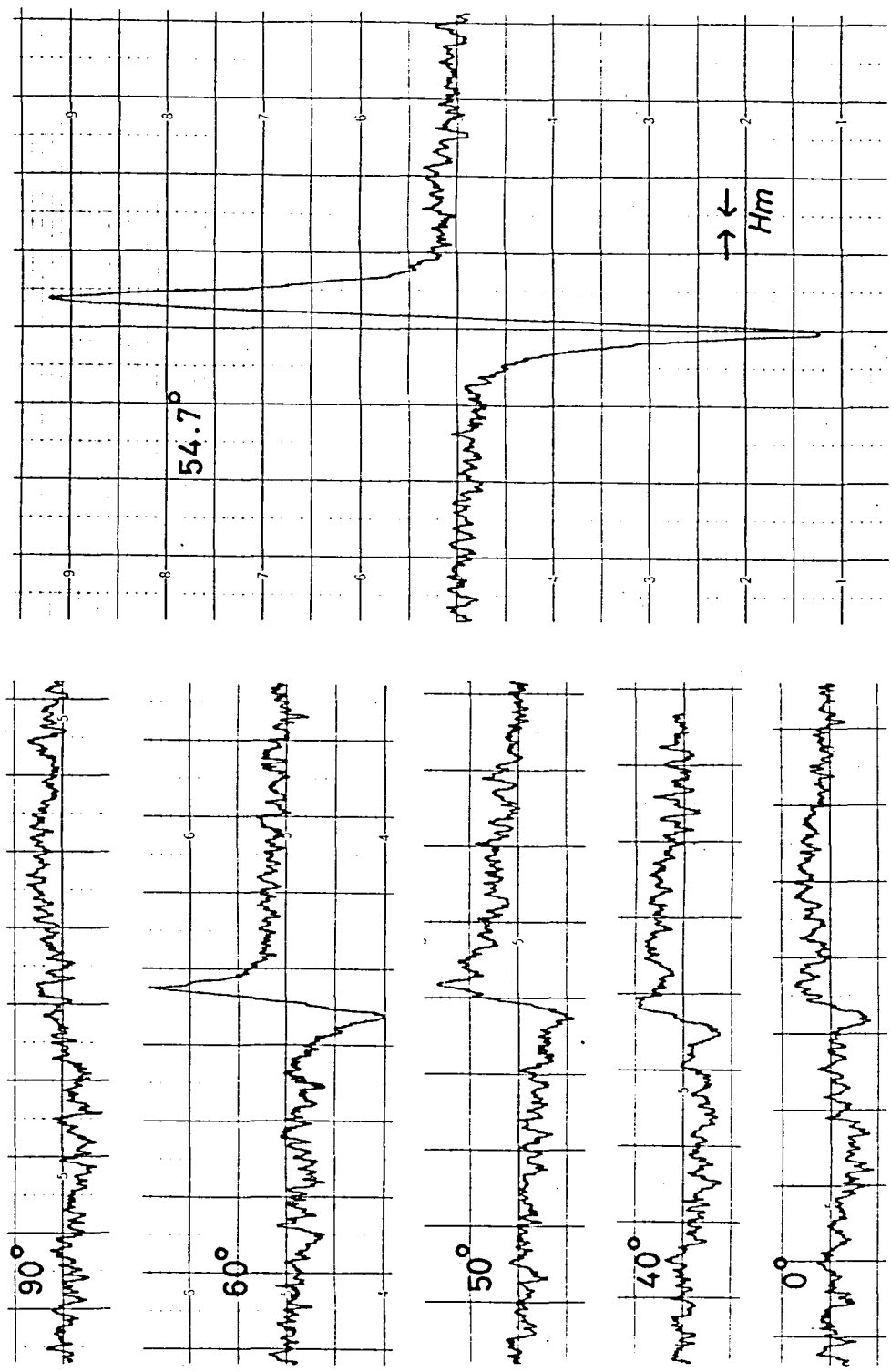


Fig. VII-6. Rotation pattern of the proton NMR spectrum in the SB mesophase (323.2 K) of HBT. The gain of the detection amplifier was doubled compared with that in Fig. VII-5. The other conditions are the same.

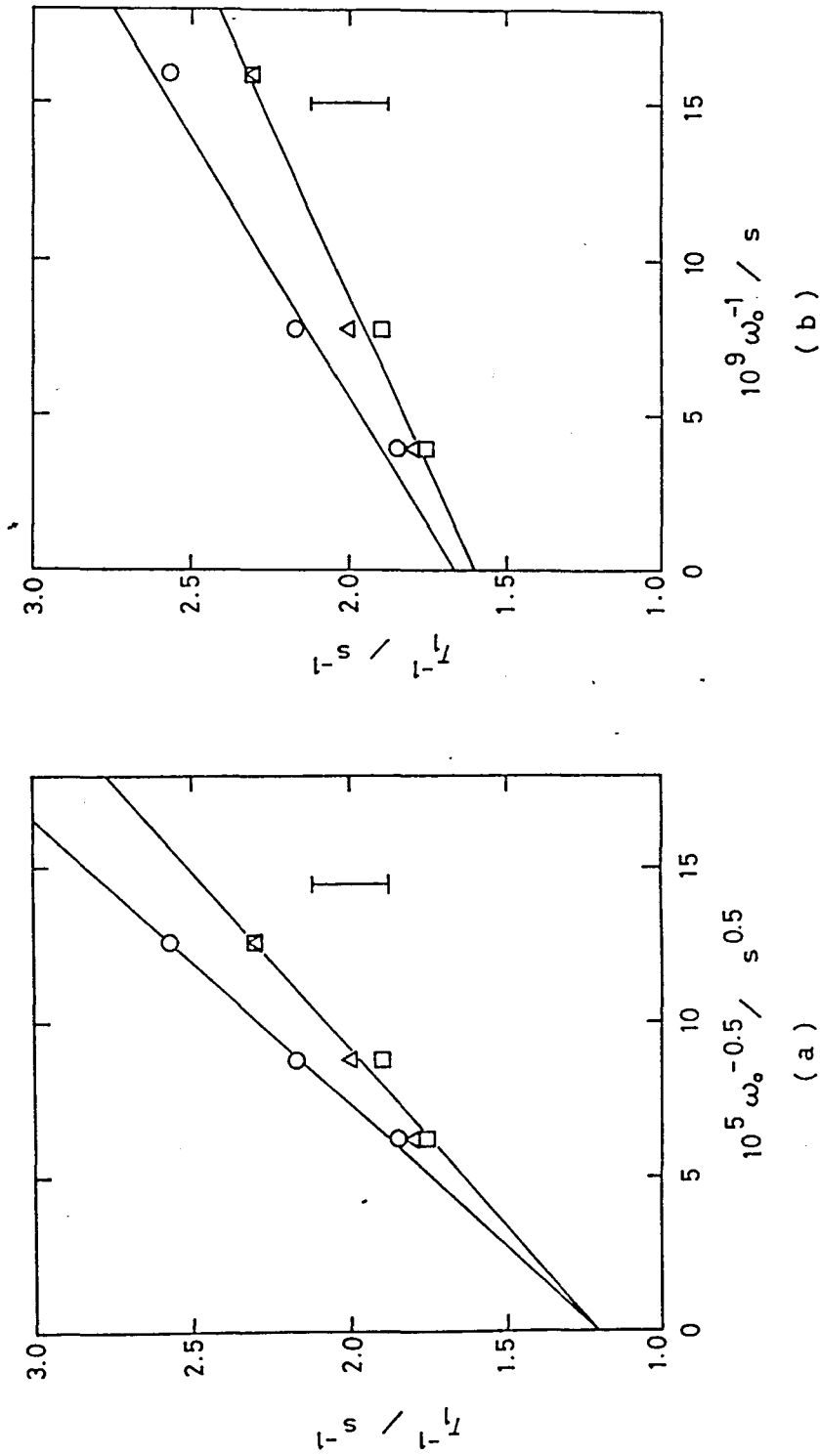


Fig. VII-7. Frequency-dependence of proton spin-lattice relaxation rate in the SB mesophase of HBT, plotted against $\omega_0^{-0.5}$ (a), and ω_0^{-1} (b). The data were taken at 325.5 K (○), 324.1 K (□), and 321.9 K (△). A typical experimental uncertainty is indicated.

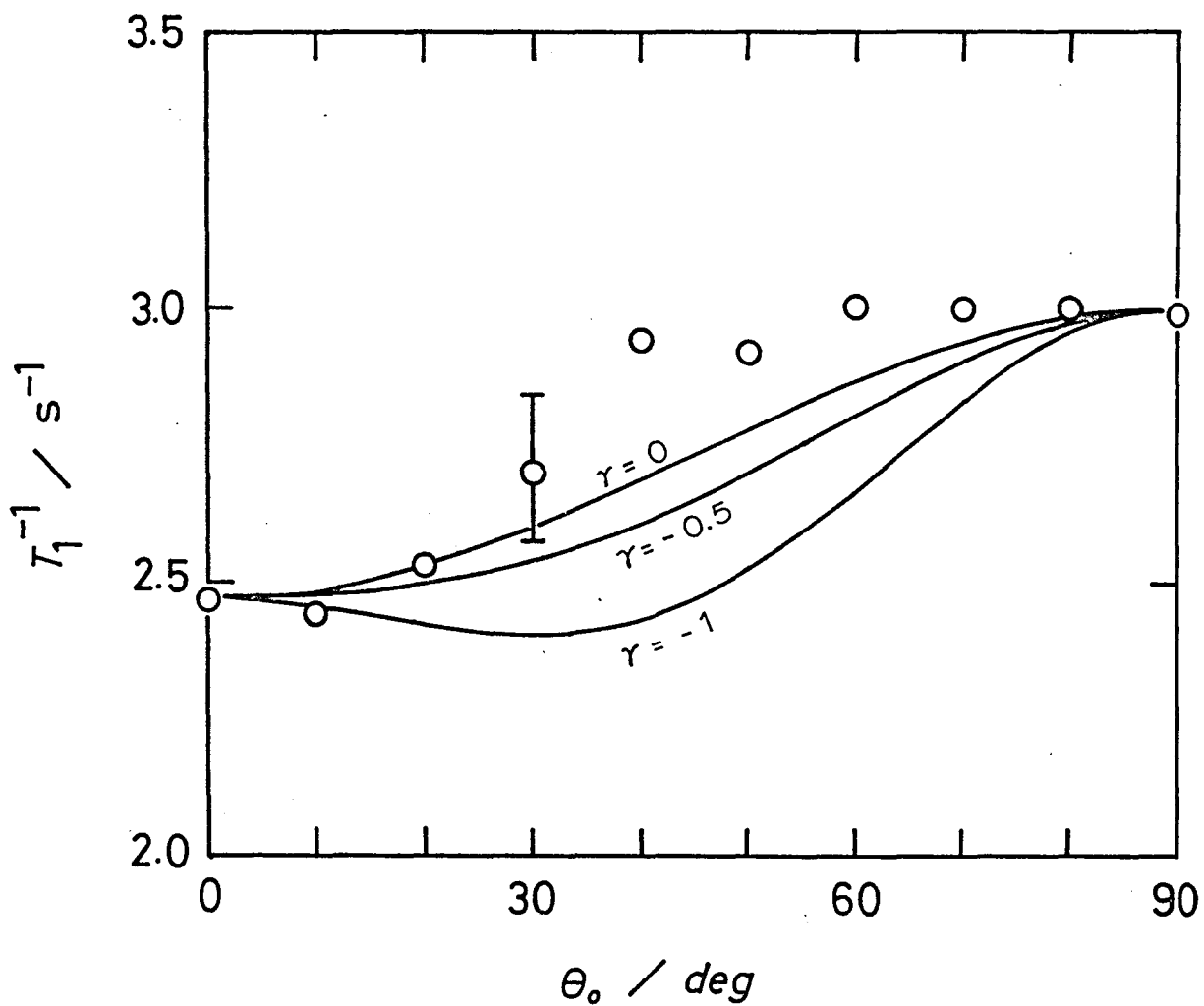


Fig. VII-8. Angular-dependence of proton spin-lattice relaxation rate in the SB mesophase (at 325.7 K) of HBT measured at 10.0 MHz. The three theoretical lines are calculated by eqs. (II-22,23, & 32), and by fitting to the data. A typical experimental uncertainty is indicated.

References to chapter VII

- 1) for a reference on the motion of the methyl group bonded to the benzene ring, see for instance,
J. Haupt and M. Warmuth: Zeit. Naturforsch. 23a (1968) 208.
- 2) R. K. Sarna, B. Bahadur, and V. G. Bhide: Mol. Cryst. Liq. Cryst. 51 (1979) 117.
- 3) P. E. Cladis: Phys. Rev. Lett. 35 (1975) 48.
- 4) P. E. Cladis: 8th Int. Liq. Cryst. Conf. (1980, Kyoto).
- 5) K. Negita: private communications.

Chapter VIII A Phenomenological Theory of Viscosity
and Self-Diffusion in Nematic Liquid Crystals

§ VIII-1. Theory

We will present here a simple phenomenological theory of viscosity and self-diffusion in nematic liquid crystals, and examine it using the data so far available for PAA, MBBA, and HBAB.

Our model is nothing but an extension of the theory of viscosity and diffusion based on Eyring's theory of significant liquid structure.¹⁾ The essential points of Eyring's theory are: (1) the liquid state consists of solid-like molecules and gas-like mobile molecules adjacent to the holes, (2) viscosity and diffusion can be treated on the common physical basis by supposing that the two phenomena are related to the friction against molecules jumping into holes. Eyring et al. developed their theory for isotropic liquids, and we will now treat the case of anisotropic system.

Diffusion constant tensor in a three-dimensional system is defined by the Fick's first law,

$$\vec{J} + D \vec{\nabla} c = \vec{0}. \quad (\text{VIII-1})$$

Here, c and \vec{J} denote the concentration and the flow density, respectively. If we take a coordinate in which the z -axis is parallel to \vec{n} , the D tensor can be diagonalized reflecting the cylindrical symmetry of the system,

$$D = \begin{bmatrix} D_{\perp} & & 0 \\ & D_{\perp} & \\ 0 & & D_{\parallel} \end{bmatrix}, \quad (\text{VIII-2})$$

and eq. (VIII-1) consists of three independent differential equations. If the velocity of flow is represented by \vec{u} , and taking in mind the relation $\vec{J} = c \vec{u}$, the following set of equations hold for the flow in the direction of q_j (q denotes the coordinate, and $j = x, y, z$),

$$c u_j + D_{jj} \frac{\partial c}{\partial q_j} = 0. \quad (\text{VIII-3})$$

On the other hand, viscosity η is generally defined by the shear stress divided by the velocity gradient. When the direction of shear stress is q_j , and the direction of velocity gradient is q_i , the viscosity coefficient η_{ji} is represented by

$$\eta_{ji} = \frac{\left(\frac{F_j}{A_i} \right)}{\left(\frac{\partial u_j(q_i)}{\partial q_i} \right)}, \quad (\text{VIII-4})$$

where F_j and A_i denote the shear force in the direction of q_j , and the area on which the shear force acts. If we consider a gas-like molecule jumping into the nearby hole getting over the friction of solid-like molecules, the denominator in eq. (VIII-4) is replaced by u_j/λ_i (λ_i is the nearest neighbor

distance in the direction of q_i), and eq. (VIII-4) is replaced by

$$\eta_{ji} = \left(\frac{\lambda_i}{A_i} \right) \cdot \frac{F_j}{u_j} \quad . \quad (\text{VIII-5})$$

The F_j is related to the activity a by a simple thermodynamical consideration to obtain

$$F_j = - k T \frac{\partial \ln a}{\partial q_j} \quad . \quad (\text{VIII-6})$$

Combining eqs. (VIII-3, 5, & 6) yields a modified Stokes-Einstein equation

$$\eta_{ji} = \frac{\lambda_i}{A_i} \cdot \frac{k T}{D_{jj}} \cdot \frac{\partial \ln a}{\partial \ln c} \quad . \quad (\text{VIII-7})$$

Now let us introduce a specific expression of viscosity in nematic liquid crystals. In nematic liquid crystals, viscosity depends on the orientation of the director \vec{n} with respect to the direction of flow (q_j) and the velocity gradient (q_i), the latter of which depends on the experimentally determined boundary conditions. Miesowicz²⁾ gave definitions of the three principal viscosity coefficients corresponding to the cases in which \vec{n} is (1) parallel to the velocity gradient, (2) parallel to the flow, and (3) perpendicular to both the flow and the velocity gradient. These orientations are drawn in Fig. VIII-1, in which the definitions of η_1 , η_2 , and η_3 are the same as those by Helfrich,³⁾ Gähwiller,⁴⁾ and Knepe and

Schneider,⁷⁾ but different (η_1 and η_2 are interchanged) from those by Miesowicz,¹⁾ Franklin,⁵⁾ and Porter and Johnson.⁶⁾

The three principal viscosity coefficients can be expressed by eq. (VIII-5) if a suitable set of the geometrical factors, A_i and λ_i , are chosen.

We will now present a very simple model treatment for these factors. The nematic liquid crystal media is regarded to be closely packed with elongated regular hexagonal prisms as is shown in Fig. VIII-2, except the existence of holes at some concentration. The symbols a and νa represent the dimensions of individual molecules. The ν may be called the anisotropy factor of the molecular shape. This model corresponds to the perfect orientational order. By utilizing this model structure, A_i and λ_i can be determined in a purely geometrical manner for each of the three Miesowicz viscosity coefficients: in the case of η_2 , all of the six side-planes suffer shear, whereas in the

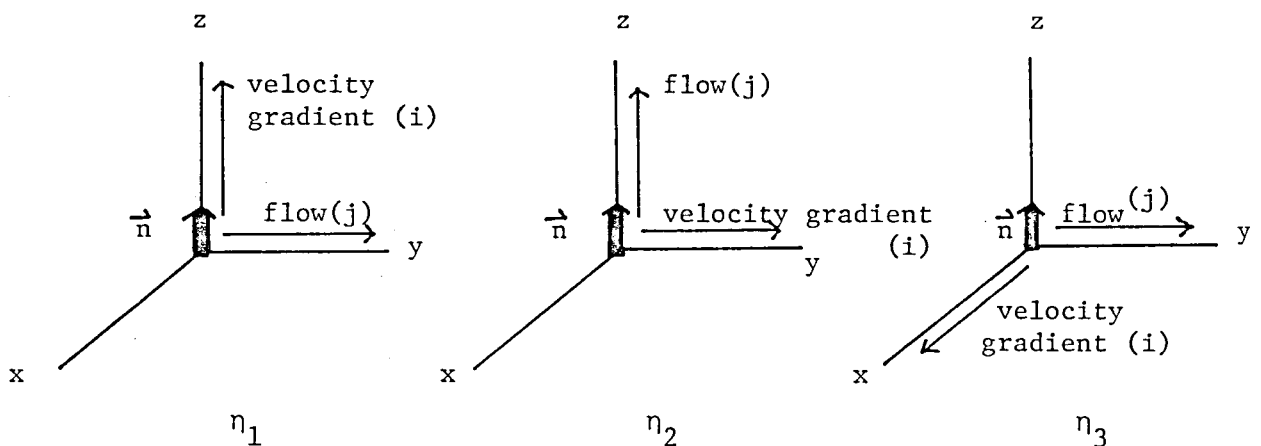


Fig. VIII-1. Geometries for the three Miesowicz viscosity coefficients in a wall-aligned nematic liquid crystal system.

case of η_1 , the two base hexagons, and in the case of η_3 , the two side-planes do, respectively. The quantity λ_i is νa for η_1 whereas $\sqrt{3} a$ for η_2 and η_3 . The following equations are thus obtained from eq. (VIII-7),

$$\eta_1 = \frac{\sqrt{3} \nu}{9 a} \cdot \frac{k T}{D_{\perp}}, \quad (\text{VIII-8})$$

$$\eta_2 = \frac{\sqrt{3}}{6 \nu a} \cdot \frac{k T}{D_{\parallel}}, \quad (\text{VIII-9})$$

$$\eta_3 = \frac{\sqrt{3}}{2 \nu a} \cdot \frac{k T}{D_{\perp}}. \quad (\text{VIII-10})$$

These three equations give phenomenological relations between

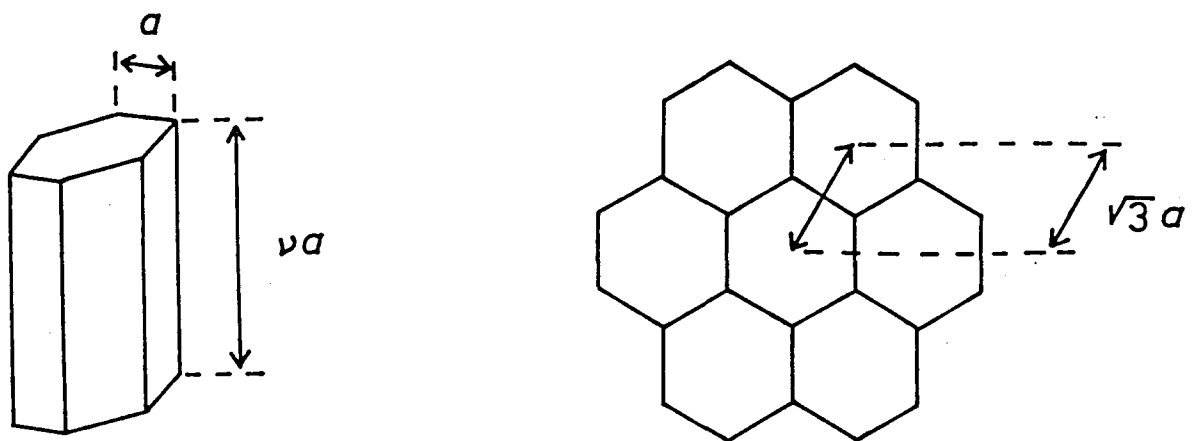


Fig. VIII-2. Model of packing of molecules in nematic liquid crystals under perfect orientational order.

the viscosity coefficients and the diffusion constants. It should be noted that the two viscosity coefficients η_1 and η_3 can be distinguished because the direction of velocity gradient can be determined by utilizing the wall-aligned nematic system. In the experiment of diffusion measurements, on the other hand, the direction of velocity gradient cannot be specified because usually a bulk sample oriented by an external field is utilized. A useful relation

$$\nu = 3 \left(\frac{\eta_1}{2 \eta_3} \right)^{1/2}, \quad (\text{VIII-11})$$

is obtained from eqs. (VIII-8 & 10) which enables us to determine the anisotropy factor ν when the experimental data of viscosity coefficients are available. Anisotropy of diffusion constant is predicted by eqs. (VIII-8 & 10) to be

$$\frac{D_{\parallel}}{D_{\perp}} = \frac{\eta_3}{3 \eta_2} = \frac{3 \eta_1}{2 \nu^2 \eta_2}. \quad (\text{VIII-12})$$

§ VIII-2. Comparison with Experiment

When one wishes to compare the present theory with the experimental data, one will find that the experimental uncertainty connected with the measurements of anisotropic diffusion constant is larger than that of viscosity coefficients. So we will present the discussion of this section by calculating D_{\parallel} and D_{\perp} by utilizing the viscosity data and the equations in

Table VIII-1. Experimental data of Miesowicz viscosity coefficients

sample	temperature T / K	Miesowicz viscosity coefficients		
		η_1	η_2	η_3 / Pa s
PAA ^{2,8)}	395.15	9.2×10^{-3}	2.4×10^{-3}	3.4×10^{-3}
MBBA ⁷⁾	298.15	0.1361	0.0240	0.0413
HBAB ⁴⁾	345.0	0.058	0.0186	0.0115

the present theory, and compare them with the experimental data on diffusion.

Miesowicz viscosity coefficients were measured by Miesowicz²⁾ for PAA, by Gähwiller⁴⁾ for MBBA and HBAB, and by Knepe and Schneider⁷⁾ for MBBA. These data are tabulated in Table VIII-1. Anisotropic self-diffusion constants of nematic liquid crystals were first measured by Yun and Frederickson⁹⁾ for PAA by means of ¹⁴C radioactive tracer technique, and later by Zupančič et al.¹⁰⁾ for MBBA by means of NMR pulsed field gradient technique coupled with multiple-pulse line-narrowing technique. The only data for diffusion of HBAB is our NMR relaxation data.¹¹⁾ These are tabulated in Table VIII-2.

In the first place the anisotropy factor ν of the molecular shape was calculated by eq. (VIII-11). The values 3.49 (PAA), 3.85 (MBBA), and 4.76 (HBAB) obtained are quite reasonable.

The theoretical values of D_{\parallel} and D_{\perp} were calculated by utilizing eqs. (VIII-8 ~ 10), viscosity data, and the values of

Table VIII-2. Comparison of the theoretical prediction with the experiment.

sample	T / K	ν theory	D_{\parallel} theory	D_{\perp} theory	D_{\parallel}/D_{\perp} theory
			D_{\parallel} exper.	D_{\perp} exper.	D_{\parallel}/D_{\perp} exper.
PAA	395.15	3.49	6.5×10^{-10}	1.4×10^{-9}	0.5
			4.1×10^{-10}	3.2×10^{-10}	1.3
MBBA	298.15	3.85	4.4×10^{-11}	7.7×10^{-11}	0.6
			1.2×10^{-10}	9.0×10^{-11}	1.3
HBAB	345.0	4.76	5.4×10^{-11}	2.6×10^{-10}	0.2
			$(\overset{2.7}{4.2} \times 10^{-10})$	$(\overset{1.7}{2.6} \times 10^{-10})$	(1.6)

Experimental data are quoted from ref. 10 (NMR pulsed field gradient) for MBBA, from ref. 9 (^{14}C tracer) for PAA, and the present work (NMR relaxation) for HBAB. The experimental data D_{\parallel} and D_{\perp} of HBAB are less trustworthy because $D_{\parallel}/D_{\perp} = 2.0$ was assumed to derive them (see chapter V, this thesis).

estimated above. The value of a ($\sqrt{a} = 0.50 \text{ nm}$) was quoted from the x-ray work.¹²⁾ The results are presented in Table VIII-2. The values of D_{\parallel} and D_{\perp} are in satisfactory agreement with the experiment, but the anisotropy of the diffusion constants D_{\parallel}/D_{\perp} are in poor agreement showing the limitation of this simple theory.

The origin of this disagreement will now be examined. Our model theory of self-diffusion takes into account only shear stress as a hindering force for self-diffusion, and ignores steric hindrance. This simplification will result in

overestimate of diffusion coefficient perpendicular to \vec{n} .

(As can be seen from Fig. VIII-2, self-diffusion perpendicular to \vec{n} will suffer strong steric hindrance.)

The effect of steric hindrance may be incorporated into the theory in a lowbrow manner by introducing Eyring's phenomenological parameter κ (transmission coefficient, $0 < \kappa < 1$) for transverse diffusion. This parameter depends on the local structure of the intermolecular potential surface near its saddle point. By utilizing this transmission coefficient for transverse diffusion, eqs. 8, 10, & 12 are replaced by

$$\eta_1 = \frac{\sqrt{3} \kappa \nu}{9 a} \frac{k T}{D_{\perp}}, \quad (\text{VIII-13})$$

$$\eta_3 = \frac{\sqrt{3}}{2 \nu a} \frac{k T}{D_{\perp}}, \quad (\text{VIII-14})$$

$$\frac{D_{\parallel}}{D_{\perp}} = \frac{\eta_3}{3 \kappa \eta_2} = \frac{3 \eta_1}{2 \kappa \nu^2 \eta_2}. \quad (\text{VIII-15})$$

The value $\kappa \approx 0.4$ can explain the anisotropy of diffusion in PAA and MBBA well.

VIII-3. Discussion

It has been demonstrated that our simple phenomenological theory can give us a good insight into the relation between viscosity and self-diffusion in nematic liquid crystals. Note that our model is based on the perfect orientational order of the system. We never expect that these equations would

quantitatively explain the phenomena of diffusion and viscosity in the nematic liquid crystal because these relations were derived from purely geometrical model without any further reflection on the dynamical mechanism of diffusive motion of flexible long molecules in a medium with imperfect orientational order. But we believe that these relations will give a simple and qualitative perspective to the transport properties in nematic liquid crystals.

Franklin⁵⁾ developed a theory of self-diffusion in nematic liquid crystals by modifying Kirkwood's theory^{13,14)} of macromolecular diffusion in isotropic solvents. Franklin's theory is far more detailed and thorough than ours, including intermolecular friction constants, anisotropy factor of a molecule, so-called "molecular segment sum," orientational order parameter, and the viscosity coefficients, in the theoretical expression of diffusion constant. The most essential difference between Franklin's treatment and ours lies in that the former theory takes into account the flexibility of a molecule and consequently the effect of intramolecular interactions between segments on self-diffusion, whereas the latter ignores them and treats the diffusion of a rigid hexagonal prism. The latter can be compared with experiment far more easily.

References to chapter VIII

- 1) H. Eyring and Mu Shik John: " Significant Liquid Structures " (John-Wiley & Sons, Inc., 1969), chapter 5.,
H. Eyring and T. Ree: Proc. Natl. Acad. Sci. (U. S.)
47 (1961) 526.
- 2) M. Miesowicz: Nature 17 (1935) 261., *ibid.* 158 (1946) 27.
- 3) W. Helfrich: J. Chem. Phys. 50 (1969) 100., *ibid.* 53
(1970) 2267.
- 4) Ch. Gähwiller: Mol. Cryst. Liq. Cryst. 20 (1973) 301.
- 5) W. Franklin: Mol. Cryst. Liq. Cryst. 14 (1971) 227.,
Phys. Lett. 48A (1974) 247., Phys. Rev. 11A (1975) 2156.
- 6) R. S. Porter and J. F. Johnson: J. Phys. Chem. 66 (1962)
1826.
- 7) H. Knepe and F. Schneider: Mol. Cryst. Liq. Cryst. 65
(1981) 23.
- 8) S. Chandrasekhar: " Liquid Crystals " (Cambridge Univ.
Press, 1977) chapter 3.
- 9) C. K. Yun and A. G. Frederickson: Mol. Cryst. Liq. Cryst.
12 (1970) 73.
- 10) I. Zupancic, J. Pirs, M. Luzar, and R. Blinc: Solid State
Commun. 15 (1974) 227.
- 11) chapter V, this thesis.
- 12) A. J. Leadbetter, P. M. Richardson, and C. N. Colling:
J. Phys. (Paris) 36 (1975) C1-37.
- 13) J. G. Kirkwood: J. Polymer Sci. 12 (1954) 1.
- 14) H. Yamakawa: " Modern Theory of Polymer Solutions "
(Harper & Row Publishers, 1971) chapter VI.

Chapter IX Summary

NMR studies were carried out in a series of liquid crystalline compounds, HBAB, HBAC, and HBT. Various motional aspects which are exhibited in a variety of thermodynamical phases in this series of compounds were examined with special emphasis on the kinds of modes and their time-scales. Informations on successive excitation of modes were obtained in relation to liquid crystalline polymorphisms.

Theory of spin-lattice relaxation due to orientational fluctuation in smectic liquid crystals was developed on the basis of elastic continuum theory. The order of magnitude of proton spin-lattice relaxation rate, and its frequency-, temperature-, and angular-dependences were deduced theoretically.

Another theoretical contribution was made for the phenomenological relation between viscosity and diffusion coefficients in nematic liquid crystals, which is an extension of Eyring's theory of significant liquid structure. The theory was compared with experimental data on PAA, MBBA, and HBAB almost successfully.

The experimental results are summarized below.

(1) The ordered crystalline phase (CII) of HBAB and HBT was characterized by the NMR relaxation due only to the terminal methyl reorientation. On the other hand, in the high temperature phase (CI) of HBAB, motional disorder with respect to conformation of the hexyloxy chain was detected. Although the rotational modes of segmental motion are excited up to the

propyl group, the nature of these modes are considered to be that of jump rotation with activation barriers of $9 \sim 19 \text{ kJ mol}^{-1}$, and does not correspond to the melting of the hexyloxy chain. This is the first report on motional disorder exhibited by the high-temperature crystalline modification of mesogenic compounds. Motional states of CI of HBT is not so different from that of CII because an additional relaxation mode is observed only in the highest temperature region of CI. In the crystalline state of HBAC, a kind of large angle oscillatory mode was detected in the high temperature region.

(2) The qualitative change in dynamical nature when the sample is heated from crystal to smectic liquid crystal are the melting of the alkoxy chain and the excitation of self-diffusion of molecules, which are reflected on the qualitative change in NMR lineshape. At the transition from crystal to smectic liquid crystal, the Gaussian envelope of the signal disappears, and there appear a narrow central component (which is well approximated by a Lorentzian) and outer doublets. From this point of view (i.e., as far as the NMR time-scale is concerned), the unidentified phase III of HBAC has a character of crystal. If this phase is justifiably classified into crystal, it follows that the three compounds melts into mesophase at the common temperature, $334.1 \pm 0.2 \text{ K}$.

(3) The nature of smectic liquid crystal was examined for the SB and SA phases of HBAC and the SB phase of HBT. The frequency-, temperature- and angular-dependences of T_1^{-1} were most reasonably accounted for by assuming collective excitation

of orientational fluctuation in all the phases, although agreement between the theory and the experiment is not quantitative. A fast rotational mode of the chain motion gave contribution, which is independent of frequency, to T_1^{-1} in the SB mesophase of HBAC. The contribution from translational self-diffusion to T_1^{-1} was small in SB, and seems to be larger in SA.

(4) The T^* - (T/T_c) dependences of the second rank orientational order parameter $\langle p_2 \rangle$ were examined in the nematic phases of HBAB and HBT. Both of the results showed the failure of the mean field theories. The $\langle p_2 \rangle$ of HBAB was smaller than that of HBT in the entire region of T^* , but some common features were recognized: $\langle p_2 \rangle = 0.71$ at the transition point CI/N, and $\langle p_2 \rangle \simeq 0.78$ at the limit of undercooling. The effect of terminal substituent on lowering $\langle p_2 \rangle$ and on stability enhancement of the nematic state was discussed. The idea that the cyano end group assists molecular association was supported.

(5) Molecular dynamics in the nematic liquid crystal were examined, and it was revealed that translational self-diffusion is the dominant mechanism of T_1^{-1} in the low temperature region of nematic HBAB. A quantitative analysis of the diffusion constants was attempted. An additional relaxation enhancement on approaching the N/I transition point will be due to the order director fluctuation.

(6) The time-scale of self-diffusion in the isotropic liquid phase is faster than that in the nematic phase. But the apparent activation enthalpies obtained from the temperature-dependence of T_1^{-1} in the isotropic phases of HBAB, HBAC, and

HBT were 40, 46, and 43 kJ mol^{-1} , respectively, which are greater than the activation enthalpy for self-diffusion in the nematic HBAB (31 kJ mol^{-1}), This point suggests that self-diffusion in the isotropic phase will be strongly correlated with large amplitude rotation of a molecule or of a cluster of molecules, which has become possible as the one-dimensional long-range orientational order has vanished in this phase.

Appendix. Kinetics of Phase Transition between Two Crystalline Modifications of p-n-Hexyloxybenzylideneamino-p'-Benzonitrile (HBAB) as Studied by Nuclear Magnetic Relaxation.*

abstract

Pulsed proton NMR was applied to the study of kinetics of the first order phase transition of a nematogen compound, HBAB. The change of behavior in magnetization recovery was measured during the transition from the undercooled Crystal I to the stable Crystal II was proceeding. Transition kinetics is analyzed by the nucleation/growth theory with constant nucleation rate. A distinct deviation from the well-known master curve of Johnson and Mehl was observed when about 70 % of the transition was achieved. This slowing-down of transition rate is interpreted by introducing an improved treatment on impingement among growing domains of the stable crystal. A possible mechanism of transition kinetics is suggested which is related to motional disorder in the parent crystal.

*) This paper was submitted by S. Miyajima, N. Nakamura, and H. Chihara to J. Chem. Soc. Faraday I, and is now in press.

The physical properties of nematic liquid crystal, p-n-hexyloxybenzylideneamino-p'-benzonitrile (HBAB), have been investigated by various techniques, e.g., viscosity,¹⁻³ density,³ dielectric constant and relaxation,⁴ and flow alignment^{2,5,6} etc. None of these studies, however, reported on polymorphism of HBAB in the solid state. Recently thermodynamic studies⁷ showed that this compound shows a first order phase transition between its two crystalline modifications at 306.98 K with the heat of transition, 5.11 kJ mol⁻¹. Tsuji et al.⁷ also found that a metastable crystal (undercooled Crystal I, the high-temperature crystalline phase) could exist at room temperature, which was gradually transformed to the stable crystal (Crystal II) on standing at room temperature. These two crystal modifications differ in colour, Crystal I being pale yellow and Crystal II being yellow.

Sluggish phase transitions in non-metallic solids are scarce (see for example ref.8). The fact that a nematogenic compound such as HBAB has a phase transition is particularly interesting because it may be a manifestation of successive acquisition of molecular degrees of freedom of motion. In fact, in the course of recent NMR study of HBAB,⁹ we found that the segmental motion of the hexyloxy chain differs in the two crystalline phases: Crystal I has a motional disorder with respect to chain conformation, whereas Crystal II is

the ordered phase.

Apart from such a point of view, the kinetics of solid-solid phase transition attracts a particular attention because it will give us a clue to the nature of the molecular motion that is responsible for the mechanism of the transition.

In this paper we report NMR spin-lattice relaxation measurements for studying the kinetics of the first order phase transition in crystalline HBAB. The method employed here will find applications to other similar systems under certain conditions.

PRINCIPLE OF THE METHOD

In the first place we will examine how the transition kinetics can be studied by NMR spin-lattice relaxation measurements. The transition of HBAB in question is of the first order and this fact constitutes the basis on which the following analysis can be made justifiable.

We take for simplicity the following three assumptions¹⁰.
(i) When domains of the two phases coexist, the nuclear spin system in each phase forms a canonical ensemble and the coupling of each spin system with the lattice is stronger than the coupling between the two spin systems, enabling us to define two different spin temperatures and two different spin-lattice relaxation times. (ii) Bloch equation holds separately for the recovery of the longitudinal component of magnetization in each phase. (iii) The time required for growth

of the stable phase, τ_g (which will be defined exactly, later) is much longer than either of the two spin-lattice relaxation times, T_{1s} in the stable phase and T_{1m} in the metastable phase. All of these assumptions were justified experimentally in the present case.

The experimental method is to observe the rate of recovery of the proton magnetization by a pulsed NMR (in the present experiment, saturation- τ - $\pi/2$ pulse sequences were utilized). Because τ is chosen as $\tau \approx T_{1s}, T_{1m}$ in such an experiment, $\tau \ll \tau_g$ is always satisfied for such a slow phase transition. Therefore the equation

$$M_z(\tau) = p M_O^S \left[1 - \exp(-\tau/T_{1s}) \right] + (1 - p) M_O^m \left[1 - \exp(-\tau/T_{1m}) \right] \quad (1)$$

is valid because the value of p , which is the mole fraction of the stable phase domain or the extent of the transition, can be regarded as a constant under the time scale of spin-lattice relaxation measurements. In eqn (1), $M_z(\tau)$ is the observable longitudinal component of the magnetization at a time τ , and M_O^S and M_O^m are the equilibrium values of M_z in the stable and the metastable phases, respectively. Eqn (1) can be transformed into

$$\frac{M_O - M_z(\tau)}{M_O} = \frac{p \alpha \exp(-\tau/T_{1s}) + (1-p) \exp(-\tau/T_{1m})}{p \alpha + (1-p)} \quad (2)$$

where $\alpha \equiv M_O^S/M_O^m$ and $M_O \equiv p M_O^S + (1-p) M_O^m$. The values of T_{1s} , T_{1m} and α can be determined from experiments for the pure phases.* If the difference of the two spin-lattice relaxation times are sufficiently large, eqn (2) as a function of α can be solved for p , enabling us to determine the rate of growth of the stable phase domains.

* (footnote) In determining α , it is important to obtain nuclear signals from the same number of nuclei in the two phases. A small error may have been incorporated in the value that arises from the volume change at the transition.

EXPERIMENTAL

The sample of HBAB was kindly offered by Dr. K. Tsuji.⁷ We further purified it by the molecular distillation method, and sealed it in a glass ampoule under 4 kPa of helium exchange gas after evacuation for ten hours with three freeze-and-thaw cycles. Proton NMR relaxation was measured at 10.0 MHz; details of the apparatus was described elsewhere.¹¹

The experimental procedure is as follows. The spin-lattice relaxation time T_1 was measured for the pure Crystal II at 293 K, and the sample was then heated to 330 K in order to bring it to Crystal I. After standing at 330 K for three hours, the magnetization recovery was observed, which exhibited an exponential recovery showing that the transition into Crystal I had been completed. Then, the sample was

cooled down to 293 K, where Crystal I survived as a metastable phase. The change of spin-lattice relaxation behaviour was monitored continuously for fifteen days using the saturation- τ - $\pi/2$ method while maintaining the sample temperature at 293.0 ± 0.1 K.

RESULTS AND DISCUSSION

JOHNSON-MEHL MECHANISM

Some of the magnetization recovery curves obtained on different days are presented in fig. 1. Three of them

Fig. 1 here

clearly show nonexponential recovery showing that the phase transition is underway. The spin-lattice relaxation times for the two phases were determined as $T_{1s} = 10.0$ s and $T_{1m} = 0.60$ s, and the value of α was 0.7 at 293 K. By utilizing these values and fitting the experimental data with eqn (2), the values of p were assessed. The results of calculation together with the values of p are also given in fig. 1.

The experimental values of p thus obtained are plotted in fig. 2 as a function of time. Fig. 2 is usually called

Fig. 2 here

the master curve of the phase transition. The origin of the time axis was taken as the time when the annealing at 293 K was started. We can see from fig. 2 that the phase transition began after some induction period of about 10^5 s, and that the master curve has a breakpoint at $t \approx 7 \times 10^5$ s.

Johnson and Mehl developed a theory of transformation kinetics based on the homogeneous nucleation/growth mechanism and derived a rate law of the form^{12,13}

$$p = 1 - \exp \left[-(t/\tau_g)^n \right], \quad (3)$$

where τ_g is the growth time which is the time to reach $p = 1 - (1/e) = 0.632$. When the rate of nucleation per unit volume of the parent matrix, I , and the radial velocity of the surface of the growing domains, G , are constant, the index n is shown to be four, and τ_g is expressed as $\tau_g = (\pi I G^3 / 3)^{-1/4}$. Eqn (3) is transformed into

$$\log \log \left(\frac{1}{1-p} \right) = n \log t - n \log \tau_g - 0.362. \quad (4)$$

In fig. 3, the double logarithm of $1/(1-p)$ is plotted against

Fig. 3 here

$\log t$ to see how eqn (3) fits the experimental results.

Fig. 3 shows that $n = 4$ and $\tau_g = 6.6 \times 10^5$ s reproduce the

experimental data quite satisfactorily for $t \leq 7 \times 10^5$ s where eqn (4) begins to deviate appreciably. Formally, this deviation can be viewed as a decreased value of n but it shows inadequacy of the original treatment of Johnson and Mehl.

A REFINED TREATMENT OF IMPINGEMENT AMONG GROWING DOMAINS

The most crucial step in the theory of Johnson and Mehl is the treatment of "impingement" among growing domains of the stable phase. They assumed for randomly distributed domains,

$$\frac{A}{A_x} = f(p) = 1 - p, \quad (5)$$

where A is the sum of the real surface of the growing domains, A_x is the so called "extended surface" which would have existed if all domains had grown without impingement, p is the mole fraction of the stable phase. This assumption has an intrinsic difficulty that the differential coefficient $f'(p) = -1$ over the whole region of p , whereas actually $f'(0)$ should be equal to zero and $f(p)$ should decrease more gradually for small p . It should be also noted that A/A_x at the completion of the transition has actually a certain nonzero value which depends on the size and the shape of crystallites, whereas eqn (5) assumes that $f(1) = 0$. If the nuclei are distributed more or less uniformly in the

parent crystal, growth impingement will not take place until a certain critical value of p is reached, where $f(p)$ begins to decrease rapidly. In order to take into account such a nonlinear behaviour of $f(p)$, we assumed a simple analytical function having a blurred stepwise behaviour in the form,

$$f(p) = \frac{1}{1 + \exp\left(\frac{p-p_0}{\delta}\right)} \quad (6)$$

In eqn (6), p_0 represents the value of p corresponding to $f(p) = 0.5$ and δ represents diffuseness of the critical region. Physically, p_0 is related to the value of p at which impingement causes the greatest effect and δ reflects the non-uniformity of the distribution of the nuclei. By replacing eqn (5) by eqn (6) in the treatment of Johnson and Mehl, the master equation for the transition kinetics is derived as

$$p + \delta \exp\left(-\frac{p_0}{\delta}\right) \left[\exp\left(\frac{p}{\delta}\right) - 1 \right] = \left(\frac{t}{\tau_g}\right)^4 \quad (7)$$

In deriving eqn (7), the rate of nucleation, I , has been assumed to be homogeneous within the parent matrix and independent of p , and the radial velocity G of the growing domain is also assumed constant. The τ_g is identical with that defined earlier. If $p \ll p_0$ (free growth stage), eqn (7) may be approximated by $p \approx \left(t/\tau_g\right)^4$ which is

essentially the same as eqn (3) for small p . If, however, $p \gg p_0$ (strong impingement stage), eqn (7) is approximated by,

$$p \approx \frac{4 \delta}{\log e} (\log t - \log \tau_g) + p_0. \quad (8)$$

In this region the master curve, i.e., the p vs. $\log t$ plot, becomes a straight line with the gradient $4 \delta / \log e$. If δ is taken to be small, eqn (7) gives a clear bending in the master curve as was really observed in the present

Fig. 4 here

experiment. Fig. 4 shows a plot of eqn (7) with an appropriate set of parameters, $p_0 = 0.95$, $\delta = 0.10$ and $\tau_g = 6.8 \times 10^5$ s. Agreement with the experiment is quite satisfactory.

CAHN'S MECHANISM OF GRAIN BOUNDARY NUCLEATED GROWTH

Cahn¹⁴ developed a different theory by assuming that nucleation may be effected on boundary surfaces of grains, the area of which should drop off faster than does the mole fraction of the parent crystal as the phase transition proceeds. He named such a loss of nucleation sites the "site saturation". According to his theory, the index n in eqn (3) changes from four to unity in the vicinity of half

reaction if the nucleation predominates on the grain boundary surfaces. The time at which the site saturation effect is expected to occur is $t \approx (I_s G^2)^{-1/3}$, where I_s is the rate of nucleation per unit area of the grain boundary. It should be noted that this mechanism can also give a formal explanation of the present experimental results (See fig. 3).

The treatment of Cahn and ours provide two different approaches for reforming Johnson-Mehl theory to accommodate it to bending of the master curve. Cahn modified the process of nucleation, whereas we improved the treatment of impingement among growing domains. If the parent matrix in which domain growth takes place has such a rigid structure that the sites of nucleation may be readily identified, Cahn's idea will probably be a good model. However, if there are considerable degrees of motional disorder in the parent matrix, recrystallization in the parent matrix will be constantly taking place and our model will be a more realistic one. It is to be admitted that either model alone corresponds to an oversimplified situation.

ON THE MECHANISM OF PHASE TRANSITION IN HBAB

It is difficult at this stage to speculate about the molecular mechanism of the phase transition in HBAB because of the lack of structural information. It is, however, possible to predict a probable mechanism of the transition.

Our phenomenological treatment suggested that the domains of Crystal II grow considerably freely until $p \approx 0.7$ is reached (See fig. 4) and that collisions among growing domains take place more or less suddenly. This may possibly arise from the motional disorder in the parent Crystal I. Because the motion of the hexyloxy chain is highly excited at this temperature in Crystal I⁹, the parent matrix is "soft", and the growing "stiff" domains may be rearranged in the "soft" matrix thus escaping direct impingement at least during the initial stages of phase transition. It is interesting to note that packing fraction of the face-centred cubic lattice with spheres of equal size is 0.74.

The authors are grateful to Dr. Kazuhiro Tsuji of Kwansai Gakuin University for the loan of the sample.

REFERENCES

- 1 Ch. Gähwiller, Mol. Cryst. Liq. Cryst., 1973, 20, 301.
- 2 S. Meiboom and R. C. Hewitt, Phys. Rev. Lett., 1973, 30, 261.
- 3 A. E. White, P. E. Cladis and S. Torza, Mol. Cryst. Liq. Cryst., 1977, 43, 13.
- 4 M. Schadt, J. Chem. Phys., 1972, 56, 1494.
- 5 Ch. Gähwiller, Phys. Rev. Lett., 1972, 28, 1554.
- 6 P. Pieranski and E. Guyon, Phys. Rev. Lett., 1974, 32, 924.
- 7 K. Tsuji, M. Sorai, H. Suga and S. Seki, Mol. Cryst. Liq. Cryst., 1979, 55, 71.
- 8 H. Chihara and S. Seki, Bull. Chem. Soc. Japan, 1959, 32, 897.
- 9 S. Miyajima, N. Nakamura and H. Chihara, unpublished results.
- 10 for a general reference on nuclear magnetic relaxation in condensed matter, see for instance, C. P. Slichter, Principles of Magnetic Resonance, second revised and expanded edition (Springer-Verlag, Berlin, Heidelberg and New York, 1978).
- 11 T. Tsuneyoshi, N. Nakamura and H. Chihara, J. Magn. Reson., 1977, 27, 191.
- 12 W. A. Johnson and R. F. Mehl, Trans. Amer. Inst. Min. Met. Eng., 1939, 135, 416.

- 13 J. Burke, The Kinetics of Phase Transformations in Metals (Pergamon Press, 1965), chapters 2 and 7.
- 14 J. W. Cahn, Acta Metall., 1956, 4, 449.

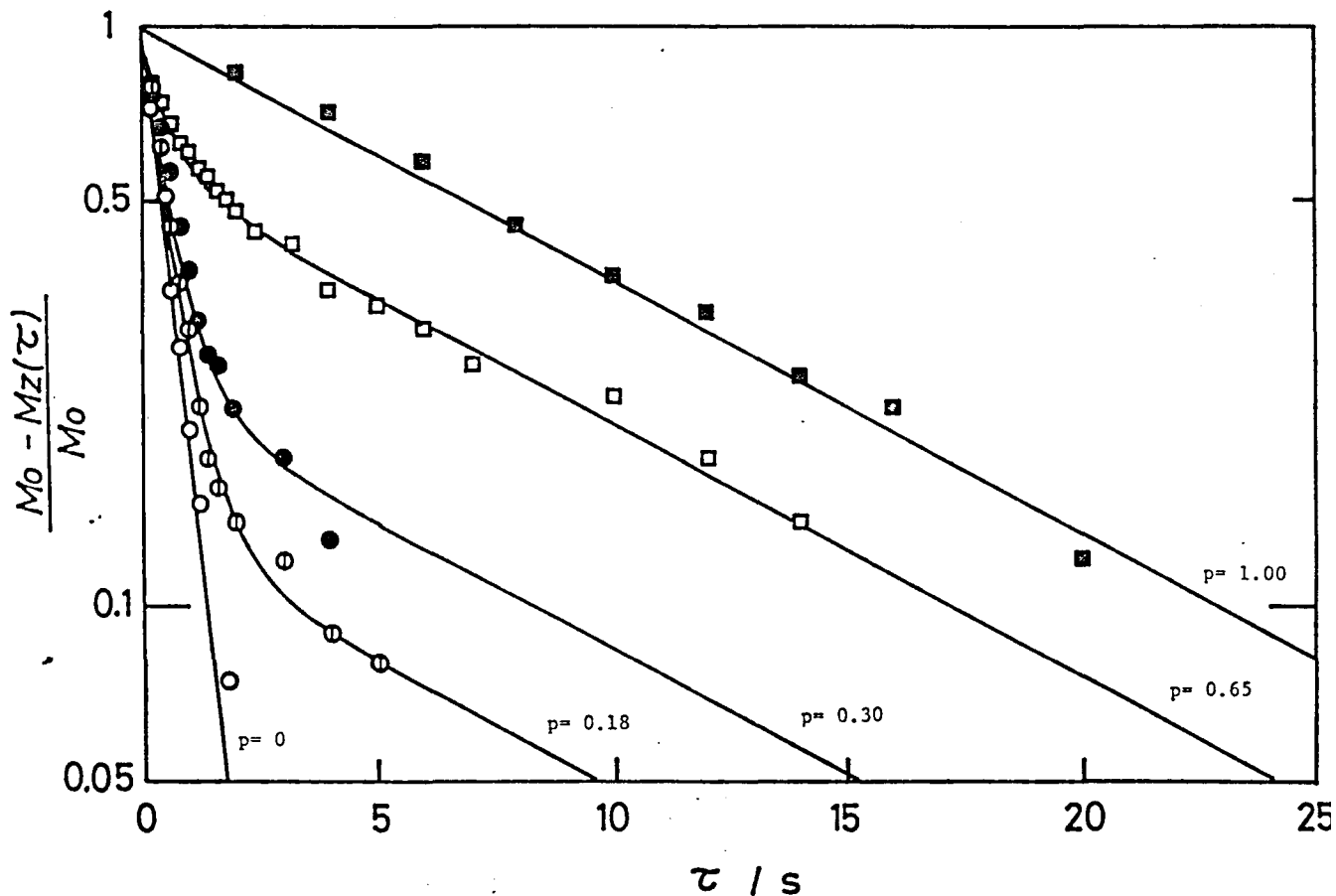


Fig. 1. Proton NMR (at 10.0 MHz) magnetization recoveries at 293 K at different times from the beginning of annealing. The points \circ and \blacksquare represent the data taken for pure Crystal I and Crystal II, respectively. The points \odot represent the data taken at $t = 4.12 \times 10^5$ s, \bullet at 5.00×10^5 s, and \square at 6.73×10^5 s. The four solid lines correspond to eqn (2) for different p values with the parameters given in the text.

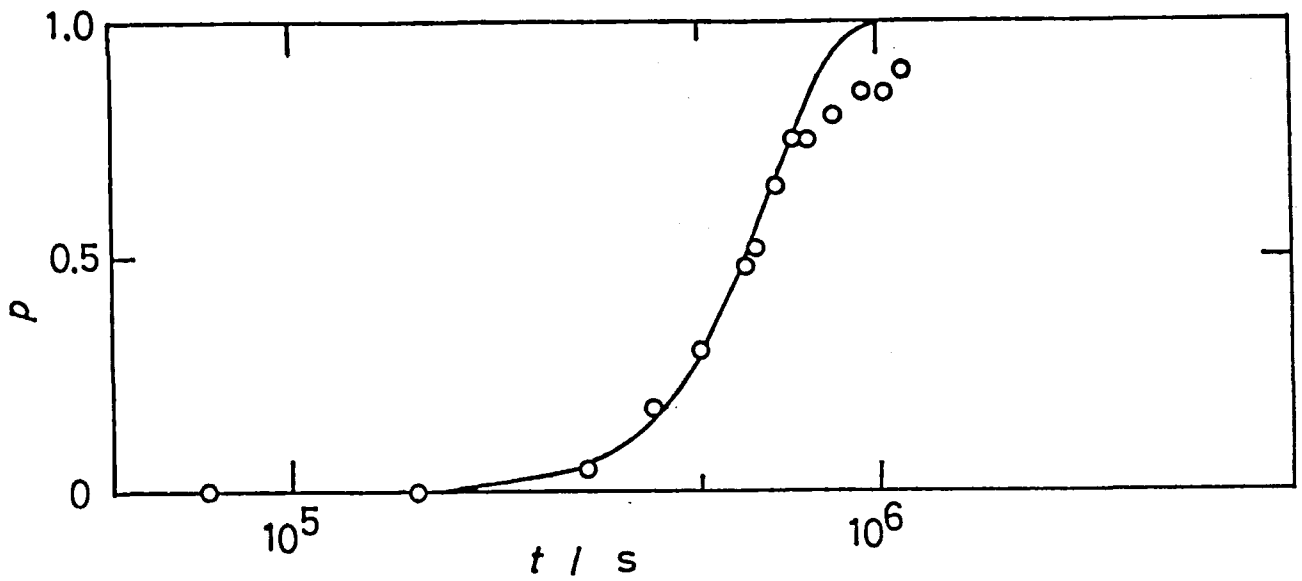


Fig. 2. Time-evolution of the stable phase fraction at 293 K. The solid line corresponds to eqn (3) (Johnson-Mehl curve) with $n = 4$ and $\tau_g = 6.6 \times 10^5$ s.

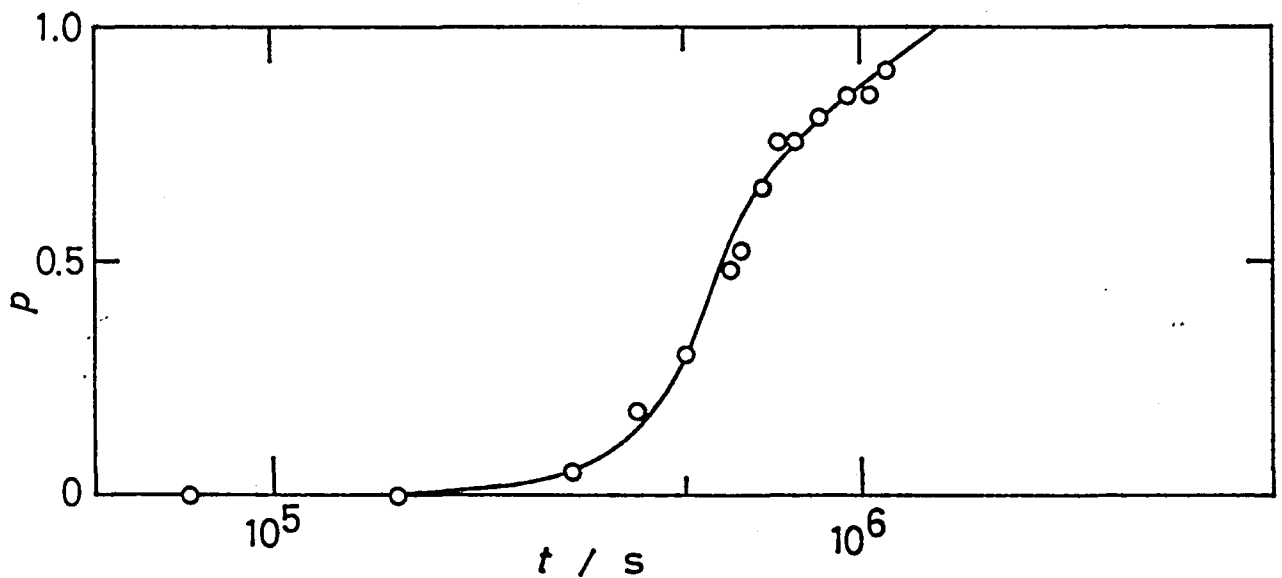


Fig. 4. Time-evolution of the stable phase fraction at 293 K. The solid line represents eqn (7) (present theory) with the parameters $p_o = 0.95$, $\delta = 0.10$, and $\tau_g = 6.8 \times 10^5$ s.

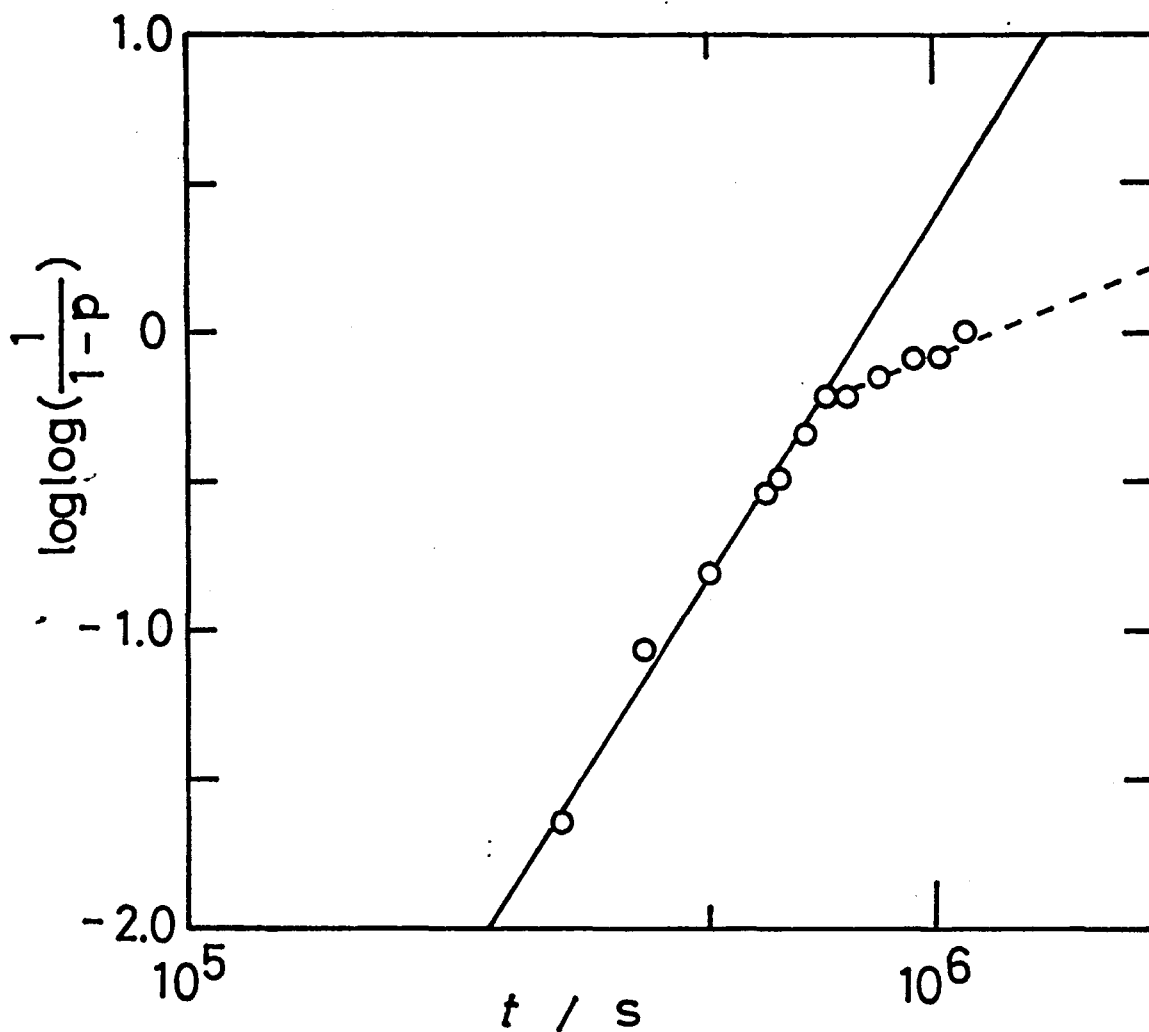


Fig. 3. Time-evolution of the stable phase fraction at 293 K in the form of $\log \log [1/(1-p)]$ against $\log t$. Experimental data are presented by circles. The solid line represents eqn (4) with $n = 4$ and $\tau_g = 6.6 \times 10^5$ s, whereas the broken line corresponds to $n = 1$.